

Finding information-rich electrocardiographic biomarkers to characterize atrial fibrillation.

Présentée le 7 juin 2023

Faculté des sciences et techniques de l'ingénieur
Groupe SCI STI JMV
Programme doctoral en génie électrique

pour l'obtention du grade de Docteur ès Sciences

par

Anna Mary MC CANN

Acceptée sur proposition du jury

Prof. J.-Ph. Thiran, président du jury
Dr J.-M. Vesin, Prof. P. Vandergheynst, directeurs de thèse
Prof. L. Sörnmo, rapporteur
Prof. G. Carrault, rapporteur
Prof. K. Aminian, rapporteur

The world is full of magic things, patiently
waiting for our senses to grow sharper.

— W. B. Yeats

Change depends on the questions we ask.
Always providing we are willing to ask them.
And at a certain point, I set out to find those questions.

— Eavan Boland

ACKNOWLEDGEMENTS

Thank you to everyone who has been there for me during the past four years, to share in the good moments and encourage me during the difficult moments. Your support is what allowed me to finish this thesis and remain relatively intact.

To my thesis supervisor, Jean-Marc Vesin, I would like to thank you for giving me the opportunity to come to EPFL and pursue a PhD in your lab. Thank you for giving me the freedom and resources to work on different projects and explore my curiosity. Thank you for your guidance and sharing your extensive knowledge with me. I came to EPFL to learn about cardiac signals and that I most certainly did, thanks to you. Not only that, you have also been an excellent French teacher! Thank you also to my thesis committee—Kamiar Aminian, Guy Carrault, Leif Sörnmo, and Jean-Philippe Thiran—for the interest and enthusiasm you showed in my work and the valuable feedback you provided.

To my thesis co-supervisor, Etienne Pruvot, thank you for giving me the opportunity to attend ablation procedures and to work with your patients' data. It was a real pleasure to have such a close clinical collaboration with you. To Alexandre, Gerhard, and Gerry from Medtronic, thank you for all your technical assistance with collecting vest ECG data.

To my ASPG colleagues, Adrian, Lester, Vincent, and Yann, thank you for welcoming me into the lab. Special thanks to our beloved secretary Anne, you simplify the lives of the many of us that pass through your door and take special care that we work under the best possible conditions.

To Pierre Vanderghenst, thank you for welcoming me into LTS2. It was a privilege to spend the last few months of my PhD in your lab, and I will miss working in the environment you have created. To all my LTS2 friends and colleagues, especially Ali, Anaïs, Jirka, Maria, Nikos, and Vamsi, thank you for welcoming me to the lab with open arms. Though it may not have always seemed like it, I appreciated the foosball sessions, coffee breaks, and random hug interruptions more than you could imagine. To all my other friends and colleagues who pass through the kitchen upstairs, thank you for the great lunch breaks and coffee chats. It makes me extremely happy to see how life has come back in the upstairs corridor after the pandemic.

To my friends in Switzerland, especially Ben, David, Mariko, and Nouha, I could not thank you enough for the joy you bring to my life. I was incredibly lucky to cross paths with you, and my life in Lausanne changed when I met you. Here's to many more walks, hikes, brunches, iftars, weekends, and finally a first silent disco!!

To my friends from school and university, especially Ami, Maxime, and Sara, thank you for understanding me and for believing in me. While I wish we could see each other more often, I am comforted knowing you are always there for me. Your accomplishments never cease to inspire me, and I look forward to seeing where the wind takes you.

Acknowledgements

Finally to my family. To my little niece Coraline, you arrived just as I was starting my PhD and have been a constant source of joy since. To my sister-in-law, Elizabeth, thank you for always being there for me, thank you for supporting me and encouraging me and reassuring me. Your positivity and enthusiasm are contagious, and without fail, talking to you is an assured source of motivation and inspiration. To my brothers, Kevin, Gerard, and John, thank you for your love, support, and encouragement. To Guillaume, I met you only two years ago and yet here you are, a part of my family. Thank you for making me laugh, for letting me cry, for inspiring me, for believing in me. But especially for your brioches and your help with matrix algebra ;) If this PhD led to crossing paths with you, then I would do it again. And to my parents, Gerry and Teresa, thank you for encouraging my curiosity and independence, for supporting me, for trusting me, and most of all, for loving me unconditionally.

Lausanne, May 4, 2023

A. McCann

ABSTRACT

Atrial fibrillation (AF) is the most common cardiac arrhythmia; it will affect one in four adults worldwide in their lifetime. AF has serious consequences, including drastically increased risk of stroke. Catheter ablation surgery is an established treatment option for persistent AF, that is, an advanced form of AF that does not terminate spontaneously. However, while estimates vary widely by study, health care center, and exact ablation strategy, a common figure for post-ablation AF recurrence for patients with persistent AF is 50%. There is therefore great interest in developing pre-ablation screening to select persistent AF patients most likely to benefit from undergoing the surgery.

The clinical diagnosis of AF requires recording an electrocardiogram (ECG). This signal provides a wealth of information about the function of a patient's heart. Many studies have investigated the ECG for calculating digital biomarkers related to ablation outcomes. These studies have resulted in the development of signal processing algorithms that aim to quantify AF disease complexity from a patient's recorded ECG in an electrophysiologically interpretable way. In this thesis, we propose, test, and evaluate digital predictive biomarkers obtained through signal processing of ECG recorded pre-ablation for noninvasive selection of patients most likely to benefit long term from ablation. We additionally track the progression of the biomarkers throughout ablation to see whether they evolve differently according to procedural ablation outcome.

We used standard 12-lead ECG recorded in a persistent AF patient cohort before and during catheter ablation. We applied two distinct analysis approaches. In the first, fibrillatory wave extraction was applied to the ECG recorded on several precordial leads to allow for direct analysis of the atrial component. We then calculated spatiotemporal biomarkers correlated with AF complexity over the course of catheter ablation surgery. In the second approach, RR-interval sequences were extracted from ECG lead II, and heart rate variability (HRV) analysis was performed, to quantify the relationship between HRV and procedural and clinical ablation outcomes. In both approaches, we found that higher levels of AF organization measured pre-ablation using the ECG biomarkers were associated with AF termination by catheter ablation and long-term maintenance of sinus rhythm thereafter.

We then recorded body surface potential mapping (BSPM) ECG including 252 leads distributed across the torso. Atrial fibrillatory wave extraction was again applied to allow for a spatiotemporal analysis of all BSPM leads. We propose two novel BSPM biomarkers inspired by spatiotemporal signal processing methods that quantify regularity in space and time of the high-dimensional ECG and analyze their association with clinical ablation outcomes. It was found that increasing regularity in the high dimensional BSPM signal was associated with AF

Abstract

termination and long-term maintenance of sinus rhythm. These biomarkers were also shown to be performant for predicting ablation outcome.

The results of this thesis demonstrate that ECG biomarkers were predictive of catheter ablation outcomes for the persistent AF populations tested. The use of such biomarkers could help guide treatment planning for both doctors and patients and would aid in the creation of an informed and transparent treatment pathway tailored to each patient's individual needs.

Keywords: atrial fibrillation, atrial fibrillation recurrence, risk stratification, digital predictive biomarkers, catheter ablation, electrocardiogram, heart rate variability, instantaneous frequency, principal component analysis

RÉSUMÉ

La fibrillation auriculaire (FA) est l'arythmie cardiaque la plus fréquente au monde : un adulte sur quatre sera touché au cours de sa vie. La FA engendre des conséquences graves. Elle multiplie notamment le risque de subir un accident vasculaire cérébral. L'ablation par cathéter est une intervention chirurgicale bien établie pour traiter la FA persistante, c'est-à-dire une forme de FA avancée qui ne se termine pas spontanément. Toutefois, chez les patients en FA persistante, le taux de récurrence après l'ablation est de l'ordre de 50%. Il convient de noter que les chiffres exacts varient en fonction de l'étude, la clinique et la stratégie précise d'ablation appliquée. Il y a par conséquent un grand intérêt à développer une méthode de tri avant ablation permettant de sélectionner les patients en FA persistante pour qui la chirurgie pourrait être la plus bénéfique.

Le diagnostic clinique de la FA nécessite l'enregistrement d'un électrocardiogramme (ECG). Ce signal fournit une mine d'informations sur le fonctionnement du cœur du patient. De nombreuses études ont analysé l'ECG pour calculer des biomarqueurs numériques liés aux résultats de l'ablation. Ces études ont abouti au développement d'algorithmes de traitements des signaux permettant de quantifier la complexité de la FA d'une manière qui peut être interprétée sur le plan électrophysiologique, à partir des signaux ECG enregistrés avant l'ablation. Dans cette thèse, nous proposons, testons, et évaluons des biomarqueurs prédictifs numériques basés sur le traitement des signaux ECG enregistrés avant l'ablation pour la sélection non-invasive des patients pour qui l'ablation pourrait être la plus bénéfique à long terme. Nous suivons également la progression des biomarqueurs tout au long de l'ablation pour déterminer s'ils évoluent différemment en fonction de l'issue procédurale de l'ablation.

Nous avons travaillé à partir de l'ECG standard à 12 dérivations enregistré sur une cohorte de patients en FA persistante, avant et pendant l'ablation par cathéter. Nous avons appliqué deux approches d'analyse distinctes. Dans la première, l'extraction des ondes de fibrillation a été effectuée sur l'ECG enregistré sur plusieurs dérivations précordiales, pour permettre une analyse directe de la composante atriale. Nous avons ensuite calculé des biomarqueurs spatiotemporels corrélés à la complexité de la FA au cours de la chirurgie d'ablation par cathéter. Dans la deuxième approche, des séquences d'intervalle RR ont été extraites de la dérivation II de l'ECG. Une analyse de la variabilité de la fréquence cardiaque (VFC) a ensuite été réalisée afin de quantifier la relation entre la VFC et les résultats procéduraux et cliniques de l'ablation. Dans les deux approches, nous avons trouvé que des niveaux plus élevés d'organisation de la FA mesurés avant l'ablation à l'aide des biomarqueurs ECG étaient liés à l'élimination de la FA par ablation par cathéter, et au maintien à long terme du rythme sinusal par la suite.

Nous avons ensuite enregistré un ECG à haute dimension (BSPM, body surface potential

Résumé

mapping, cartographie des potentiels de surface du corps), avec 252 dérivations réparties sur le torse. L'extraction des ondes de fibrillation a de nouveau été réalisée pour analyser spatio-temporellement toutes les dérivations BSPM. Nous proposons deux nouveaux biomarqueurs BSPM inspirés des méthodes de traitement des signaux spatiotemporelles afin de quantifier la régularité spatiale et temporelle de l'ECG à haute dimension. Nous analysons ensuite leur lien aux résultats cliniques de l'ablation. Nous avons trouvé qu'une grande régularité dans les signaux était liée à l'élimination de la FA et au maintien à long terme du rythme sinusal. Ces biomarqueurs se sont également avérés performants pour prédire le résultat clinique de l'ablation.

Les résultats de cette thèse démontrent que les biomarqueurs ECG proposés étaient capables de prédire le résultat de l'ablation par cathéter, pour la population de patients atteints de la FA persistante analysée. L'utilisation de ces biomarqueurs pourrait guider la planification des traitements, tant pour les médecins que pour les patients et contribuer à la création des plans de traitement transparents et adaptés aux besoins individuels de chaque patient.

Mots-clés : fibrillation auriculaire, récurrence de la fibrillation auriculaire, stratification du risque, biomarqueurs prédictifs numériques, ablation par cathéter, électrocardiogramme, variabilité de la fréquence cardiaque, fréquence instantanée, analyse en composantes principales

CONTENTS

ACKNOWLEDGEMENTS	i
ABSTRACT	iii
RÉSUMÉ	v
1 INTRODUCTION	1
1.1 Motivation	1
1.2 Objectives	3
1.3 Organization	3
1.4 Contributions	4
2 CARDIAC PHYSIOLOGY AND ELECTROCARDIOGRAPHY	7
2.1 Cardiac Anatomy and Physiology	7
2.1.1 Overview	7
2.1.2 Cardiac cycle	8
2.1.3 Electricity in the heart	9
2.1.4 Electrical conduction system	13
2.2 Electrocardiography	16
2.2.1 Electrocardiogram	17
2.2.2 Lead systems	21
3 ATRIAL FIBRILLATION	29
3.1 Definition	29
3.2 Epidemiology	30
3.3 Symptoms	33
3.4 Diagnosis	34
3.5 Causes and Mechanisms of AF	34
3.6 Disease management	40
4 SPATIOTEMPORAL SIGNAL PROCESSING METHODS FOR 12-LEAD ECG	45
4.1 Methods	47
4.1.1 Study Population	47
4.1.2 Ablation procedure and signal acquisition	47
4.1.3 ECG signal preprocessing	48
	vii

Contents

4.1.4	Instantaneous frequency estimation	50
4.1.5	Calculation of ECG-based organization indices	54
4.1.6	Patient group comparison at each ablation step	55
4.1.7	Statistical analysis	57
4.2	Results	58
4.2.1	Study Population	58
4.2.2	ECG organization indices before and during ablation	58
4.2.3	Temporal IF and AOI evolution throughout stepwise catheter ablation	59
4.2.4	Temporal evolution of AF organization post-PVI	59
4.3	Discussion	61
5	HEART RATE VARIABILITY ANALYSIS IN ATRIAL FIBRILLATION FOR ASSESSING RESPONSE TO CATHETER ABLATION	69
5.1	Recurrence in a dynamical system	71
5.1.1	Dynamical systems, phase spaces and their trajectories	71
5.1.2	Recurrence plot	72
5.1.3	Recurrence quantification analysis	74
5.2	Methods	75
5.2.1	RR-interval sequence extraction	76
5.2.2	HRV analysis	77
5.2.3	Statistical analysis	78
5.3	Results	79
5.3.1	Change in HRV metrics from BL to endABL	79
5.3.2	Association between HRV metrics and ablation outcome	81
5.3.3	Predictive power of HRV metrics for ablation outcome	82
5.4	Discussion	87
5.4.1	Change in HRV before and at the end of ablation	88
5.4.2	Association between HRV and ablation outcome	90
5.4.3	HRV predictive power for ablation outcome	90
6	SPATIOTEMPORAL SIGNAL PROCESSING METHODS FOR BSPM	95
6.1	Introduction	95
6.2	Methods	96
6.2.1	Study population	96
6.2.2	BSPM signal acquisition and preprocessing	96
6.2.3	AA-BSPM reconstruction using a subset of BSPM electrodes	98
6.2.4	Electrode subset selection and comparison	100
6.2.5	Novel spatiotemporal indices ER_{NRMSE} , ER_{ABSE}	101
6.2.6	Performance metrics and statistical analysis	102
6.3	Results	103
6.3.1	Study population	103
6.3.2	AA-BSPM reconstruction with BSPM electrode subsets	103
6.3.3	BSPM AF spatiotemporal indices and CA outcome	104

6.3.4	Predictive power of spatiotemporal indices for outcome classification . .	106
6.4	Discussion	107
6.4.1	Electrode subset capacity to represent AA-BSPM	109
6.4.2	Statistical comparison of novel indices	111
6.4.3	Assessment of clinical impact of novel indices	112
6.4.4	Limitations	113
7	CONCLUSION	115
7.1	Main findings	115
7.2	Contributions	116
7.3	General discussion and perspectives	116
	APPENDIX	119
A	ATRIAL ACTIVITY EXTRACTION	121
A.1	Spatiotemporal QRST Cancellation Technique	122
A.1.1	Methods	122
A.2	Single-beat method	124
B	THE CONCEPT OF INSTANTANEOUS FREQUENCY	127
	BIBLIOGRAPHY	129
	CURRICULUM VITAE	147

1 INTRODUCTION

1.1 MOTIVATION

Atrial fibrillation (AF) is a cardiac arrhythmia that occurs when groups of cells outside the sinoatrial node spontaneously discharge electrical impulses in a chaotic fashion. AF is incredibly common, particularly in older populations and in certain parts of the world. Current estimates project that 1 in 3 people of European descent, 1 in 5 people of African descent, and 1 in 7 people of Asian descent will develop AF in their lifetime. The irregular heart rhythm caused by AF has serious health, social, and economic consequences, increasing drastically the risk of stroke, reducing quality of life, and costing health care systems billions of dollars worldwide. Yet despite decades of research, the molecular mechanisms underlying the genesis, progression, and maintenance of AF remain poorly understood. Treatment for AF is therefore naturally subpar, focusing on controlling heart rate or rhythm rather than tackling the molecular mechanisms behind the arrhythmia. The exact type of treatment administered to a patient depends on their disease stage and refractoriness to other kinds of treatment, though ongoing research and guidelines for what therapy to apply and at what stage are constantly evolving. The last few decades have resulted in improvements for the management of AF, but no definitive cure exists, and patient response to treatment remains unpredictable. It is widely hoped that a better understanding of the causes and mechanisms of AF would allow for the design of better treatment tools, both via pharmacological and non-pharmacological means. In the meantime, there is a need to provide tools that would help both doctors and patients choose patient-tailored treatment plans from the myriad of options available. This would result in better patient outcomes, as well as add transparency for patients about the types of health outcomes they could reasonably expect from their treatment. The work presented in this thesis addresses these concerns.

AF Management

Options for AF treatment include medication, electrocardioversion, and catheter ablation surgery. Medication is often effective for treating AF, particularly for younger patients and those with *paroxysmal AF*, meaning AF episodes which are sporadic and resolve on their own before progressing to a more advanced form (Hindricks et al., 2021). However, for older patients, who have had AF for a long time, i.e. who suffer from *persistent AF*, medication often fails to restore a normal heart rate or rhythm, or satisfactory quality of life. Persistent AF is formally defined as AF which lasts for at least 7 days and does not resolve on its own, in

1 Introduction

contrast to paroxysmal AF.

A breakthrough in AF treatment came with the development of a surgical procedure called catheter ablation, developed by Haissaguerre et al. (1998). Catheter ablation is a rhythm control strategy that is usually prescribed when both medication and electrocardioversion have failed to restore sinus rhythm. In this procedure, surgeons attempt to block electrical conduction from arrhythmogenic groups of cells located in the pulmonary veins to the left atrium, blocking arrhythmia-causing electrical impulses from reaching the heart. These procedures have been shown to be very effective in restoring a normal heart rhythm in patients who have paroxysmal AF. However, scarred tissue in the pulmonary veins can heal, rendering conduction again possible, and in persistent AF, changes in the electrical and mechanical structure of the atria themselves may contribute to arrhythmia progression. Electrically isolating the pulmonary veins is therefore not sufficient to terminate persistent AF. Estimates vary widely by study, health care center, and exact ablation strategy, but a common figure for post-ablation AF recurrence in persistent AF patients is 50%.

Therefore, predictive analysis that could provide an indication of the likelihood of success for persistent AF patients undergoing catheter ablation would help both doctors and patients choose whether to include this costly procedure as part of their treatment pathway. This would contribute to the ongoing effort to personalize patient treatment and include patients in the decision-making process. Such predictive analysis relies on finding patient-specific information thought to be related to likelihood of AF recurrence following catheter ablation. Work has been done in this area, with predictive analysis including both clinical biomarkers, as well as electrocardiographic biomarkers.

The electrocardiogram (ECG) non-invasively measures the electrical activity of the heart using electrodes placed on a patient's limbs and thorax, where they are capable of recording fluctuations in electrical currents generated by the waves of cardiac electrical activation. The ECG is by far the most widely used and analyzed electrical signal of physiological origin. It is also the most widely used non-invasive clinical tool to diagnose and characterize AF. The disordered electrical pathways responsible for the initiation and perpetuation of AF result in distinctive electrical patterns that can be seen on the ECG. Various studies have investigated whether these patterns could be used not only for diagnosis of AF, as is currently the case, but also for characterization of AF dynamics and severity of AF, which have been shown to be linked to AF catheter ablation outcomes. These studies have resulted in the development of signal processing algorithms relying on spatial, temporal, spectral, and non-linear methods that aim to quantify AF disease complexity, structure, and organization from a patient's recorded ECG signal in an electrophysiologically interpretable way. Therefore, the ECG can be used as a digital biomarker to provide objective information regarding AF disease state (Kornej et al., 2020), in addition to clinical biomarkers.

To summarize, AF is a cardiac arrhythmia of growing concern for which no cure exists and for which current treatments are subpar for some patients. ECG is a ubiquitous and low-cost

tool that has shown promise for non-invasively characterizing AF, however, its potential is underdeveloped, as its current use in clinical practice for AF is limited to its diagnosis. Further investigation into the potential applications of ECG analysis to guide treatment planning for both doctors and patients would be helpful for an informed and transparent decision-making processing, tailored to each patient's individual needs.

1.2 OBJECTIVES

The main questions explored in this thesis are as follows:

Are ECG biomarkers known to be associated with AF disease complexity associated with both procedural and clinical AF outcomes following catheter ablation, when measured pre-ablation?

Can these ECG biomarkers also be used to predict, on the level of individual patients, AF termination by catheter ablation and long-term maintenance of sinus rhythm thereafter?

What advantage, if any, can be offered using high-dimension body-surface potential map ECG relative to the two questions above?

The main chapters of this thesis answer these questions using two kinds of ECG, standard 12-lead ECG, and high dimensional body-surface potential map (BSPM) ECG. Direct analysis of the atrial component of the ECG, and indirect analysis of the atrial response via analysis of the ventricular response were both performed.

1.3 ORGANIZATION

In **Chapters 2** and **3**, we provide an introduction to cardiac anatomy and physiology, electrocardiography, and the epidemiology and management of AF. These concepts are important for understanding the origin of the ECG in AF. The thesis continues with its main chapters as follows:

Chapter 4 begins by describing the patient cohort, resulting database, and pre-processing methods used for the 12-lead ECG analysis performed in this thesis. The chapter continues with the calculation of spatiotemporal ECG biomarkers known to be associated with AF disease complexity before and over the course of catheter ablation, and statistically analyzes whether significant changes in their values occur between different ablation steps. The ECG biomarkers measured prior to ablation are compared between patient groups and found to be associated with AF termination by ablation but not with long-term maintenance of sinus rhythm. The results of this chapter demonstrate that ECG biomarkers associated with AF complexity change in value over the course of ablation, therefore showing their potential value as tools to track the progress of ongoing ablation.

1 Introduction

Chapter 5 continues with the analysis of the 12-lead ECG. However, a different approach is taken, in which the ventricular response is analyzed as a proxy for the atrial response. The chapter proposes the use of several heart rate variability (HRV) metrics thought to be correlated with atrial fibrillatory rate, an indicator of AF organization, as well as HRV analysis using recurrence quantification analysis (RQA), thought to be useful for dynamical analysis of physiological time series like the ventricular response in AF. The HRV metrics are calculated prior to and at the end of ablation, to analyze not only whether their pre-ablation values are associated with AF outcome, but also whether changes in the ventricular response can be measured at the end of ablation. The results of this chapter show the promise of HRV metrics to be included as ECG biomarkers indicative of ablation outcomes for persistent AF patients.

Chapter 6 begins with a discussion of the analysis of BSPM signals in the context of AF. The chapter then presents the patient cohort, resulting database, and pre-processing of BSPM signals. The chapter continues with the development of two novel ECG biomarkers for BSPM data, drawing inspiration from signal-processing methods used for both the 12-lead ECG and BSPM. The novel BSPM biomarkers are tested and evaluated for their association with and predictive power of ablation outcomes and compared with other biomarkers suggested in the literature. The results of this chapter show that BSPM biomarkers can be used for AF outcome prediction, but do not clearly answer whether they provide an advantage over 12-lead ECG biomarkers.

Finally, the thesis concludes with **Chapter 7**, which provides a summary of the main findings and contributions of this work, as well as a reflection of its place within the context of current research in the field.

1.4 CONTRIBUTIONS

This thesis is composed of the following papers and articles:

Chapter 4 McCann, A., Vesin, J.-M., Pruvot, E., Roten, L., Sticherling, C., and Luca, A. (2021b). ECG-based indices to characterize persistent atrial fibrillation before and during stepwise catheter ablation. *Frontiers in physiology*, 12:654053.

Chapter 5 McCann, A., Luca, A., Pruvot, E., Roten, L., Sticherling, C., and Vesin, J.-M. (2021a). Ventricular response regularity in atrial fibrillation and its relationship to successful catheter ablation. In *2020 28th European Signal Processing Conference (EUSIPCO)*, pages 910–914. IEEE.

McCann, A., Luca, A., Pruvot, E., Roten, L., Sticherling, C., and Vesin, J.-M. (2023). Heart rate variability analysis in atrial fibrillation for assessing response to catheter ablation. *Physiological measurement*. In submission.

Chapter 6 McCann, A., Luca, A., Pascale, P., Pruvot, E., and Vesin, J.-M. (2022). Novel spatiotemporal processing tools for body-surface potential map signals for the prediction of

catheter ablation outcome in persistent atrial fibrillation. *Frontiers in physiology*, 13:1001060.

During my doctoral studies, I also co-authored the following papers, which do not appear in this document:

Luca, A., Pittet, A., Buttu, A., McCann, A., Vesin, J.-M., Pascale, P., Le Bloa, M., Herrera, C., Park, C.-I., Rollin, A., et al. (2020). Severe and uniform bi-atrial remodeling measured by dominant frequency analysis in persistent atrial fibrillation unresponsive to ablation. *Journal of interventional cardiac electrophysiology*, 59(2):431–440.

Luca, A., Baskaralingam, A., McCann, A., Vesin, J., Pascale, P., Le Bloa, M., Herrera, C., Roten, L., Kuhne, M., Spies, F., et al. (2022). Amplitude of fibrillatory wave correlates with long-term maintenance of sinus rhythm after ablation in persistent atrial fibrillation. *Europace*, 24(Supplement_1):euac053–063.

Pithon, A., McCann, A., Buttu, A., Vesin, J.-M., Pascale, P., Le Bloa, M., Herrera, C., Park, C.-I., Roten, L., Kühne, M., et al. (2021). Dynamics of intraprocedural dominant frequency identifies ablation outcome in persistent atrial fibrillation. *Frontiers in physiology*, 12:731917.

2 CARDIAC PHYSIOLOGY AND ELECTRO-CARDIOGRAPHY

The purpose of this chapter is to give an overview of cardiac anatomy and physiology (Sec. 2.1), including normal heart anatomy and function, and the electrocardiogram (ECG) (Sec. 2.2). These concepts will be necessary to understand the overview of AF given in Chapter 3, as well as to appreciate the ECG signal analysis techniques presented in this thesis.

2.1 CARDIAC ANATOMY AND PHYSIOLOGY

2.1.1 OVERVIEW

The heart is a muscular organ that contracts, or beats, to pump blood through blood vessels of the circulatory system, delivering blood and nutrients to and removing metabolic waste from the body's tissues, organs, and cells. A representation of the human heart and its structures is shown in Fig 2.1. The heart is made up of four chambers: the upper right and left atria, and the lower right and left ventricles. The atria are smaller than the ventricles. All four chambers contract according to carefully timed electrical impulses, with each atrial contraction pumping blood to the ventricles, and with each ventricular contraction pumping blood to the lungs or rest of the body (right and left ventricular contraction, respectively). The right side of the heart pumps oxygen-deficient blood, while the left side of the heart pumps oxygen-rich blood. A healthy heart beats (pumps blood) with a rhythm determined by a group of pacemaker cells that make up a structure called the sinoatrial node (SA node), located in the right atrium (Fig. 2.4). These cells create electrical impulses called action potentials which are conducted to the entire heart, causing it to contract via electromechanical coupling¹. The resulting heart rhythm is called *sinus* rhythm, since it is determined by the sinoatrial node. The rate at which the pacemaker cells generate electrical impulses is controlled by the brain and nervous system, therefore the heart can respond to the body's metabolic needs by slowing the heart rate at rest, and accelerating the heart rate during times of exercise or stress. The heart's pacemaker cells and the electrical impulses they generate will be discussed in more detail in Sec. 2.1.3, but first, an overview of how blood flows through the heart during each heart beat will be discussed in the next section.

¹ *Electromechanical coupling* in the heart refers to the fact that electrical impulses in most types of cardiac cells cause the cell to mechanically contract

2 Cardiac Physiology and Electrocardiography

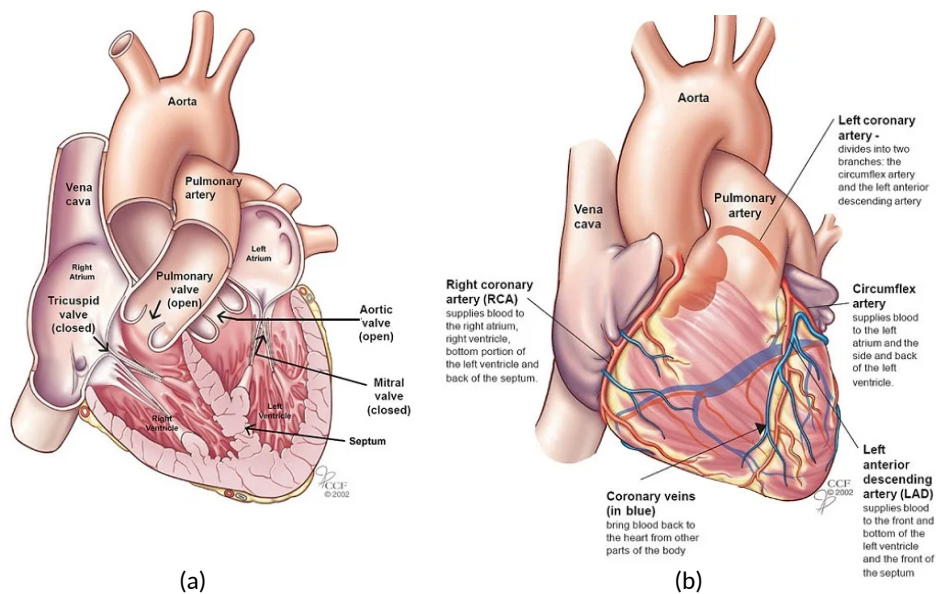


Figure 2.1: **Heart anatomy.** (a) Anterior cross-sectional view of heart. (b) Anterior view of heart. Figure adapted from the Cleveland Clinic.

2.1.2 CARDIAC CYCLE

In this section, the flow of blood throughout the heart during a single beat will be presented. Please refer to Fig. 2.1 for the anatomical structures mentioned. Oxygen-deficient blood from the lower part of the body enters the right atrium through the inferior vena cava, while blood from the upper part of the body enters the right atrium through the superior vena cava. Once filled with blood, the right atrium contracts, its high pressure pushes open the tricuspid valve, and blood flows to the right ventricle. Once filled with blood, the right ventricle contracts (via the same, but delayed electrical impulse that caused the atrium to contract). The high pressure in the contracted ventricle pushes open the pulmonary valve and pumps the oxygen-deficient blood to the lungs, which remove carbon dioxide and replenish the oxygen level in the blood. The oxygen-rich blood from the lungs then enters the left atrium through the four pulmonary veins.² The left atrium contracts, and its resulting high pressure pushes open the mitral valve and pumps blood into the left ventricle. Finally, the left ventricle contracts, pushing open the aortic valve and pumping blood through the aorta, which branches into smaller arteries to deliver blood to all the body's organs and tissues .

It is important to note that the two atria contract at the same time, and the two ventricles contract at the same time. Therefore, while the right atrium is filling with oxygen-deficient blood from the body, the left atrium is filling with oxygen-rich blood from the lungs, and while the right ventricle is pumping oxygen-deficient blood to the lungs, the left ventricle is pumping oxygen-rich blood to the the body. Each atrial and ventricular contraction is controlled by the

²Ectopic pacemaker cells in the pulmonary veins are thought to play an extremely important role in the initiation of atrial fibrillation. These important cells will be discussed further in Chapter 3.

same electrical impulse (beat) created in the sinus node, with the electrical activation and resulting contraction occurring first and simultaneously in the atria, and then after a delay simultaneously in both ventricles.

An important concept which has not yet been discussed is the mechanisms that cause the various chambers of the heart to contract in the coordinated manner discussed above. The contractions of the heart are assured by its electrical conduction system, which will be presented in Sec. 2.1.4. To understand the electrical conduction system as a whole, its building blocks - cardiac action potentials and cardiac cell types - will be discussed in the next section.

2.1.3 ELECTRICITY IN THE HEART

As briefly mentioned, electrical signaling pathways are responsible for coordinating the rapid and sequential activation and contraction of the heart's chambers. To understand the details of these pathways, a brief introduction to the origin and conduction of electrical phenomena in the body, and more specifically the heart, will be given below.

Cells in the body are enclosed by a special *double-phospholipid membrane* about 5 nm thick (Fig. 2.2), separating the intracellular fluid from the extracellular fluid. Both the intra- and extracellular fluids are conducting media, made up of electrolytes. A voltage exists across the cell membrane (transmembrane voltage) because different concentrations of various types of ions (mostly Na^+ , K^+ , and Ca^{2+}) accumulate inside and outside cells. The cell membrane therefore acts as a capacitor, across which a potential difference, called a *resting membrane potential* of about -90 mV, measured as the intracellular potential minus the extracellular potential when the cell is at rest, exists. Nerve and muscle cells (skeletal, heart, and smooth) are *electrically excitable* in the sense that they can selectively change their membrane conductivities to Na^+ , K^+ , and Ca^{2+} , thereby altering the ion concentrations on either side of the membrane, and causing the transmembrane voltage to deviate from the resting membrane potential. *Depolarization* refers to an increase in the transmembrane voltage (more positive voltage), while *hyperpolarization* refers to a decrease in the transmembrane voltage (more negative voltage). Changes in transmembrane voltage are caused by electrical or chemical stimuli that modify the properties of ion channels and ion pumps embedded in the cell membrane (Fig. 2.2). Ion pumps guarantee proper ion concentration gradients across the cell membrane. They require energy to function, since they pump ions against their electrical gradient. Ion channels selectively allow the passive diffusion of ions down their electrical gradient but can be opened or closed in response to stimuli. Both ion pumps and ion channels are protein macromolecules.

If a nerve or muscle cell, in response to an electrical or chemical stimulus depolarizes up to a voltage called the *threshold potential* of about -60 mV, this causes a very rapid and irreversible increase in the transmembrane voltage (depolarization), which overshoots to positive values before returning to the resting membrane potential (repolarization). When the transmembrane voltage is plotted versus time, this phenomenon resembles an electrical

2 Cardiac Physiology and Electrocardiography

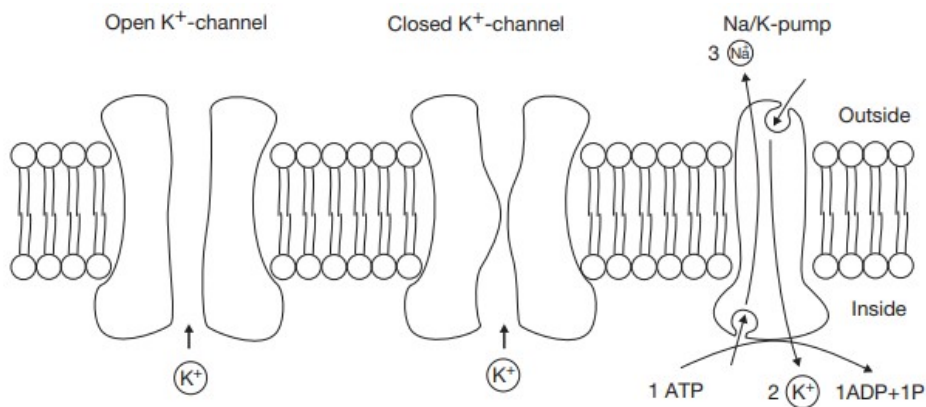


Figure 2.2: **The excitable cell membrane.** Phospholipid double layer with examples of protein macromolecules: opened K^+ channel, closed K^+ channel, and active Na $^+$ -K $^+$ pump. Figure adapted from Werner (2014).

impulse that is called an *action potential*, a generalized example of which is shown in Fig. 2.3. Cells which can generate action potentials are said to be *electrically excitable*. The impulse width of the action potential is about 1 ms for nerve cells, 5 ms for skeletal muscle cells, and 250 ms for heart muscle cells. The transient depolarization and repolarization are triggered either by external mechanisms, such as motor nerve stimulation of skeletal muscle, or cell-to-cell depolarization in the heart, or by intracellular, spontaneous mechanisms, such as occurs in cardiac pacemaker cells. Conserved propagation of action potentials from cell to cell is what constitutes the transmission of electrical signals in the body. The mechanisms which drive the rapid changes in transmembrane voltage that occur during cardiac action potentials will be discussed in the next section.

Cardiac action potentials

Action potentials occur in all cardiac cells, but take one of two forms depending on which type of cardiac cell generates them. *Cardiac pacemaker cells* display automaticity, depolarizing and discharging an action potential spontaneously without external stimuli. All other *cardiac muscle cells* must receive a triggering electrical impulse, such as the action potential from a neighboring cell, to generate an action potential. The form of each type of action potential, and the associated underlying ionic mechanisms, are shown in Fig. 2.4.

Cardiac pacemaker cells that make up the SA node and other secondary pacemakers in the heart have no true resting potential. Instead, immediately following repolarization, Na $^+$ current begins leaking into the pacemakers cells and increasing their transmembrane voltage. This inward current is referred to as Phase 4 and is shown in green in Fig. 2.4a. Once the threshold potential is achieved, voltage-gated Ca $^{2+}$ channels open, and the inward Ca $^{2+}$ current triggers complete depolarization of the cell. Finally, K $^+$ channels open, this time resulting in an outward K $^+$ current, resulting in the cell's repolarization. The cycle then repeats itself and

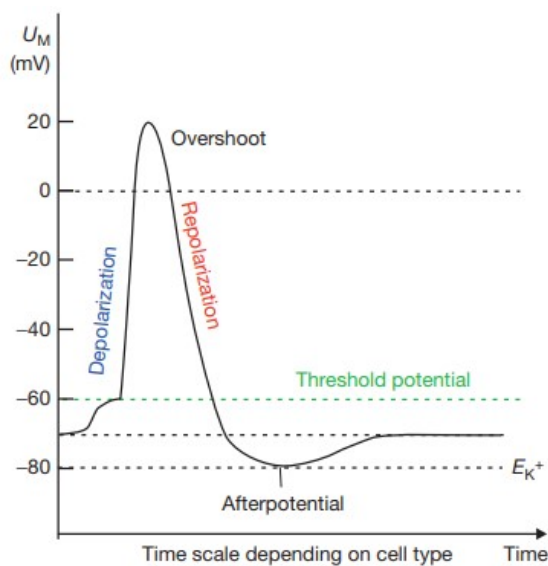


Figure 2.3: **Action potential generation.** Figure adapted from Werner (2014).

Na^+ again begins leaking into the cell, explaining the automaticity of pacemaker cells.

All other cells making up the atrial and ventricular myocardium (contractile muscle cells) display a different form of action potential. These cells remain at a true resting potential of around -90 mV, referred to as Phase 4 and shown in red in Fig. 2.4b. They must be stimulated via an incoming impulse from a neighboring cell to reach the threshold potential. Once the threshold potential is reached, fast Na^+ channels open causing a rapid inward current that depolarizes the cell (Phase 0), reaching a maximum membrane voltage of about 20 mV. The opening of K^+ channels causes a brief outward current, generating a brief early repolarization (Phase 1). Following the early repolarization, a plateau phase is caused by the opening of Ca^{2+} channels (Phase 2) at about the same time as the opening of the K^+ channels, resulting in a steady inward current that maintains a positive transmembrane voltage for a relatively long duration, allowing the majority of the myocardium to contract simultaneously. Finally, repolarization (Phase 3) occurs when Ca^{2+} channels close and K^+ channels open, resulting in an outward current. The cell returns to its resting phase (Phase 4) until it is triggered by a new incoming stimulus.

For most of the action potential, myocardial cells are *absolutely refractory* to stimulation, meaning that even if another stimulus were to arrive, the cell could not generate a new action potential (Fig. 2.5). A *relative refractory period* follows the absolutely refractory period, during which time a strong stimulus may trigger a new action potential. The relative refractory period has clinical implications which will be discussed in a later part of the chapter.

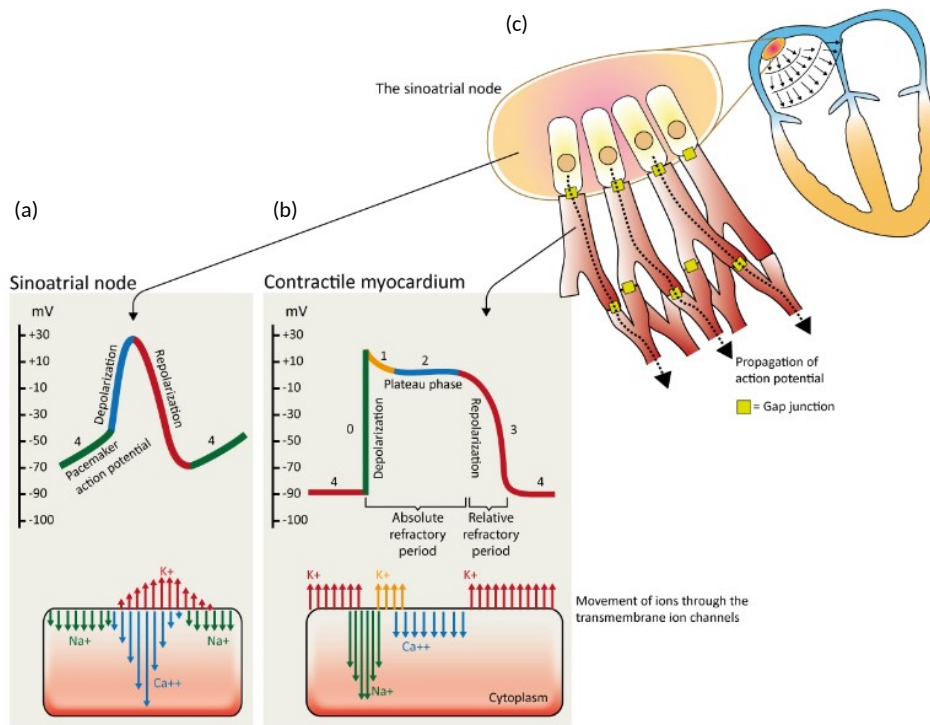


Figure 2.4: **Cardiac action potentials.** (a) The action potential of the pacemaker cells of the SA node is shown in the first panel and includes no true rest phase due to the spontaneous leakage of Na^+ current into the cell. (b) The action potential of contractile myocardial cells is shown in the second panel, and includes a plateau phase (Phase 2) due to incoming Ca^{2+} currents and a true rest phase (Phase 4). (c) Depiction of SA node in the heart and outward propagation of action potential. Figure adapted from Verma et al. (2015).

Cardiac cell types and architecture

Apart from the pacemaker and non-pacemaker cell distinction in the heart, there is another important distinction between two types of cells in the heart. *Conduction cells*, as part of the heart's specialized electrical conduction system (discussed in the next section) have fast conduction velocity and exist only to propagate the action potential to the contractile myocardium, via fiber networks that extend into the myocardium. These cells do not contribute to contraction of the heart. *Contractile myocardial cells* make up the vast majority of cardiac cells. These muscle cells are capable of transmitting the action potential, but at a much lower speed than conduction cells. However, importantly, these cells contract in response to the action potential, thus contributing to the entire heart's coordinated contraction. Depolarization activates these myocardial cells such that cellular processes are induced that cause the cell to contract. This direct link between the spread of an electrical impulse and a mechanical event in the form of cell contraction is called electromechanical coupling. It is during the plateau phase of the contractile myocardium cells (Phase 2 in Fig. 2.4b) that the cells contract. Because this phase is long, and the electrical impulse is efficiently transmitted to nearly all

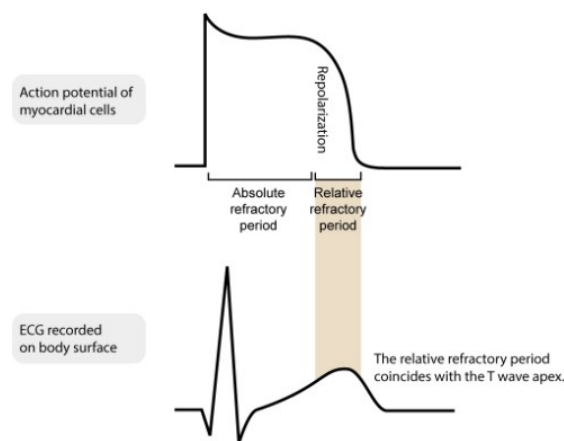


Figure 2.5: **Excitable cell refractory period.** Absolute and relative refractory periods during the cardiac action potential. Figure adapted from ECG & Echo Learning (2022).

parts of the heart simultaneously, and the cells contract almost simultaneously, contributing to the heart's efficient pumping mechanism. The long duration of the cardiac action potential and refractory period ensure that one action potential can produce only a single contraction followed by relaxation, in accordance with the heart's function of pumping blood to the body using synchronized pulses.

Cardiac cells are long and display a branch-like morphology (Fig. 2.4)c. They are connected along their long axis via *intercalated disks*, which are composed of cell membrane proteins. Some of these proteins form channels between the cells called *gap junctions* (yellow squares in Fig. 2.4c) through which electrically charged ions can flow, thus connecting adjacent cells electrically. This is how action potentials are propagated from one cell to the next. The cell architecture allows the network of cells to function as one unit. In Fig. 2.4c, the way in which conduction cells can be interconnected with contractile cells is shown. The next section will elaborate the specialized parts of the heart's *electrical conduction system* that contribute to the rapid conduction of electrical activation throughout the heart.

2.1.4 ELECTRICAL CONDUCTION SYSTEM

As discussed in Sec. 2.1.2, the atria and ventricles work together, alternately contracting and relaxing to create the pressure changes that pump blood through the heart and to the body. The atria and ventricles must be activated rapidly and sequentially for this to work properly. Rapid activation is important in order to activate as much of the myocardium simultaneously as possible. The heart pumps blood most efficiently when all myocardium cells of either the atria or ventricles contract at the same time. Sequential activation is necessary so that the atria contract before the ventricles and can fill them with the correct volume of blood before ventricular contraction. This rapid and sequential activation is coordinated by the heart's *electrical conduction system*, shown in Fig. 2.6a. This system is composed of special

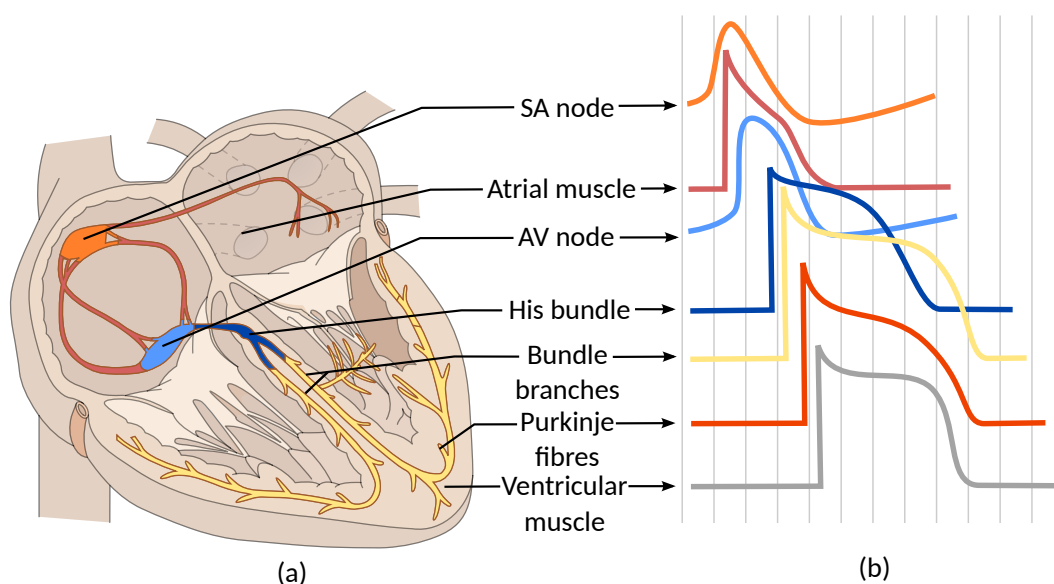


Figure 2.6: **Electrical conduction system of the heart.** (a) Parts of the electrical conduction system of the heart. (b) The form, duration, and timing of action potentials associated with each type of cardiac conduction and contractile cell. Figure adapted from ECG & Echo Learning (2022).

myocardial cells, called conduction cells, which have no contractile function and act only to spread action potentials to the contractile myocardium cells in the atria and ventricles, as discussed in Sec. 2.1.3. The parts of the electrical conduction system shown in Fig. 2.6a, and their role in coordinating the cardiac cycle, will be briefly enumerated below, following the natural order of the spread of action potentials within the heart. Also shown in Fig. 2.6b are the forms and relative duration and timing of the action potentials generated by the different types of conduction cells and contractile cells within the heart.

The sinoatrial node

The sinoatrial node (SA node) is a small oval structure located near the entrance of the superior vena cava in the right atrium. The SA node is made up of specialized cells that display automaticity, that is, they can depolarize and discharge an action potential spontaneously as discussed in Sec. 2.1.3. The SA node is referred to as the heart's primary or natural pacemaker, with an intrinsic rate discharging about 70 beats per minute³. The intrinsic rate of spontaneous

³Note, the heart also contains secondary (latent) pacemakers in parts of the atrial myocardium, myocardium near the AV node, and the His-Purkinje network. However, these pacemakers have a lower intrinsic rate than the SA node, thus the SA node dominates by depolarizing before secondary pacemakers and resetting them before they can discharge their own action potential. Additionally, parts of the heart can display ectopic automaticity and become abnormal pacemakers, which plays a role in the initiation of atrial fibrillation. This will be discussed in detail in Chapter 3

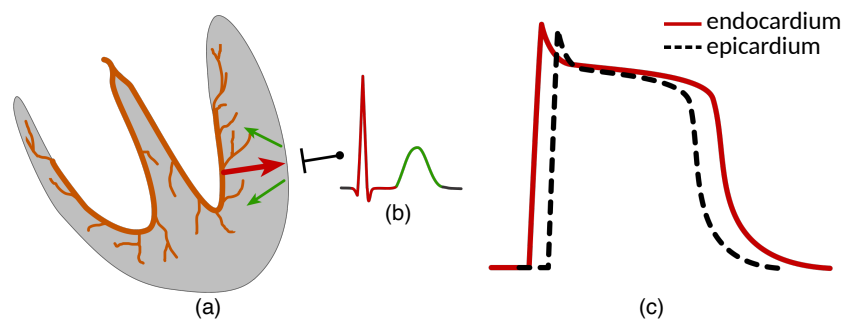


Figure 2.7: Ventricular wall activation. (a) Ventricular activation spreads from the endocardium, in contact with the heart's conduction system, to the epicardium (red arrows). Repolarization spreads in the opposite direction, from the epicardium to the endocardium (green arrows). (b) The resulting electrocardiogram traced during ventricular activation (red) and repolarization (green). (c) Repolarization occurs in the opposite direction to activation since the duration of the action potential, traced as a dashed black line, is shorter in epicardial cells, so repolarization begins there and spreads back to the endocardium, whose longer duration action potential is traced in red. Figure adapted from Klabunde (2019).

depolarization in the SA node can be modified by the autonomic nervous system⁴, increasing the rate via sympathetic stimulation dominates during physical exercise and at times of stress, or decreasing the rate during rest.

Impulse transmission

The cells of the conduction system do not have contractile function and serve only to spread the depolarization rapidly and sequentially to contractile myocardium cells. However, the conduction cells are only in direct contact with part of the contractile myocardium. Therefore, the contractile cells which are not in direct contact with conduction cells receive the traveling impulse via myocardium cell-to-cell transmission, which is significantly slower than transmission through conduction fibers (about 0.5 m/s). This effect can be seen in the activation and contraction of the ventricular wall muscle. The specialized conduction fibers extend into the endocardium of the ventricular walls but not beyond a third of the wall thickness. Therefore, activation and contraction start in the endocardium and spread via slower myocardium cell-to-cell transmission to the epicardium (Fig. 2.7).

Atrial impulse transmission

While the atria do not contain the specialized and distinct conduction structures found within the ventricles, there is some evidence that distinct conduction fiber bundles exist, and a structure called the Bachmann's bundle conducts the impulse from the right to left atrium.

⁴The *autonomic nervous system* is a component of the peripheral nervous system that regulates involuntary physiologic processes including heart rate, blood pressure, respiration, digestion, and sexual arousal. It contains three anatomically distinct divisions: sympathetic, parasympathetic, and enteric.

Otherwise, the atria rely on myocardial cell-to-cell transmission to spread the impulse (0.5 m/s).

Atrioventricular node

Conduction of the depolarization wave from the atria to the ventricles is mostly blocked by a fibrous barrier of nonexcitable cells, and is only possible via a structure called the atrioventricular node (AV node). Conduction across the specialized fibers of the AV node is about 10 times slower (0.05 m/s) than conduction in the atrial myocardium, owing to properties of specialized AV node fibers. These fibers have a smaller diameter, and their depolarization is largely governed by slower Ca^{2+} channels, as opposed to the fast Na^{+} channels. Additionally, the AV node has a low density of gap junctions.⁵ The transmission delay, about 100 ms, allows the atria to complete their contraction and fill the ventricles completely with blood before ventricular contraction begins.

The His bundle, bundle branches, and Purkinje fibers

The AV node is connected to the His bundle, which itself splits into the left and right bundle branches that line the ventricular septum. Both the His bundle and bundle branches have fast impulse conduction velocity (2 m/s). The bundles branch into smaller bundles and ultimately to the Purkinje fibers. These fibers transmit the impulse very quickly (4 m/s) and extend into the ventricular myocardium where they deliver the depolarizing impulse to contractile myocardium cells. Therefore, activation starts in the endocardium and spreads toward the epicardium as shown in Fig. 2.7. The fast impulse transmission allows the ventricular myocardium to be activated and then contract simultaneously, contributing to efficient pumping. The parts of the heart's electrical conduction system and contractile myocardial cells are summarized in Table 2.1.

2.2 ELECTROCARDIOGRAPHY

Electrocardiography is the process of recording the heart's electrical activity. The excitatory and conductive processes which produce waves of depolarization and repolarization within the heart (the heart's electrical activity) may be analyzed using electrical signals, recorded either with electrodes placed directly in the heart (intracardiac electrogram), or with electrodes placed on the body surface. The potential difference between two electrodes placed on the body surface generates a trace of heart activity in the form of voltage versus time called the electrocardiogram (ECG). For example, Fig 2.8b shows the ECG trace associated with lead II, which is the difference in potential recorded by an electrode placed on the left leg and right arm. These two electrodes are indicated by black arrows in Fig 2.8a. The study of ECG

⁵The slow conduction has extremely important physiological implications. In atrial fibrillation, the AV node protects the ventricles from the extremely high atrial rate.

Table 2.1: Conduction of electrical impulses in the heart.

Structure	Function
Sinoatrial Node	Heart's natural pacemaker. Spontaneous action potential generation produces a wave of depolarization which spreads to the atria.
Atrial muscle	Wave of depolarization quickly spreads to both atria via contractile cell-to-cell transmission (0.5 m/s), producing coordinated atrial contraction.
Atrioventricular node	Normal pathway for depolarization wave to spread from atria to ventricles. Slows wave propagation (0.05 m/s), introducing a delay and allowing atria to contract and fill ventricles with blood before they can contract.
His bundle	Speeds up conduction to ventricular muscle (2 m/s).
Bundle branches, Purkinje fibers	Continue fast spread of depolarization wave to septum (bundle branches - 2 m/s) and to ventricular wall endocardium (Purkinje fibers - 4 m/s)
Ventricular muscle	Wave of depolarization spreads from endocardium to epicardium via contractile cell-to-cell transmission (0.5 m/s), producing coordinated ventricular contraction.

biomarkers for treatment planning in AF is the backbone of this thesis, therefore, the ECG will be discussed in detail below. While intracardiac electrogram analysis was performed during this thesis, it did not lead to any significant contributions; therefore, it will not be discussed.

2.2.1 ELECTROCARDIOGRAM

It is possible to place electrodes on the body surface and measure cardiac potentials because the body acts as a volume conductor of the electrical currents generated by the heart. Time-dependent changes in potential differences recorded between electrodes at two points on the body surface are essentially determined by the spread of electrical excitation within the heart and the resulting changes in the electric field in surrounding body tissue.

The recorded trace of how the voltage changes with time between two recording electrodes placed at different positions on the body surface is called the electrocardiogram (ECG). The ECG represents a global view of the underlying electrical activity in the heart. The form of the ECG depends on the relative positions of the electrodes and which electrode is taken as the reference electrode. Usually, several electrodes are used, and different pairs of electrodes are taken to record different views of the heart. Each trace that is generated by taking the difference of these pairs of electrodes is called a lead. For example, lead II of the 12-lead ECG (to be discussed in more detail at the end of this chapter) is formed by taking the potential

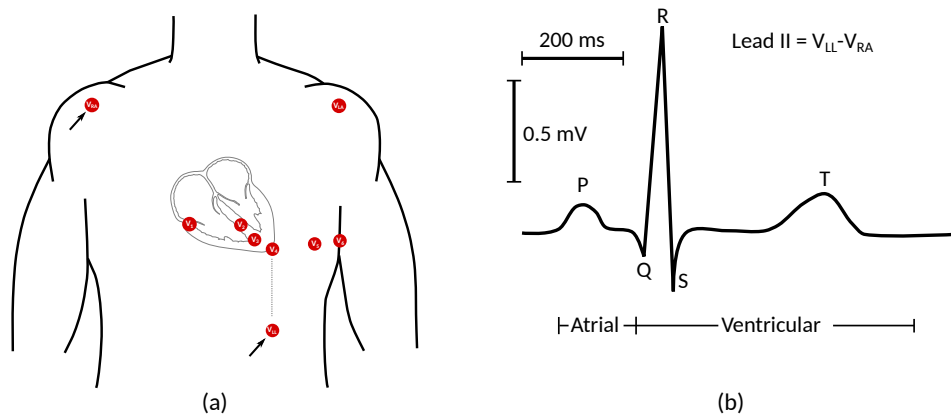


Figure 2.8: Electrocardiogram. (a) Red dots indicate standardized electrode positions to record the 12-lead ECG. Note one “ground” electrode is also placed on the right leg and is not shown. The left leg and right arm electrodes used to form lead II are indicated by black arrows. The left leg electrode should in reality be placed at the hip bone just below the navel. (b) The resulting lead II waveform, corresponding to one normal heartbeat. Figure inspired by Macfarlane et al. (2010) and Yoo (2014).

difference between recordings from electrodes placed at the left leg and the right arm:

$$II = V_{LL} - V_{RA} \quad (2.1)$$

where V_{LL} is the potential recorded by the electrode (positive, or exploring electrode) placed on the left leg, and V_{RA} is the potential recorded by the electrode (negative, or reference electrode) placed on the right arm (indicated by black arrows in Fig. 2.8a). The trace shown in Fig. 2.8b demonstrates a typical lead II ECG recording associated with one heartbeat. Different electrode configurations used for recording the ECG will be discussed at the end of the chapter. The objective of the remainder of this section is to (1) first describe the details behind why recording the ECG is possible; (2) describe the link between the electrical processes occurring within the heart, and the resulting waveforms recorded by the ECG; (3) describe various electrode configurations used for recording ECG.

Origin of the electrocardiogram

Recording electrical cardiac activity using electrodes placed on the body surface is possible because the waves of depolarization and repolarization passing through the atria and ventricles cause electric currents to flow outside the myocardium. Since the heart is surrounded by conducting body tissues and fluids, despite the torso-air boundary at the body surface, the changing electric fields set up by electric cardiac sources are still perceptible at electrodes placed on the body surface, and therefore electric potential differences can be recorded between electrodes. It is important to note that at any given point in time, there are many

separate waves of depolarization or repolarization traveling in different directions relative to the fixed positions of the body surface electrodes. The instantaneous amplitude of the measured potential on each electrode depends on its orientation relative to the instantaneous direction and magnitude of the sum of all the underlying individual depolarization waves. This sum is called the *mean electrical vector*. Therefore, the amplitude and direction of the potential difference recorded between two electrodes depends heavily on the alignment of the two electrodes relative to both the heart and to each other.

To understand how the electric fields are created, consider what happens in the extracellular space during the fundamental unit of cardiac activation: the propagation of an action potential across a single cardiac muscle cell placed in a homogeneous conducting medium, with recording electrodes at each of its ends (Fig. 2.9). Before depolarization, the transmembrane voltage along the length of the cardiac fiber is at the resting transmembrane potential of about -90 mV, therefore, no currents flow along the surface of the cell and no potential difference exists between the two electrodes (Fig. 2.9a). If an electrical stimulus enters the cell at its left side (Fig. 2.9b), it effectively discharges the transmembrane capacitance and depolarizes the membrane above the threshold level, leading to a complete depolarization. However, because cardiac cells are long, the different ends of the stretched muscle fiber (the partially depolarized region where the excitation wave is passing and Na^+ currents are entering and the fully polarized region still ahead of the advancing action potential) will be at different electric potentials. At the left electrode, the outside of the cell appears to have a negative potential with respect to the inside of the cell, while at the right side of the cell, the outside of the cell has a positive potential with respect to the inside of the cell. Therefore, a potential difference exists between the positive and negative electrodes. This results in a large intracellular axial current that carries the impulse propagation. These processes occur within the membrane because of its ability to change conductivities in an ion-selective manner, resulting in relatively positive potentials in the extracellular space near the current source (left side of the cell) and relatively negative potentials near the current sink (right side of the cell). Similarly, during repolarization (Fig. 2.9c), the left hand side of the cell returns first to the resting membrane potential while the right hand side is still depolarized. Therefore, positive charges collect at the outer surface of the cell near the negative electrode, and negative charges collect near the positive electrode, resulting in a negative voltage between the two electrodes.

The relationship between a passing depolarization or repolarization wave can be summarized as follows. A wave of net depolarization travelling toward a positive electrode results in a positive deflection in the ECG trace, while a wave travelling away from a positive electrode results in a negative deflection. A wave of net repolarization travelling toward a positive electrode results in a negative deflection, while a wave of repolarization travelling toward a negative electrode results in a positive deflection. Finally, a depolarization or repolarization wave travelling perpendicular to the line formed by connecting two electrodes results in no net deflection. Since the myocardium has a large number of fibers each with different lengths, thicknesses, spatial directions, and excitatory states, the mean electrical vector associated with a depolarization or repolarization wave is found by summing the contributions of the

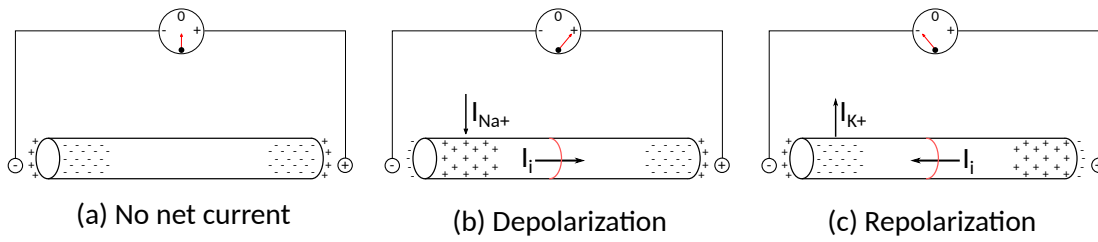


Figure 2.9: Single cell conduction. (a) Cell at rest, no potential difference between two electrodes. (b) Entering electrical stimulus results in depolarization first at left hand side of cell, while the right hand side is still polarized, which causes the flow of an intracellular action potential current I_i and creates a positive potential difference between the two electrodes. (c) The left hand side of the cell repolarizes first while the right hand side is still depolarized, resulting in a negative potential difference between the two electrodes.

individual cells.

The normal surface electrocardiogram

Extending the propagation of an action potential in a single cell with two recording electrodes at each end to the recording of the changing excitatory state of the heart using two electrodes placed on the body surface, the recorded trace, with its series of deflections, corresponds to the sequential activation of different parts of the myocardium. Figure 2.10b demonstrates the typical deflections seen during one cardiac cycle on lead II of the 12-lead ECG, along with the underlying mean electrical vectors associated with activation of the different parts of the atrial and ventricular myocardium. As mentioned, lead II takes the left leg as the positive electrode, and the right arm as the negative electrode (Eq. 2.1). Therefore, the electrodes are approximately positioned in relation to the heart as shown in Fig. 2.10a. Conduction begins at the heart's dominant pacemaker, the SA node and spreads to the atrial myocardium towards the AV node (purple arrow in Fig. 2.10). The coordinated electrical activation of the atrial myocardium produces the P wave on lead II of the ECG. The P wave is followed by an isoelectric line during which time the AV node and other components of the electrical conduction system are activated, however, the associated electric field changes cannot be seen on ECG due to their small amplitude. This is followed by activation of the ventricular myocardium, first from the left septum wall to the right septum wall (blue arrow in Fig. 2.10a), resulting in the negative Q deflection, however, the activation of the large left ventricular wall, with the depolarization wave travelling from endocardium to epicardium (orange arrow in Fig. 2.10a), results in a large positive deflection called the R wave, which returns to the negative S wave as the upper parts of the ventricular walls are activated. The relatively long segment between the S deflection and the T wave is the time in which the ventricles mechanically contract. Finally, the T wave is the result of ventricular repolarization. The T wave on lead II is also positive, because the repolarization wave starts first in the epicardium and travels to the endocardium, shown as the green arrow in Fig. 2.10a. This means the repolarization wave travels away from the positive electrode and toward the negative electrode, resulting

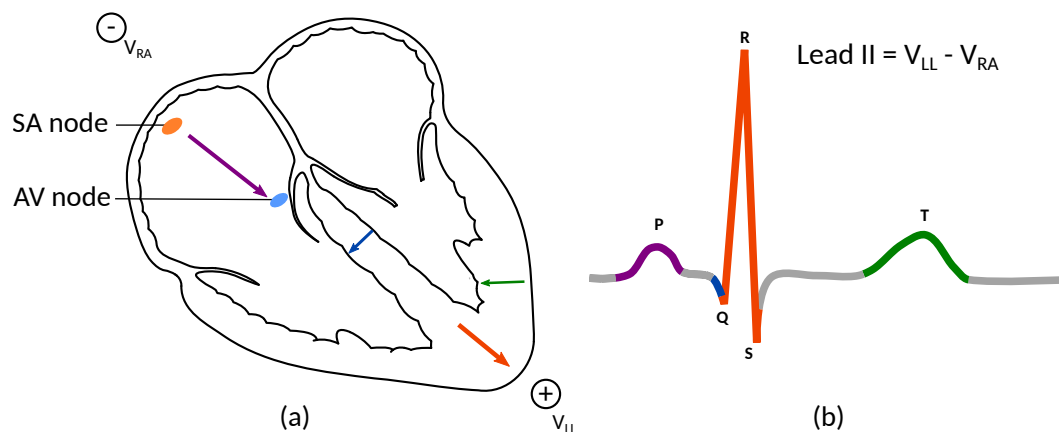


Figure 2.10: **Cardiac activation and ECG waveforms.** (a) Spread of depolarization (purple, blue, and orange arrows) and repolarization (green) waves in the heart. (b) Corresponding deflections on ECG. The P wave corresponds to atrial myocardium activation, while the QRS complex results from ventricular myocardium activation. The T wave results from ventricular repolarization. Atrial repolarization is masked on ECG by the much larger QRS complex.

in a positive deflection on lead II. Note that the signal associated with atrial repolarization is masked by the QRS complex of the much larger ventricles. The series of deflections presented in Fig. 2.10b therefore represent the underlying cardiac activity as seen by lead II of the ECG for one cardiac cycle.

2.2.2 LEAD SYSTEMS

As already mentioned, an ECG electrode is a conductive pad that is attached to the skin to record electric potential resulting from underlying cardiac activity. An ECG lead is a trace showing electrical activity of the heart and is obtained as the difference between the potential recorded at two or more electrodes. An ECG machine, or electrocardiograph, compares, amplifies, and filters the potentials recorded by the electrodes, and presents the result as electric potential differences (leads) between the electrodes, generating a trace of voltage versus time either on a screen or recording paper (Fig. 2.11).

Several standardized configurations of recording electrodes for ECG exist. By far the most common in clinical practice is the standard 12-lead ECG, recorded using 10 electrodes. In ambulatory situations, a Holter monitor, which uses two or three electrodes, may be used. Finally, high density body surface potential mapping systems use tens or hundreds of electrodes covering the entire torso. These lead systems will be elaborated below.

12-lead ECG

As mentioned, the standard 12-lead ECG is extremely common in clinical practice for analyzing heart health and diagnosing cardiac illnesses like atrial fibrillation, which will be discussed

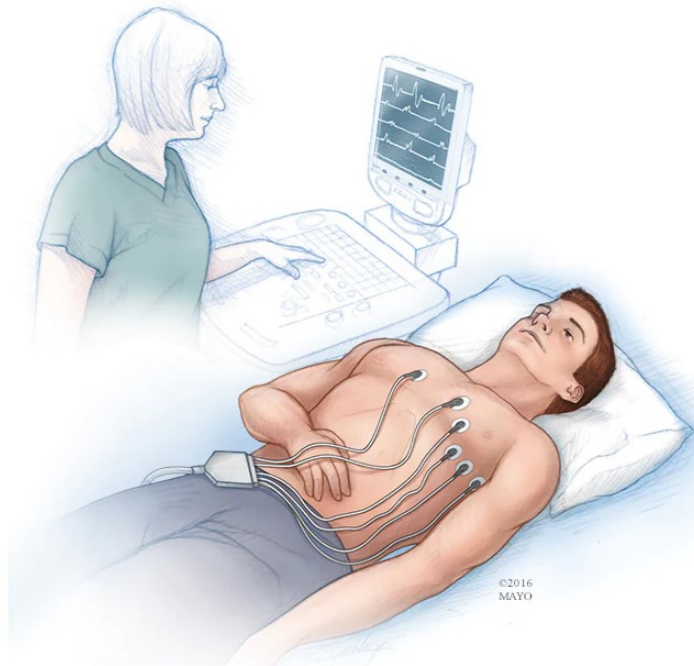


Figure 2.11: **Recording ECG.** To record an ECG, electrodes are placed on the chest to record the heart's electrical signals. The signals are shown on a screen or recording paper as waves formed by leads, or potential differences between different pairs of electrodes. Figure adapted from the Mayo Clinic.

in more detail in Sec. 3.4. The 12 leads are obtained using 10 electrodes (whose positions are shown in Fig. 2.8a) and consist of *limb* leads and *chest* or *precordial* leads. Three leads, the limb leads, are simply found by comparing electric potentials recorded by two electrodes placed on either the left arm, V_{LA} , right arm, V_{RA} , or left leg, V_{LL} :

$$\begin{aligned} I &= V_{LA} - V_{RA} \\ II &= V_{LL} - V_{RA} \\ III &= V_{LL} - V_{LA} \end{aligned}$$

The remaining leads compare an exploring (positive) electrode with a reference (negative) electrode that is actually a combination of two or three electrodes. These include the augmented limb leads, defined as the potential difference between one limb electrode and the mean of the two remaining limb electrodes:

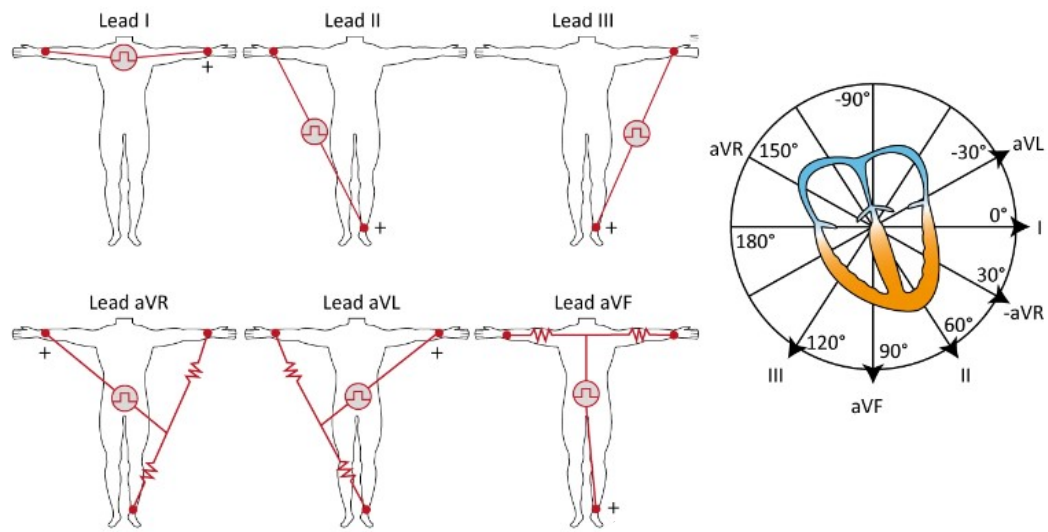


Figure 2.12: **The limb leads.** The limb leads are used primarily to detect electrical activity in the frontal plane. Each lead “views” the heart from the angle of its exploring (positive) electrode. Shown in the right panel is the coordinate system giving the angle from which each lead observes the heart. Figure adapted from ECG & Echo Learning (2022).

$$aVR = V_{RA} - (V_{LA} + V_{LL})/2$$

$$aVL = V_{LA} - (V_{RA} + V_{LL})/2$$

$$aVF = V_{LL} - (V_{LA} + V_{RA})/2$$

The letter **a** stands for **augmented**, **V** for **voltage**, **R** for **right arm**, **L** for **left arm**, and **F** for **foot**. The limb leads, shown schematically in Fig. 2.12, have both the exploring and reference electrode placed in the frontal plane, therefore they are useful for detecting mean electrical vectors travelling in this plane. For example, lead I takes its exploring electrode to be on the left arm and its reference electrode to be on the right arm, therefore, a mean depolarization vector moving from right to left should yield a positive deflection in lead I, and lead I defines 0° in the frontal plane in the coordinate system presented in the right panel of Fig. 2.12, meaning lead I “views” the heart from an angle of 0°, or it “views the lateral wall of the left ventricle.” Similar principles can be applied for lead II and lead III. For the augmented limb leads, take for example lead aVF, which has its exploring electrode on the left leg and its reference electrode is the average of the two arm electrodes, yielding a reference directly above the left leg electrode. A mean depolarization vector moving downwards should yield a positive wave in lead aVF. Therefore, lead aVF views the heart’s electrical activity from an angle of 90°, or it “views the inferior wall of the left ventricle.”

The six chest, or precordial leads, are obtained by comparing the potential recorded at six

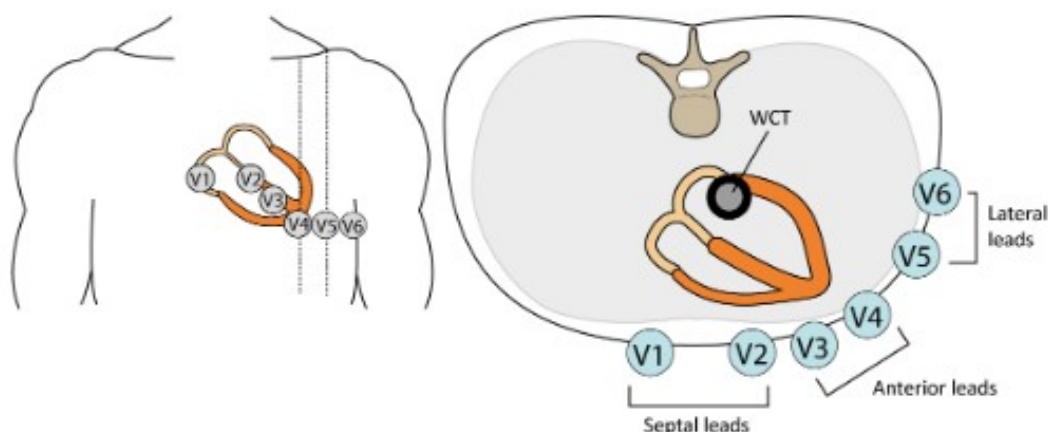


Figure 2.13: **The chest (precordial) leads.** The chest leads are used primarily to detect electrical activity in the horizontal plane between WCT and the six exploring electrodes placed on the chest anterior wall. WCT = Wilson's central terminal. Figure adapted from ECG & Echo Learning (2022).

exploring electrodes placed on the chest near the heart to a reference “electrode” which is taken as the average of the three limb electrodes, called Wilson's central terminal (WCT):

$$WCT = \frac{V_{LA} + V_{RA} + V_{LL}}{3}$$

Wilson's central terminal is an artificially constructed reference that is assumed to be a steady and near zero amplitude during the cardiac cycle. This terminal is a theoretical reference point located approximately in the center of the thorax, or in the center of Einthoven's triangle. WCT serves as the reference point for each of the six electrodes which are placed on the anterior part of the chest wall (Fig. 2.13), and the chest leads, $V_1 - V_6$, are derived by comparing the potentials recorded by the six chest electrodes to the averaged WCT potential. Each chest lead provides unique information that cannot be derived mathematically from the other leads. The chest leads primarily observe vectors moving in the *horizontal plane*, since both the exploring and reference electrode are positioned in that plane. Leads V_1 and V_2 reflect the activity of the ventricular septum and occasionally right ventricular wall, leads V_3 and V_4 reflect the activity of the left ventricular anterior wall, and V_5 and V_6 reflect the activity of the left ventricular lateral wall.

The 12 leads are presented according to their anatomical angles in Fig. 2.14 (Cabrera format). Note that lead -aVR is shown rather than aVR. Lead aVR may be flipped to instead view -aVR to fill the gap between leads I and II in the coordinate system, and improve diagnostics of certain conditions (Menown and Adgey, 2000). Note that none of the leads in the 12-lead ECG are adequate to observe vectors of the right ventricle.

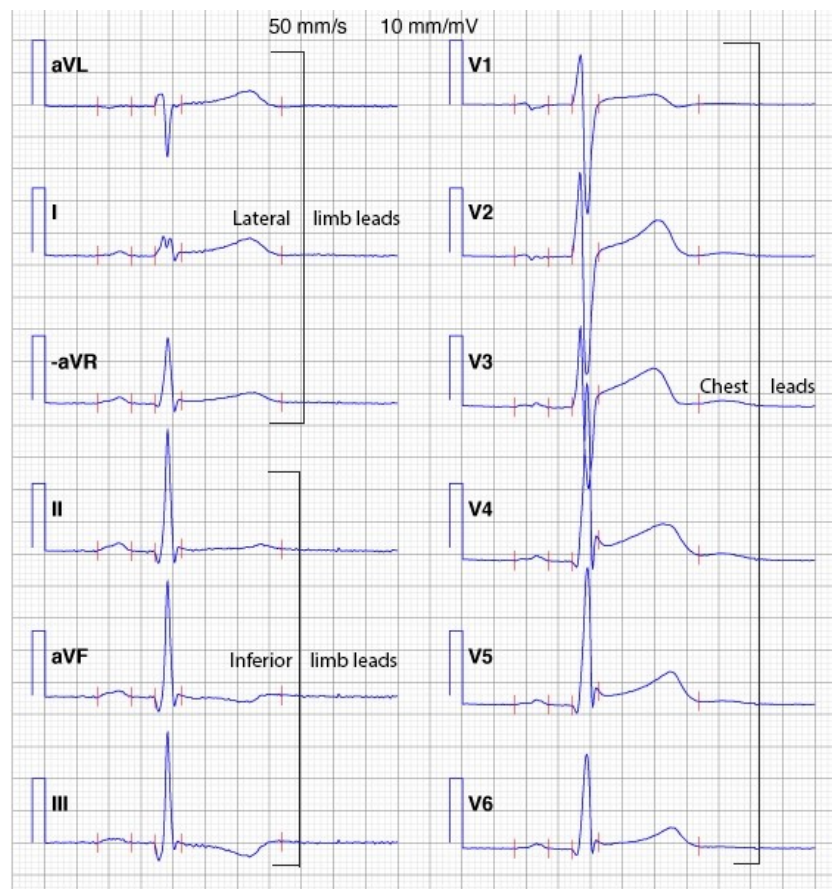


Figure 2.14: **Presentation of the 12-lead ECG.** Traces of all 12 lead shown according to their anatomical positions (Cabrera format) and lead aVR inverted to -aVR. Figure adapted from ECG & Echo Learning (2022).

Body-surface potential mapping

While the 12-lead ECG is by far the most widely used ECG technique in clinical practice, it has been suggested that its electrode placement may not be optimal for diagnosing acute coronary syndromes like acute cardiac ischemia and myocardial infarction, since the coverage of the standard chest leads over the thorax is limited (Aetna Inc., 2022). It has been suggested that the use of additional electrodes covering the entire torso, called body surface potential mapping (BSPM), could be advantageous for diagnosing and analyzing various cardiac diseases.

While extremely useful, the 12-lead ECG provides only a low resolution projection of cardiac activity on the body surface. Electrocardiogram systems using tens or hundreds of electrodes covering the entire torso in the form of a vest or grid have been developed, and are often called body surface potential mapping (BSPM) systems. These systems use 64, 128, 252, or more electrodes to record and measure electrical cardiac activity over a much larger portion of the torso than the traditional 12 lead ECG, to provide a comprehensive 3-D picture of the effects of electrical currents from the heart on the body surface. The use of BSPM is not

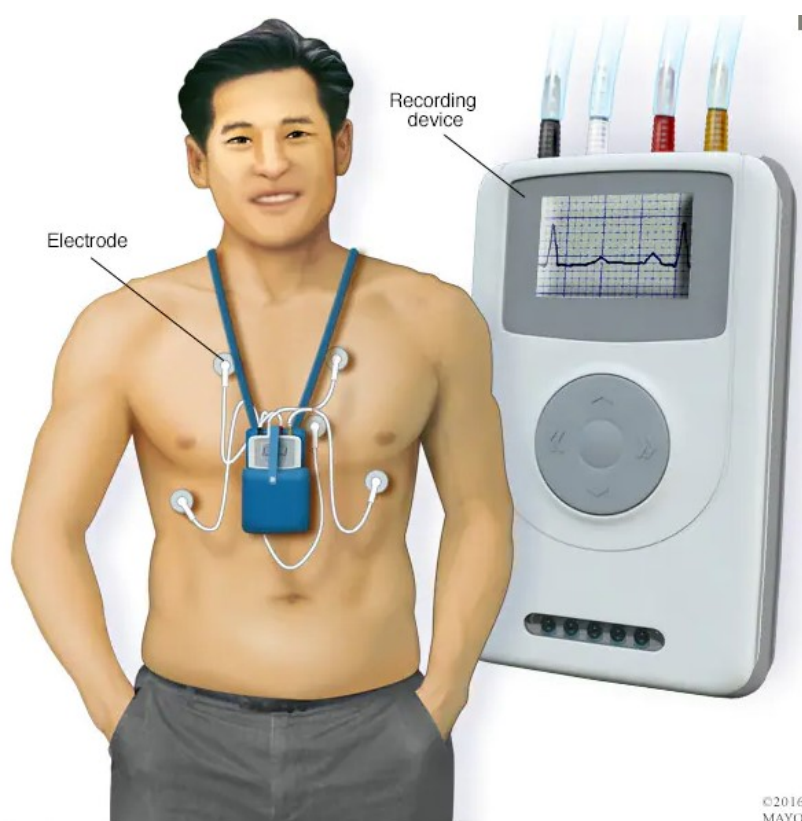


Figure 2.15: **Holter monitor.** A Holter monitor uses electrodes and a recording device to track the heart's rhythm for 24 up to 72 hours. Figure adapted from Mayo Clinic (2022).

mentioned in official guidelines for management of patients with heart disease, myocardial infarction (Heidenreich et al., 2022), or atrial fibrillation (Hindricks et al., 2021), due to a lack of a sufficient amount of evidence to justify its being used instead of 12-lead ECG. The applications for which BSPM has been tested, with a particular focus on its potential role in atrial fibrillation analysis, will be discussed in more detail in Chapter 7.

Ambulatory ECG

While the 12-lead ECG is preferred, it is not always practical in ambulatory⁶ or long-term monitoring situations. In these situations, an ambulatory ECG is used, which can monitor electrical cardiac activity while a person is performing their normal activities.

For example, a **Holter monitor**, shown in Fig. 2.15 is a type of ambulatory electrocardiography device that monitors ECG heart activity, and is used for observing occasional cardiac arrhythmias that occur transiently. As with the standard 12-lead ECG, the Holter monitor records electrical signals from the heart using between three and eight electrodes attached to the chest. The electrodes are connected to a small device, attached to the patient's belt

⁶*Ambulatory* means in a situation where a person can move around as normal, going about their daily activities.

or hung around the neck, which keeps a log of the heart's electrical activity throughout the recording period.

Compared to all other electrograms which can be recorded from the body, ECG is the most ubiquitous and elaborated physiological and clinical technique, and has delivered reliable conclusions for cardiac processes and for clinical diagnosis of heart diseases.

3

ATRIAL FIBRILLATION

Atrial fibrillation (AF) is the most common cardiac arrhythmia¹ in Western countries (Hindricks et al., 2021). Despite decades of research aiming to better understand its pathophysiology and develop suitable treatments, its incidence rises steadily each year, causing irregular heart rate, palpitations, dizziness, shortness of breath, and tiredness, as well as being associated with increased mortality. AF costs healthcare systems worldwide millions of dollars, and money has been used to fund AF research for decades, not to mention the human cost associated with decreased quality of life caused by the condition. The most commonly cited figure for health care expenditures related to AF in the United States is \$6.65 billion, however, estimates range up to \$26 billion (Coyne et al., 2006; Kim et al., 2011). Estimates in Europe for direct costs associated with AF are as follows: €3.016 billion in France, €3.564 billion in Germany, €3.019 billion in Italy, and £1.435-£2.548 billion in the UK (Burdett and Lip, 2022; Velleca et al., 2019). Estimating the true financial burden associated with AF is difficult because different studies estimate either direct costs (those associated with in-patient treatment, out-patient treatment, and prescription drugs) or direct plus indirect costs, which are those associated with work productivity loss or support provided by caregivers.

The aim of this chapter is to give an overview of AF, starting with how it is defined (Sec. 3.1), and its epidemiology² (Sec. 3.1). Then, in Sec. 3.3 and Sec. 3.4, symptoms of AF, and how AF is diagnosed, will be covered. In Sec. 3.5, the mechanisms underlying the initiation and progression of AF will be discussed. Finally, the chapter will end with an overview of current practices for managing AF (Sec. 3.6).

3.1 DEFINITION

Atrial fibrillation (AF) is a cardiac arrhythmia in which the upper chambers of the heart (atria) beat rapidly and irregularly in a seemingly chaotic fashion, and importantly, out of sync with the lower chambers of the heart (ventricles). This is in contrast to a normal heartbeat³, in which the atria and ventricles are synchronised, contracting in a predictable fashion one after the other. AF is most easily understood by comparison with a normally beating heart, as shown in Fig. 3.1. In a healthy heart, the heart rate is controlled physiologically via the heart's natural

¹A heart *arrhythmia* is an irregular heartbeat, which occurs when the electrical signaling in the heart does not work properly.

²*Epidemiology* is the branch of medicine that studies the frequency, distribution, and causative factors of infectious diseases and other health-related conditions or behaviors in a population.

³For an overview of normal cardiac anatomy and function, please see Chapter 2.

3 Atrial fibrillation

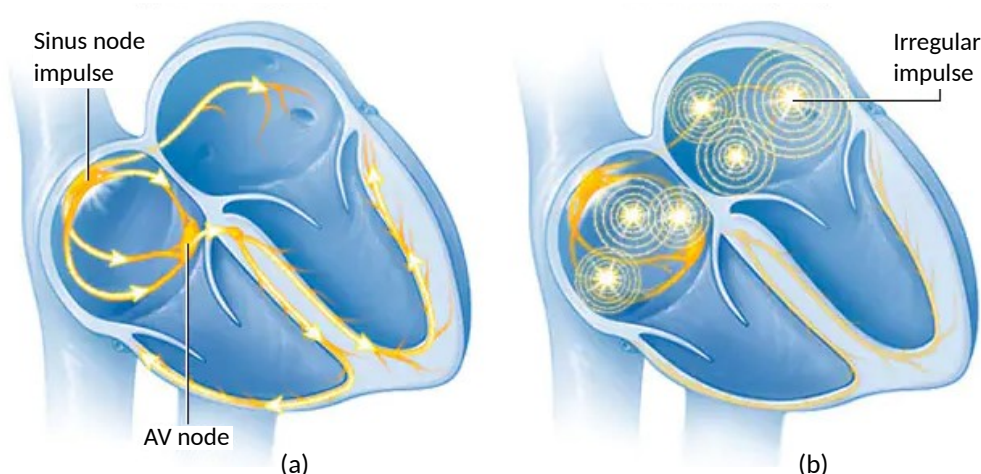


Figure 3.1: **Sinus rhythm vs AF.** A depiction of a heart in (a) sinus rhythm, (b) atrial fibrillation. AV, atrioventricular. Figure from Mayo Clinic (2023).

pacemaker, the sinoatrial node (Fig. 3.1a). This healthy heart rhythm is therefore called sinus rhythm, and maintains a rate of about 60 beats per minute at rest, and up to 180-200 beats per minute during intense exercise. The sinoatrial node is controlled by the body's autonomous nervous system, allowing the heart to respond to metabolic needs. However, during AF, cells in the atria pulse much faster, at rates of 400-600 impulses per minute. Not all of these impulses reach the ventricles due to the natural low-pass filtering action of the atrioventricular node (Fig. 3.1b). However, the ventricles still beat more rapidly than during sinus rhythm. Therefore, the resulting heartbeat is not controlled physiologically by the sinoatrial node, but rather by the interaction between the rapid atrial rate and the filtering atrioventricular node. Without drug therapy, the resulting effective heart rate during AF is around 150 beats per minute. AF was first recorded following the invention of the ECG in the early 20th century.

AF is often classified into four categories (Table 3.1), depending on its duration and how it responds to treatment (Brundel et al., 2022). Note the treatments for AF will be discussed in more detail in Sec. 3.5.

3.2 EPIDEMIOLOGY

The prevalence⁴ of AF varies widely by age, with older age being the single most important risk factor for developing AF (Schnabel et al., 2015). AF is very uncommon in young people, but its prevalence increases from 0.5% for those aged 50-59 to 10% for those aged 80 years and older (Yiin et al., 2014) in the United States and Europe (Zoni-Berisso et al., 2014). The prevalence of AF in the worldwide adult population has been estimated to be between 2% and 4% (Benjamin et al., 2019), with a 2.3-fold rise expected in prevalence due to an aging

⁴In epidemiology, *prevalence* is the proportion of a particular population affected by a medical condition at a given time.

Table 3.1: Types of AF and clinical presentation of each.

AF type	Clinical presentation
Paroxysmal	Lasts less than one week, usually terminates spontaneously, though treatment may be used.
Persistent	Lasts longer than one week, does not terminate spontaneously. Pharmaceutical and/or surgical treatment are used for rate or rhythm-control.
Long-standing persistent	Lasts longer than one year, cardioversion and pharmaceuticals unsuccessful for restoring sinus rhythm.
Permanent	Attempts to restore or maintain sinus rhythm are abandoned. Medications may be used to control heart rate and lower stroke risk.

population and higher detection rates.

AF occurs more frequently in men than women at a ratio of 1.2:1, however, more women have AF than men since they live longer (Zoni-Berisso et al., 2014). The prevalence of AF also differs by ethnicity, with the risk of developing AF highest among people of white European descent and in countries with high socioeconomic status. The lifetime risk of developing AF at an index age of 55 has been estimated at one in three for individuals of European ancestry (Staerk et al., 2018), one in five for individuals of African ancestry (Mou et al., 2018), and one in seven for individuals of Asian ancestry (Chao et al., 2018). However, the disease burden is higher in many Asian countries with a disproportionately older population, with a 2.3-fold higher prevalence estimated in China than in the United States for the year 2050 (Tse et al., 2013; Zhang et al., 2021).

Risk factors for AF can be divided into two categories, non-modifiable and modifiable 3.2. Non-modifiable risk factors for AF include older age (>65 years), male sex, ethnicity, and genetics, as over 100 genes are thought to be linked to AF (Nielsen et al., 2018a; Roselli et al., 2018). Modifiable or manageable risk factors include diseases such as hypertension, obesity, diabetes, heart disease, chronic kidney disease, sleep apnea, and thyroid problems (Chatterjee et al., 2017; Kornej et al., 2020; Zhang et al., 2021), as well as lifestyle factors such as physical inactivity and excess alcohol, tobacco, and fat consumption (Chung et al., 2020; Brundel et al., 2022). Therefore, the predicted increase in AF prevalence is due to a recognition of an aging population, as well as a worldwide shift towards lifestyle practices that are believed to be risk factors for AF.

The consequences of AF, both from a health and financial perspective, are serious and are summarized in Table. 3.2. While not itself lethal, AF is associated with both increased morbidity (ill health), increased mortality (likelihood of death), and decreased quality of life. The most serious consequence of AF is increased risk of stroke, which has been estimated to be

3 Atrial fibrillation

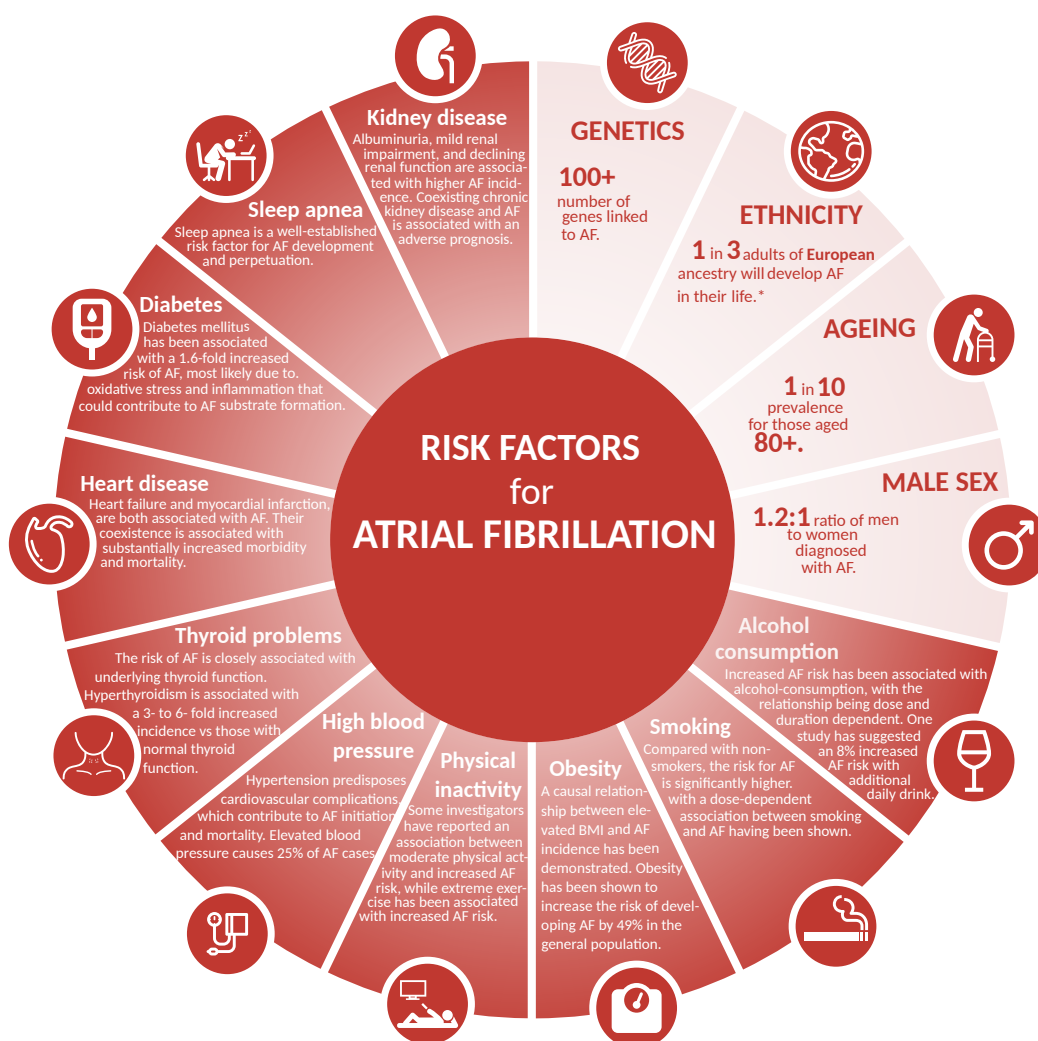


Figure 3.2: **Atrial fibrillation risk factors.** Risk factors for AF can be divided into two categories, modifiable, shown in red, and non-modifiable, shown in pink.

five times as high in patients with AF (Zoni-Berisso et al., 2014) as in those without risk factors, though the risk varies widely depending on presence of comorbidities (Hindricks et al., 2021). The increased stroke risk is due to the ineffective mechanical contraction of the fibrillating atria, which promotes blood stagnation. The stagnant blood promotes formation of clots, which can cause stroke if traveling to an artery in the cerebral circulation. Increased risk of stroke is the biggest contributor to increased mortality in AF patients. Therefore, prevention of stroke is of primary importance when managing AF, and this will be discussed further in Sec. 3.6. Overall, AF is associated with a 1.5-fold increased risk of all-cause death in men, and 2-fold increased risk in women (Benjamin et al., 1998), with the excess mortality related to stroke or comorbidities such as heart failure. Other serious complications associated with AF include heart failure, cognitive impairment, and sudden cardiac arrest, and hospitalization, as well as socioeconomic problems caused by AF symptoms (Sec. 3.3) like permanent disability,

Table 3.2: **Consequences of AF.** A summary of the implications of AF on morbidity, mortality, and quality of life. Adapted from Hindricks et al. (2021).

AF-related outcome	Frequency in AF	Mechanism
Death	1.5-3.5 fold increase	Excess mortality related to heart failure, comorbidities, stroke.
Stroke	20-30% of all ischaemic strokes, 10% of cryptogenic strokes	Stagnation of blood in heart and subsequent clot formation
Heart failure	20-30% of all AF patients	Excess ventricular rate, irregular ventricular contractions
Cognitive decline	Hazard ratio 1.4 / 1.6	Brain white matter lesions, inflammation, micro-embolism
Depression	> 15-20% of AF patients	Decreased quality of life, drug side effects
Decreased quality of life	> 60% of all patients	AF burden, comorbidities, medication
Hospitalization	> 10-40% annual hospitalization rate	AF management related to heart failure, AF symptoms, treatment complications

cognitive impairment, and absence from work (Kornej et al., 2020). The association between AF and cognitive impairment (dementia) is not fully understood (Kalantarian et al., 2013), but growing evidence supports the hypothesis that AF is an independent risk factor for cognitive decline and dementia in general and for Alzheimer's disease in particular (Dietzel et al., 2018). Patients with AF are more likely to develop anxiety disorders (Serpytis et al., 2018) and report slightly higher burden of depressive symptoms (Schnabel et al., 2013).

AF severity and consequence is more serious in women, who have greater symptom severity, increased anxiety related to their condition, increased risk of AF-associated stroke in the presence of other stroke risk factors, and increased stroke severity (Lang et al., 2017; Nielsen et al., 2018b). Additionally, quality of life in women with AF is lower (Blum et al., 2017). Women are currently underrepresented in clinical trials for AF research.

Owing to its high prevalence and association with other serious diseases, decreased quality of life, and increased risk of death, AF is considered the most common serious cardiac arrhythmia in Western countries, and its steep rise in prevalence constitutes a public health issue.

3.3 SYMPTOMS

Symptoms of AF vary widely between individuals. Some patients are asymptomatic, and their AF is only discovered from screening or while receiving care for another condition.

3 Atrial fibrillation



Figure 3.3: **Fibrillation waves on ECG.** ECG recordings with fibrillation waves (f-waves) (above), and normal sinus rhythm (below). The purple arrow indicates the P wave on the normal ECG recording, notably absent on the AF recording. Figure from Wikipedia.

However, for other patients, symptoms can be severe and drastically decrease quality of life. These symptoms include heart palpitations, chest pain, disordered sleep, dizziness, fatigue, lightheadedness, exercise intolerance, difficulty breathing, and weakness. When symptoms of AF are severe, they can lead to permanent disability, absence from work, depression, and anxiety.

3.4 DIAGNOSIS

An electrocardiogram⁵ (ECG) rhythm documentation (either 12-lead, ambulatory, or Holter) showing the absence of repeatable P-waves and irregular RR intervals is required to diagnose AF. The convention is that episodes lasting at least 30 s are considered diagnostic for AF (Steinberg et al., 2018). An example of an ECG trace recording AF is shown in Fig. 3.3. Since AF often occurs in patients with other cardiovascular risk factors or comorbidities that could be undiagnosed, patients diagnosed with AF should also receive a comprehensive assessment to check for comorbidities and AF-related symptoms (Kirchhof et al., 2016). All patients should receive a 12-lead ECG to assess ventricular rate and check for conduction defects (Hindricks et al., 2021). Following diagnosis, careful management of AF and related risks is required, which will be discussed in Sec. 3.6.

3.5 CAUSES AND MECHANISMS OF AF

Atrial fibrillation is caused by *atrial remodeling*, which is a loosely defined term used to describe changes in atrial structure and function (Nattel et al., 2008). The structural and molecular modifications (remodeling) in atrial tissue lead to disordered electrical conduction in the atria thought to be responsible for causing AF. The types of disordered electrical con-

⁵For an overview of electrocardiography, please refer to Chapter 2.

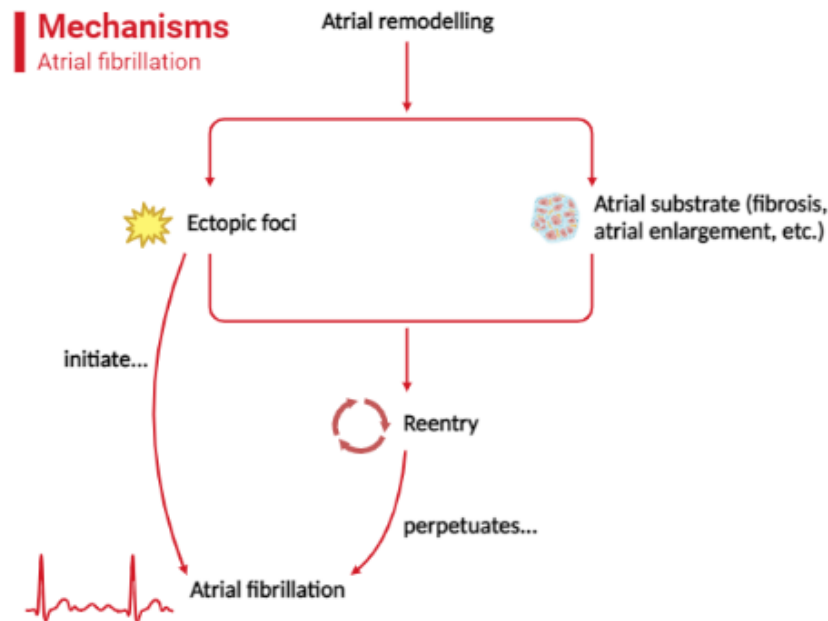


Figure 3.4: **Relationship between AF mechanisms.** A schematic representing the interplay between atrial remodeling, AF substrate, ectopic foci, and reentry as they contribute to the initiation and progression of AF. Figure inspired by Nattel et al. (2008).

duction are (1) ectopic foci^{6,7} activity, and (2) reentry.⁸ Ectopic foci, most often found in the pulmonary veins, are thought to play a large role in *initiating* AF. Both triggering activity from the ectopic foci and reentry are believed to be important for *maintaining* and *progressing* AF after its initial onset. In order for both the triggering and reentry activity to occur, a vulnerable “AF substrate” must exist. The relationships between remodeling, AF substrate, ectopic foci, and reentry are demonstrated in Fig. 3.4. The concept of an AF substrate, the role of ectopic foci in initiating AF, and the role of reentry in maintaining AF, will be discussed in the following subsections. Consideration will be given to the macroscopic modifications that occur, as well as a brief introduction to the associated underlying molecular mechanisms, for which current research is limited.

Concept of an AF substrate

In order for the mechanisms thought to initiate and sustain AF (triggered ectopic focal activity and reentry activity) to occur, changes in structural and electrical aspects of the atrial tissue must occur since these mechanisms could not be sustained in the tissue of a healthy heart. The atrial remodeling is collectively referred to as the substrate, AF substrate, or atrial

⁶ *Ectopic* in medicine means occurring in an abnormal place or position. For example, an ectopic pregnancy, which occurs outside the uterus.

⁷ *Ectopic foci* are abnormal pacemaker sites within heart structures, but outside of the sinoatrial node, that display automaticity, generating impulses outside of physiological control.

⁸ *Reentry* occurs when a propagating impulse fails to die out after normal activation of the heart.

3 Atrial fibrillation

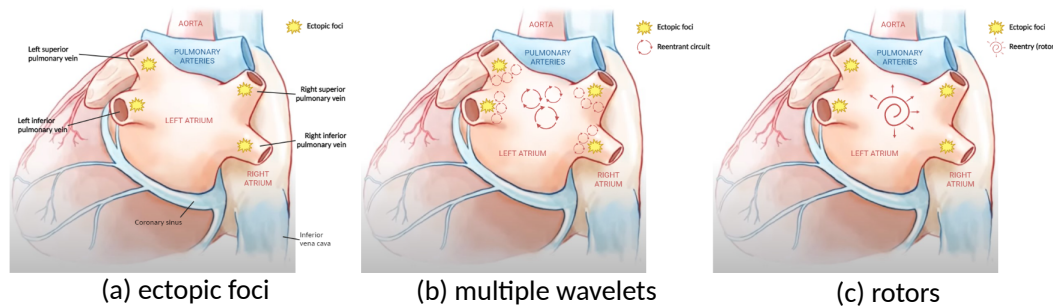


Figure 3.5: AF initiation and perpetuation. Rendering of left and right atria showing mechanisms of AF initiation and maintenance. (a) Ectopic foci located in the pulmonary veins rapidly discharge, propagating into the left atrium, which can directly initiate AF or provide the premature atrial beat for reentry. (b) Micro and macro-reentrant circuits around anatomic structures or scar tissue, driving AF (c) Functional reentry gives rise to fixed or moving spiral rotor, which drives AF. Figure inspired by Verma et al. (2015) and Calkins et al. (2018)

substrate. Debate exists about the exact types of remodeling constituting the substrate, but include hypertrophy and fibrosis. Hypertrophy refers to enlarging of atrial myocytes, which could predispose to triggering ectopic activity, while fibrosis refers to the deposition of extra collagen in the tissues surrounding and protecting the heart and could predispose to reentry by interfering with local atrial conduction by disturbing the continuous cable-like arrangement of cardiomyocytes⁹.

AF initiation: the role of ectopic foci

In a study by Haissaguerre et al. (1998), it was shown that groups of excitable cells displaying automaticity, called ectopic foci and located most often in the pulmonary veins, were responsible for the vast majority of premature atrial beats, also called ectopic beats, that initiated episodes of atrial fibrillation. Radio-frequency ablation of the ectopic foci resulted in reduced numbers of premature atrial (ectopic) beats and AF episodes, demonstrating the role of the ectopic foci in initiating AF. This remains the prevailing hypothesis by which AF is initiated. Ectopic foci, or pacemaker sites within the pulmonary veins displaying abnormal automaticity outside the sinoatrial node (and thus outside physiological control), produce premature atrial beats which are conducted from the ectopic foci to the left atrium (Fig. 3.5a). These premature atrial beats can directly induce AF paroxysms¹⁰, or can further contribute to AF progression by propagating reentrant waves in a vulnerable atrial substrate, which will be discussed further in the following section.

The mechanisms which drive the formation of ectopic foci in the pulmonary veins are debated, however, it has been suggested that the pulmonary veins have unique electric properties and a complex fiber architecture that could promote reentry and ectopic activity to

⁹A *cardiomyocyte* is a contractile, excitable heart muscle cell.

¹⁰*Paroxysms* are sudden recurrences or attacks of a disease.

initiate AF (Hocini et al., 2002). Through electrophysiological indices and image analyses, clinical studies have shown abnormalities in the pulmonary veins of patients with paroxysmal AF, including smaller electrogram voltages, slowed conduction, shorter effective refractory periods (Teh et al., 2011), and when electrically stimulated, greater vulnerability to AF induction, indicating the presence of an AF substrate (Nattel and Dobrev, 2016). The spontaneous depolarization of the ectopic foci is thought to be caused by changes in calcium ion (Ca^{2+}) handling, that cause spontaneous cardiomyocyte depolarization via early or delayed afterdepolarization (Staerk et al., 2017). Genetics are thought to play a role as well, since gene-variants associated with AF have been shown to be linked to ion channel mutations promoting the irregular current patterns associated with ectopic activity in paroxysmal AF (Hong et al., 2005; Lübkemeier et al., 2013).

AF maintenance and progression: the role of reentrant circuits

Atrial fibrillation is maintained by reentrant circuits propagating in an abnormal atrial substrate. In cardiology, reentry occurs when a propagating impulse fails to die out after normal activation of the heart, and persists to re-excite the heart after the end of the normal refractory period. This phenomenon occurs when a premature beat, such as a beat conducted from pulmonary vein ectopic foci to the left atrium, reenters conducting heart tissue that is no longer refractory from the previous sinoatrial node beat. If a vulnerable atrial substrate exists (for example, heterogeneous tissue conduction properties), the premature beat creates a self-sustaining circuit that excites the surrounding heart tissue, and that is refractory to normal heartbeats originating from the sinoatrial node. The concept of reentry is illustrated in Fig. 3.6. Fig. 3.6a shows conduction of a normal sinus beat in a schematic circuit with two splitting and reconnecting branches of conducting heart tissue that have different conductive properties. The beat is successfully propagated to surrounding heart tissue by the branch of the circuit with high conduction velocity. The beat ceases to exist within the circuit when the two propagating impulses cancel each other in the side of the circuit with slower conduction velocity. Fig. 3.6b shows the initiation of reentry. A premature atrial beat originating from ectopic foci encounters refractory tissue when propagating in one direction but is able to conduct in faster-recovering tissue in the other direction. For reentry maintenance (Fig. 3.6c), the ectopic beat must traverse the circuit slowly enough for all points to regain excitability, therefore, the impulse conduction time around the circuit has to be greater than the longest refractory period of the heart tissue in the circuit. Reentry is thus favored by short refractory periods, slow conduction, and the availability of long pathways (circumference of circuit). The impulse continues traveling around the circuit and exciting surrounding heart tissue, and blocking conduction of normal sinus beats. In reentry, the excitation of the heart tissue is not governed by physiological control (parasympathetic and sympathetic system), but rather by the frequency with which the impulse travels around the circuit. Reentry is a mechanism of not only AF, but also other arrhythmias.

Structural, architectural, and electrophysiological atrial abnormalities promote AF maintenance.

3 Atrial fibrillation

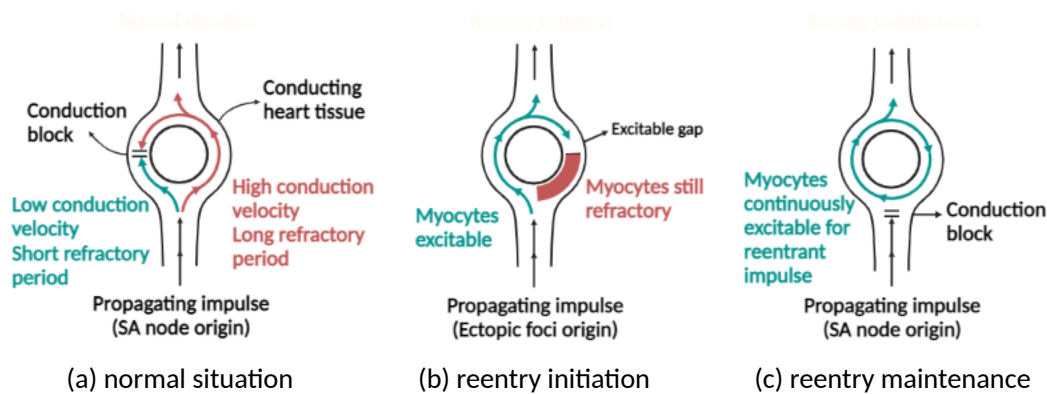


Figure 3.6: **Single-loop reentry circuit formation.** (a) Sinus beat propagation through conducting tissue. (b) An ectopic (premature) beat blocks in still-refractory cardiac tissue but propagates through tissue that has already recovered. (c) Maintenance of reentry. Figure inspired by Milaire et al. (2017)

nance and progression by stabilizing reentry circuits. There are two dominant hypotheses for the types of reentry circuits that promote AF, including micro- and macro- reentrant circuits leading to multiple independent wavelets (Moe, 1959) (Fig. 3.5b), or reentrant rotors (Pandit and Jalife, 2013) (Fig. 3.4c). While the multiple independent wavelets hypothesis was believed for many years to be the dominant reentrant mechanism at play in AF, more recent studies have lent support to the rotor hypothesis (Pappone et al., 2000; Miller et al., 2014). Finally, a third hypothesis known as the double layer hypothesis suggests that electrical dissociation of the epicardial and endocardial layers may facilitate reentry (Allessie et al., 2010).

As reentry circuits stabilize, they become the dominant factor sustaining AF, and the role of ectopic foci becomes less important. This is demonstrated in Fig. 3.7, in which the factors affecting AF initiation and maintenance as it progresses from paroxysmal to persistent are shown. Paroxysmal AF is associated with ectopic triggers that are usually located in the pulmonary veins (Fig. 3.7a), while persistent AF is usually characterized by some degree of atrial remodeling including fibrosis and electrophysiological changes in atrial myocytes (Fig. 3.7b), and ectopic foci are still present. As AF progresses further, the atrial remodeling is more extensive promotes reentry, while ectopic foci play a less important role (Fig. 3.7c). Atrial substrate caused by remodeling associated with the arrhythmia, or by effects of existing heart disease and other risk factors, is known to present an obstacle to successful treatment, partially explaining why advanced forms of AF, in which the substrate has had time to progress, are particularly difficult to treat (Blum et al., 2019).

Underlying factors and mechanisms promoting the creation of an “AF substrate” conducive to reentry include fibrosis, which can lead to heterogeneous conduction properties and conduction block in heart tissue (Everett IV and Olgin, 2007). For example, in heart failure, fibrosis combined with alterations in cardiomyocyte function result in both a slowing of conduction velocity and shortening of the refractory period, factors known to promote reentry.

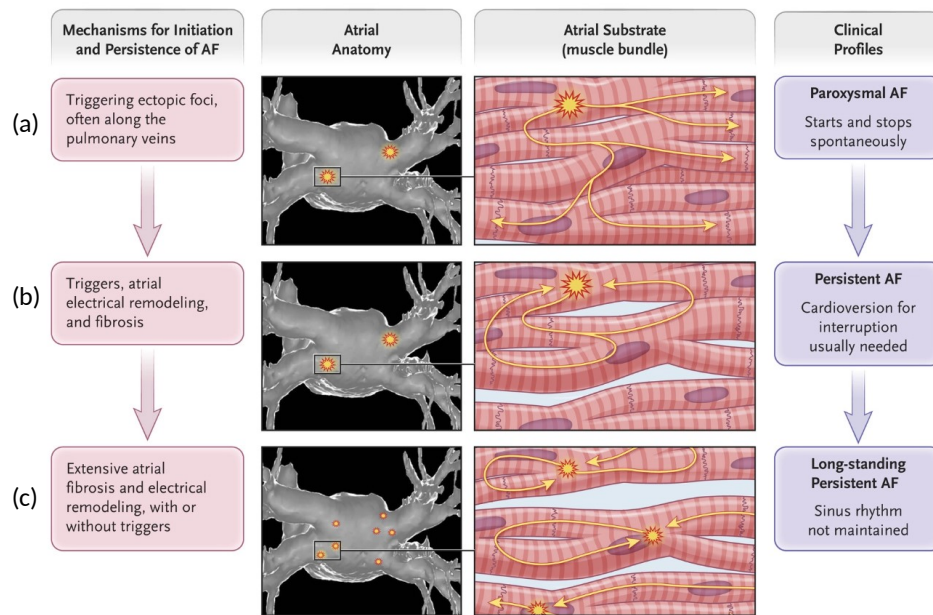


Figure 3.7: **Types and triggers of AF.** Left atrial anatomy shown on left, with clinical profiles of AF related to the underlying atrial substrate at the muscle-bundle level shown at right. (a) Paroxysmal AF. (b) Persistent AF. (c) Long-standing persistent AF. Figure from Michaud and Stevenson (2021).

Another example could be a person with congenital abnormalities that lead to a gain in K^+ channel function, also shortening the refractory period. While not the only substrate type thought to promote reentry, the degree of fibrosis in human atria has been correlated with the presence and persistence of AF (Platonov et al., 2011).

The underlying mechanisms causing the remodeling, and the resulting changes in atrial structure and function, vary in individual patients depending on the presence or lack thereof of comorbidities, as well as lifestyle, congenital, and genetic factors (Hindricks et al., 2021), since AF rarely occurs in individuals without any concomitant condition or underlying comorbidity. In the vast majority of cases, an underlying pathology coexists (Goette et al., 2016). The extent of individual variation in both remodeling and symptom manifestation makes achieving a complete understanding of the mechanisms causing atrial remodeling difficult. Additionally, debate exists about the exact types of changes in structure and function that take place during atrial remodeling and how they contribute to the initiation and maintenance of AF. Recently, more attention has been paid to understanding the molecular mechanisms underlying both the structural defects and the disordered conduction that cause AF initiation and perpetuation (Nattel et al., 2020). A fundamental understanding of the molecular basis of both the structural and electrical modifications that occur in AF could potentially open the door to new targeted treatment modalities, and explain why treatment outcomes differ so widely in AF patients.

3.6 DISEASE MANAGEMENT

As of now, no cure exists for AF. As discussed in Sec. 3.5, the molecular pathways underlying the disordered cardiac electrical conduction that drives AF are not completely understood. The resulting lack of treatment specifically targeting these pathways, and the lack of personalized diagnostic tools to determine disease severity in individuals, has resulted in sub-par treatments (Andrade et al., 2014; Heijman et al., 2016) to which patients often respond differently and unpredictably.

In the absence of a cure for AF, the main treatment goals are: (1) reducing stroke risk associated with AF (see Sec. 3.2), (2) controlling the heart rate (rate-control), (3) regaining a normal heart rhythm (rhythm-control), and more recently, (4) lifestyle and risk factor management. These treatment aims are intended to prevent AF progression, reduce AF burden, and increase quality of life for affected patients. A combination of both medications (pharmacology) and surgical procedures are used, with the exact treatment strategy depending on each patient's circumstances, physician knowledge, and the availability of resources, as optimum treatment of AF requires a well-functioning healthcare system and significant financial resources. The treatment aims for AF are summarized by the better care ABC pathway (Lip, 2017), which is a holistic treatment strategy that has been shown to be associated with better AF outcomes (Proietti et al., 2018; Pastori et al., 2019; Yoon et al., 2019) and is recommended for use in the most recent guidelines (Hindricks et al., 2021; Chao et al., 2022). The core principles of the ABC treatment pathway will therefore be enumerated below, giving an overview of the various treatment strategies that exist for AF.

'A' Avoid stroke/Anticoagulation therapy

As discussed in Sec. 3.2, AF is associated with a five-fold increased risk of stroke. Therefore, stroke prevention is one of the cornerstones of AF management. However, individual risk varies widely (Pisters et al., 2012) and should first be assessed using one of the various stroke epidemiologic risk scoring mechanisms that have been developed, such as the CHA₂DS₂VASc score (Lip et al., 2010). This score assesses risk factors such as existing congestive heart failure, hypertension, older age, diabetes, previous stroke, and female sex. Then, unless a patient is at low risk for a stroke, he or she should be offered stroke prevention therapy in the form of oral anticoagulation drugs (blood thinners) that prevent blood clots from forming, such as warfarin or non-vitamin K antagonists (Hohnloser et al., 2019), which have less food and drug interactions and don't require frequent blood testing when compared to warfarin. However, due to the use of oral anticoagulation, special attention should be paid to the increased risk of bleeding.

'B' Better symptom control

There are two approaches to symptom control in AF, one is *rate-control*, which aims to control the ventricular response rate but allows AF to persist, and the other is *rhythm-control*, which aims to restore sinus rhythm.

Rate-control is often sufficient to improve AF-related symptoms, despite allowing AF to persist (up Investigation of Rhythm Management , AFFIRM; Hindricks et al., 2021). There are several approaches to rate-control, including pharmacological and non-pharmacological strategies. Pharmacological strategies include the use of beta-blockers (Kotecha et al., 2014), calcium channel blockers (Nikolaidou and Channer, 2009), and rarely amiodarone. When drug-based therapy fails, a non-pharmacological strategy consisting of ablation of the atrioventricular node and pacemaker implantation can be used and has a low complication rate and low long-term mortality risk, at least for older patients (Lim et al., 2007). The rate-control strategy is recommended for patients with few AF symptoms and infrequent AF episodes (Antman et al., 2022).

Rhythm-control attempts to restore and maintain sinus rhythm and prevent recurrences of AF, using pharmacological and non-pharmacological strategies, or a combination of the two. Pharmacological rhythm-control is attempted using antiarrhythmic drugs, which target ion channels but are not directed at the molecular causes of AF. These drugs can have adverse effects (Andrade et al., 2014), and there is a small chance that they could destabilize the heart rhythm. If destabilization occurs in the ventricles, it could cause ventricular tachycardia and lead to death (Antman et al., 2022). Therefore, careful consideration needs to be given to which anti-arrhythmic drugs should be administered to individual patients. A non-pharmacological alternative to anti-arrhythmic drugs is catheter ablation, which is a minimally invasive surgical procedure. The core of this procedure is called pulmonary vein isolation (PVI), which attempts a complete electrical isolation of the pulmonary veins by applying linear lesions around their openings (Pappone et al., 2000; Jaïs et al., 2008) (Fig. 3.8). The reasoning behind this procedure is that AF, particularly in the early stages, usually originates with ectopic foci in the pulmonary veins. Therefore, in the pulmonary vein isolation procedure, the surgeon locates the four pulmonary veins and ablates the tissue at their openings into the left atrium using an ablation catheter in a circumferential fashion (Fig. 3.8a,b). The ablation is performed using an ablative catheter which delivers either heat (radiofrequency ablation) or freezing cold (cryoablation) to create a circle of burned tissue at the base of each vein. The procedure therefore electrically isolates the left atrium and therefore the AV node from the ectopic foci present in the pulmonary veins. However, it is known that not all AF is caused by pulmonary vein ectopic foci (particularly in the more advanced stages), therefore, more involved ablation strategies have been attempted, including applying linear lesions in the atria, or targeted ablation of complex fractionated atrial electrograms¹¹ (CFAEs), low-voltage areas, or rotational

¹¹ *Complex-fractionated electrograms* are defined as intra-atrial electrograms with a cycle-length “less than 120 ms, or that were fractionated or displayed continuous electrical activity” (Oral et al., 2007). They are thought to indicate high-frequency electrical sources in the atria, and are targeted for ablation using the stepwise approach.

3 Atrial fibrillation

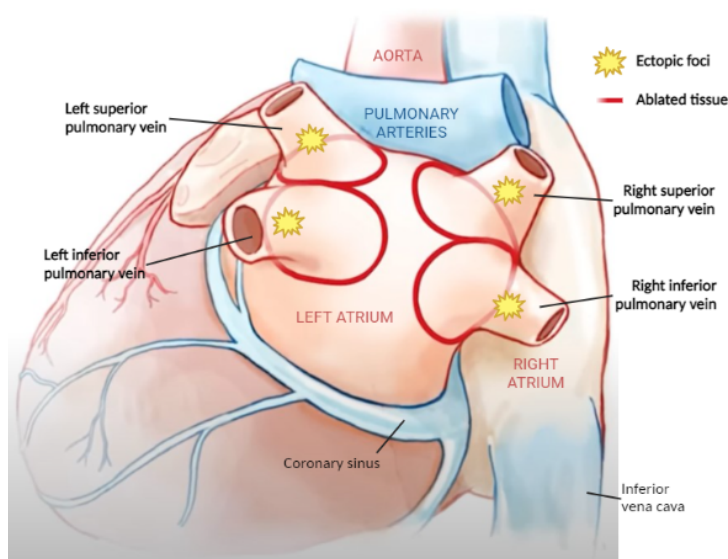


Figure 3.8: **Pulmonary vein isolation.** In pulmonary vein isolation, a catheter applies lesions around the openings of the pulmonary veins, depicted as red ovals in the figure. The ablative catheter delivers either heat (radiofrequency ablation) or freezing cold (cryoablation) to create the lesions. Figure adapted from Verma et al. (2015).

activity. This approach, first extensively used by Nademanee et al. (2004) and referred to as *stepwise ablation*, was hallmarked by several studies as improving outcomes for terminating persistent AF over PVI-only procedures (Haïssaguerre et al., 2004, 2005; Hocini et al., 2010; Rostock et al., 2011). However, later studies have called into question the effectiveness of these strategies (Tamborero et al., 2009; Verma et al., 2015), noting that such procedures are considerably more involved than pulmonary vein isolation alone.

When successful, catheter ablation treatment is considered more effective for improving quality of life and reducing risk of AF recurrence than long-term antiarrhythmic drug therapy (Wilber et al., 2010; Packer et al., 2013; Piccini and Fauchier, 2016; Nielsen et al., 2017) in patients in whom drugs have already failed, but these drugs can still be used after ablation to reduce the risk of AF recurrence (Duytschaever et al., 2018). Despite the promising nature of catheter ablation, AF recurrence can still occur following the procedure, most likely due to electrical reconnection of the pulmonary veins to the left atrium due to tissue healing. Its success rate depends highly on AF stage, providing the best results for younger patients with paroxysmal AF. The success rate is much lower in older patients and those with persistent AF (Antman et al., 2022), most likely due to enlarged left atrium size and the presence of fibrosis, making creation of effective lesions at the connecting pulmonary veins difficult.

Usually, anti-arrhythmic drugs are attempted before catheter ablation. However, ongoing debate exists regarding the merits of each strategy. Two recent studies, the EARLY-AF and STOP AF First trials, conducted across 18 centers in Canada and 24 centers across the United States, respectively, investigated the effectiveness of cryoablation versus anti-arrhythmic drugs as

initial therapy for paroxysmal AF (Andrade et al., 2021; Wazni et al., 2021). Both studies found that cryoablation resulted in lower rates of atrial fibrillation recurrence than anti-arrhythmic drugs, however, further studies would be required before recommending catheter ablation as initial therapy for most patients. The treatment modalities used for AF are therefore still evolving, and new technologies for ablation, as well as drugs targeting molecular pathways, may improve long-term AF outcomes in the future.

'C' Cardiovascular risk factors and concomitant disease management

As discussed in Sec. 3.4, many modifiable risk factors and manageable comorbidities, including obesity, alcohol and tobacco use, physical inactivity, sleep apnea, diabetes, and hypertension, increase the risk of developing AF (Fig. 3.2). Identifying and managing both risk factors and comorbidities can help reduce AF burden and symptom severity, as well as being much less invasive and expensive than traditional AF treatments. While this aspect of AF management has been under-recognized and understudied, several recent clinical studies have demonstrated benefits of risk factor reduction for the management of AF. Several studies have reported that lifestyle changes targeting weight loss, physical activity, and risk factor modification were associated with decreased AF burden (Pathak et al., 2014, 2015a,b; Middeldorp et al., 2018). Additionally, a recent study demonstrated that patients with persistent AF who received targeted intervention for hypertension, prevention of coronary and vascular events, and practicing a healthy lifestyle had higher rates of sinus rhythm one year after catheter ablation compared to patients who did not receive such intervention (75% vs. 63%, $p=0.042$) (Rienstra et al., 2018). This could indicate that risk factor reduction is particularly important for those with persistent AF, which is traditionally significantly harder to treat than paroxysmal AF.

The most recent Asian Pacific (Chao et al., 2022), Australian/New Zealand (Brieger et al., 2018), Canadian (Andrade et al., 2020), and European (Hindricks et al., 2021) guidelines recommend risk factor reduction to be included as part of AF management. Additionally, while not a formal guideline, the American Heart Association recently issued a scientific statement (Chung et al., 2020) advocating further study of the associations between risk factor management and improved outcomes for AF patients at all stages of AF.

4 SPATIOTEMPORAL SIGNAL PROCESSING METHODS FOR 12-LEAD ECG

Analysis of the surface ECG in the context of AF is based on the assumption that the abnormal electrical activity of the atria produces characteristic patterns on the recorded surface ECG. This is indeed the case, as reflected by the presence of f-waves on ECG recorded during AF, shown in Fig. 3.3. The presence of f-waves on ECG is required to diagnose AF, as discussed in Chapter 3. This begs the question of whether f-waves recorded on surface ECG bear additional information that permits not only AF diagnosis, but also characterization of AF dynamics and severity of AF, which have both been shown to be linked to AF recurrence following catheter ablation treatment.

Many studies have investigated this research question, resulting in the development of signal processing algorithms relying on spatial, temporal, spectral, and non-linear methods that aim to find patterns in ECG signals that can be linked to underlying physiological phenomena which are known to be indicative of AF disease complexity, organization, and structural remodeling (Lankveld et al., 2014). These studies generally simultaneously record (1) intracardiac electrograms from directly inside the heart, and (2) surface ECG from patients in persistent AF, or during paroxysmal AF episodes. They then attempt to show a relationship between an index calculated using the intracardiac electrograms already known to be related to AF organization,¹ and a similar index calculated on the surface ECG. As one example, it was shown that a high degree of AF organization usually implies a slower atrial activation rate than complex activation patterns, as measured using intracardiac electrograms (Konings et al., 1994), and that this measure could serve as an index of the degree of AF organization (Capucci et al., 1995), and could correlate to the length of the refractory period in AF (Kim et al., 1996).² It was then shown that the repetition rate of f-waves in ECG lead V_1 , converted to atrial cycle length, was reflective of the rate of atrial activation recorded on intracardiac electrograms (Holm et al., 1998). Therefore, one could say that atrial cycle length computed on ECG lead V_1 is a noninvasive ECG biomarker that provides objective information related to AF organization and refractory period in AF.

These and similar studies have resulted in interesting though often conflicting ideas regarding the type of f-wave measures or indices that can reliably quantify the organization or

¹ *AF organization* refers to the idea that activation patterns in AF can either possess a high degree of organization, i.e., the same conduction routes in the atria are frequently activated, or a low degree of organization, i.e., different conduction routes in the atria are activated.

² Short refractory periods in AF are known to contribute to the development of AF-perpetuating reentry circuits.

4 Spatiotemporal signal processing methods for 12-lead ECG

complexity of the underlying AF. However, the general consensus is that quantifiable metrics from surface recorded f-waves on ECG are reliable reflections of underlying AF processes. Despite this, the use of surface ECG in clinical practice remains limited to its diagnosis (Lankveld et al., 2014).

As mentioned, the surface ECG has been shown to be related to AF organization, and AF organization has been shown to be related to likelihood of AF recurrence following catheter ablation treatment. Several studies have therefore gone a step further than the analyses described above and attempted to study the relationship between surface ECG measures of AF organization and AF recurrence following catheter ablation, since the success rate of catheter ablation for treating persistent AF is subpar. While estimates vary depending on the exact ablation procedure and follow-up protocol, long-term success rates range from 25% to 80% (Rostock et al., 2011; Tilz et al., 2012; Scherr et al., 2015; Schreiber et al., 2015). For example, (Matsuo et al., 2009) examined the ability of pre-procedural clinical variables to predict both procedural and clinical outcomes of catheter ablation in patients with persistent AF, finding that among AF duration, echocardiographic parameters, presence of structural heart disease, and AF cycle length measured on ECG, only AF cycle length was an independent predictor of procedural AF termination. Surface ECG AF cycle length and AF duration were both predictive of long-term maintenance of sinus rhythm following ablation, i.e., clinical outcome. Longer AF cycle length was predictive of procedural termination of AF and long-term maintenance of sinus rhythm following ablation. Rostock et al. (2011) also found that longer pre-procedural AF cycle length was the strongest predictor for single-procedure catheter ablation success for terminating AF. Fibrillation-wave amplitude has been shown to be another ECG-derived AF complexity parameter (Lankveld et al., 2016), achieving the best independent predictive performance for both catheter ablation AF termination and long-term maintenance of sinus rhythm following the ablation procedure, when compared with other ECG or clinical only parameters. Numerous other studies have found longer baseline AF cycle length, and large fibrillation wave amplitude, to be predictive of procedural AF termination and long-term maintenance of sinus rhythm (Heist et al., 2012; Szilágyi et al., 2018). Greater f-wave amplitude has been shown to be correlated with younger age and shorter AF history, while smaller f-wave amplitude was shown to be associated with AF recurrence during the follow-up period post-ablation (Nault et al., 2009).

Higher dominant frequency (DF) and lower organization index (OI) have been associated with recurrence of AF (Buttu et al., 2013), however, their predictive performance has not been shown to be reliable enough to be adopted as a clinical tool for choosing patients most likely to benefit from catheter ablation treatment. These ECG-derived AF complexity parameters, or electrocardiographic biomarkers, are time-invariant and thus reflect only average tendencies. The work presented in this chapter aimed to analyze the temporal evolution of these parameters before and throughout catheter ablation procedures, to better understand their role in predicting AF recurrence following catheter ablation. The remainder of the chapter is organized as follows: Section 4.1 presents the time-variant methods used to analyze the ECG signals. The results are presented in Section 4.2 and discussed in Section 4.3.

4.1 METHODS

4.1.1 STUDY POPULATION

The study population consisted of 40 patients (38 M/2 F, 61 ± 8 years) who were referred for a first catheter ablation after displaying resistance to pharmacological and electrical cardioversion interventions. The patients were suffering from AF for 6 ± 4 years, sustained for 19 ± 11 months before ablation. All patients discontinued antiarrhythmic drugs for at least five half-lives prior to the catheter ablation procedure, except for amiodarone and beta-blockers. Oral anti-coagulation was prescribed for at least one month prior to the ablation procedure. The clinical characteristics of the patients recorded prior to the procedure are summarized in Table 4.1.

Table 4.1: **Stepwise patient population clinical characteristics.**

Characteristic	<i>n</i> = 40
Sex (M/F)	38/2
Age, mean \pm std, years	61 ± 8
Hypertension, <i>n</i>	27
Coronary artery disease, <i>n</i>	0
Valvular Disease, <i>n</i>	6
Diabetes, <i>n</i>	6
Left ventricular ejection fraction, mean \pm std, %	49 ± 11
Sustained AF duration, mean \pm std, months	19 ± 11
std, standard deviation	

4.1.2 ABLATION PROCEDURE AND SIGNAL ACQUISITION

Stepwise radiofrequency catheter ablation³ was performed as described in Buttu et al. (2013), under general anesthesia by the same cardiologist for all patients at Lausanne University Hospital. Briefly, the procedure consisted of pulmonary vein isolation (PVI), followed by ablation of complex fractionated atrial electrograms (CFAE), followed by linear ablation within the left atrium. The endpoint of the ablation was termination of AF into either sinus rhythm or atrial tachycardia at any step of the ablation procedure. If this endpoint was not reached, electrical cardioversion was performed in an attempt to restore sinus rhythm. Patients were then monitored throughout a follow-up period, with clinical visits scheduled at 3, 6, 12, and 18 months, then 2, 3, and 4 years after the initial ablation procedure to monitor arrhythmia recurrence, defined as atrial tachycardia, atrial flutter, or AF observed during the follow-up period and lasting more than 30 s (Calkins et al., 2018). Not all patients continued with the

³For a review of the different types of catheter ablation procedures, see Section 3.6.

4 Spatiotemporal signal processing methods for 12-lead ECG

clinical follow-up for the full duration; the mean duration was 32 ± 14 months.

12-lead ECG was continuously recorded at a sampling frequency of 2 kHz (Axiom Sensis XP, Siemens) before, during, and immediately after catheter ablation in all patients for later offline analysis. Chest lead V₆ was moved from its normal position and instead placed on the back of the patient, as this has been shown to improve recording quality of anterior to posterior activation activity of the atria (Petrutiu et al., 2009).

Based on the observed procedural and clinical outcomes, the study population was divided into the following three groups: (1) left-terminated, non-recurring (LTN, $n=8$), patients in whom catheter ablation successfully terminated AF into either sinus rhythm or atrial tachycardia at any stage of the procedure, and remained free of arrhythmia throughout the follow-up period; (2) left-terminated, recurring (LTR, $n=20$), patients in whom catheter ablation successfully terminated AF, but who experienced an arrhythmia recurrence in the follow-up period post-ablation; (3) not left-terminated (NLT, $n=12$), patients in whom the stepwise catheter ablation procedure failed to terminate AF. In the LTR and NLT groups, the arrhythmia recurrences were classified according to their form as either (1) atrial tachycardia/atrial flutter (AT/AFL) or (2) AF. The study protocol was approved by the Lausanne University Hospital Human Research Ethics Committee, and all patients provided written informed consent.

4.1.3 ECG SIGNAL PREPROCESSING

ECG signals were visually inspected before preprocessing, and signals containing excessive noise or artifacts were removed from the analysis. Recordings were then processed to remove base drift and high frequency noise by applying a 5th order bandpass filter (1-20 Hz) to the signals.

Fibrillatory-wave extraction

The aim of this study was to apply spatiotemporal techniques to continuous ECG signals to reveal information regarding atrial dynamics throughout catheter ablation. This required creating continuous signals of atrial origin. However, analysis of the component of the ECG signal of atrial origin is complicated by the fact that the atrial fibrillatory waves present in AF, called f-waves and shown in Fig. 3.3, are of much smaller amplitude than QRST complexes. Therefore, it is necessary to apply signal processing techniques to reduce and ideally eliminate the QRST complexes to obtain a signal of purely atrial origin. These techniques, referred to as atrial activity extraction, f-wave extraction, or ventricular activity cancellation, are described briefly below and in detail in Appendix A. The term f-wave extraction will be used here.

It is possible to algorithmically detect the deflections, or *fiducial points* of the QRST complex, and to analyze only the portions of the ECG which are known to be of atrial origin, the TQ segments. However, TQ segments, especially in AF, are short, often less than half a second. Therefore, if temporal or spectral analysis is desired, it is preferable to have a longer duration,

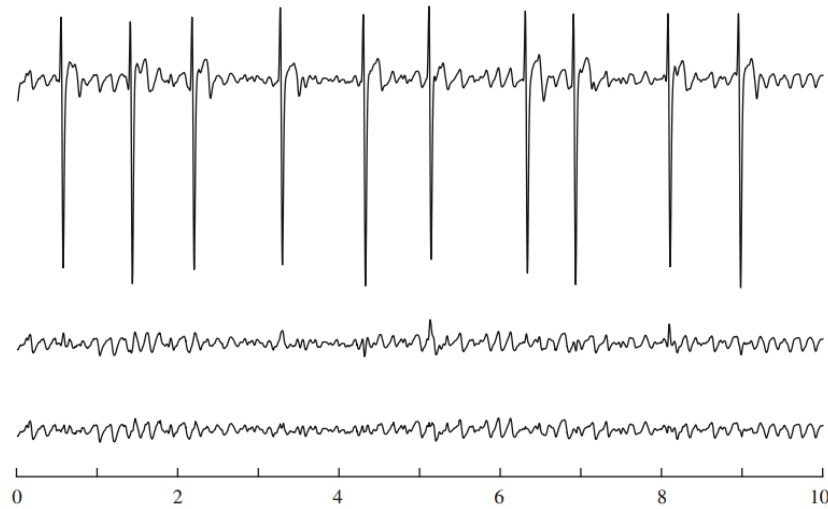


Figure 4.1: **f-wave extraction.** Top row: recorded ECG signal with f-waves characteristic of AF. Middle row: f-waves extracted using average beat subtraction. Bottom row: f-waves extracted using signal and noise dependent weighted averaging.

continuous signal available for analysis. Several algorithms have thus been developed for f-wave extraction, to allow for more robust and accurate temporal and spectral analyses on longer-duration signals of atrial origin. An example of an ECG signal containing f-waves before and after f-wave extraction (using two different algorithms) is shown in Fig. 4.1.

Most f-wave extraction algorithms rely on some form of beat averaging to remove the QRST complex. The idea is to compute an average QRST complex, obtained from an ensemble of beats with similar morphology, and subtract the resulting average from each beat of the original ECG. The algorithms used to obtain the atrial activity signals shown in Fig. 4.1b, c are both variants of this basic idea. Other algorithms use variants of principal components analysis (PCA), independent components analysis (ICA), or blind-source separation to extract an “atrial source,” assumed to be separable from the “ventricular source.”

The single-beat method, described in (Lemay et al., 2007), in which QRS and T-waves are separately processed, was used to extract atrial activity on all 12-lead ECG recordings. This algorithm is a variant of the beat averaging method and is described in detail in Appendix A.

Following application of the single-beat method, the 12-lead ECG signals were downsampled to 50 Hz, since the frequency content of interest in atrial signals is generally below 10 Hz (Holm et al., 1998). Once downsampled ECG signals devoid of ventricular activity were obtained, time and frequency domain ECG parameters quantifying organization and evolution were calculated, as will be described in the next section.

4 Spatiotemporal signal processing methods for 12-lead ECG

4.1.4 INSTANTANEOUS FREQUENCY ESTIMATION

This study aimed to examine the temporal evolution of AF organization indices in a way that would be clinically applicable. Therefore, several factors were considered when choosing appropriate analysis methods, including the non-stationary and multi-variate nature of ECG signals recorded in AF, as well as the feasibility of a real-time implementation. Various time-frequency approaches exist for estimating instantaneous frequency of non-stationary signals. The Wigner distribution (Cohen, 1995) was for example used in (Stridh and Sornmo, 2001) to estimate temporal frequency trends in ECG leads V_1 , V_2 , and V_3 . However, time-frequency distributions must obey the time-bandwidth product theorem, or uncertainty principle.⁴ Time-frequency distributions are also not designed for multivariate applications, and so do not inherently leverage the redundancy and spatial variability exhibited by signals recorded on ECG leads. Finally, computing a signal's time-frequency distribution is extremely computationally intensive, which would preclude a real-time implementation.

Another class of methods for tracking the instantaneous frequency of a non-stationary signal includes adaptive filtering algorithms (Haykin, 2002). These algorithms consist of (1) a bandpass or notch filter whose center frequency varies in time to match the signal's instantaneous frequency, and (2) a feedback mechanism to adapt the center frequency of the filter. A schematic of such a system is shown in Fig. 4.2. We chose to use adaptive filtering methods for the study presented in this chapter to overcome the difficulties mentioned in the paragraph above. Adaptive frequency tracking will be presented in the next section, and the concept of instantaneous frequency is presented in more detail in Appendix B.

Adaptive frequency tracking

The adaptive filtering algorithm used here is an extension of a harmonic frequency tracking algorithm originally proposed by Liao (2005) and later extended (Uldry et al., 2009; Van Zaen et al., 2010; Van Zaen, 2012). The adaptive frequency tracking algorithm's variations for single signal, multi-signal, and harmonic instantaneous frequency tracking will be described below.

Single frequency tracking

To demonstrate the concept of adaptive filtering for instantaneous frequency estimation, consider an input signal $x[n]$ of the form:

$$x[n] = s[n] + v[n] = A_0 \sin(\omega_0 n + \phi_0) + v[n] \quad (4.1)$$

where A_0 , ω_0 , and ϕ_0 are the instantaneous amplitude, frequency, and phase, respectively, of the signal's sinusoidal component, and $v[n]$ is an additive white noise. The single frequency

⁴The *uncertainty principle* states in no uncertain terms that a narrow waveform has a wide spectrum, and a wide waveform has a narrow spectrum, and both the time waveform and frequency spectrum cannot be made arbitrarily small simultaneously (Skolnik, 1980).

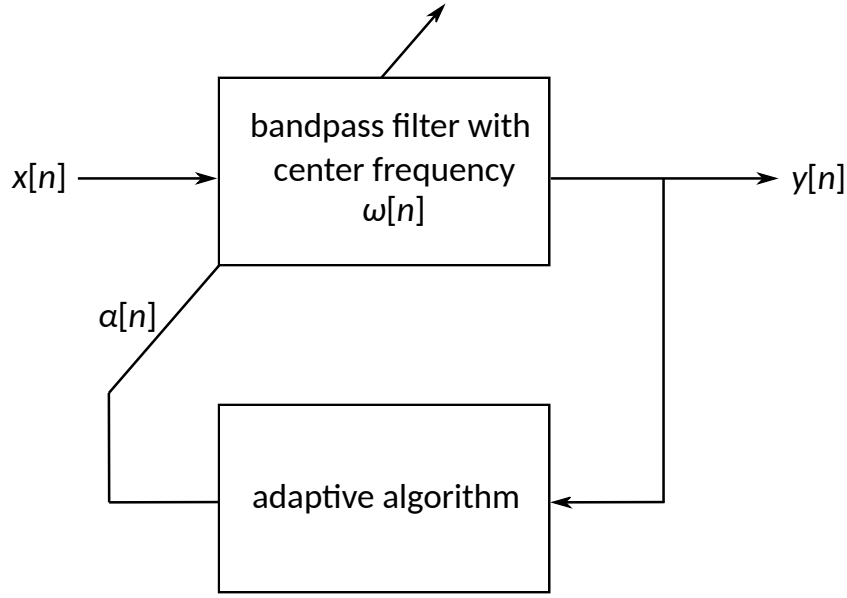


Figure 4.2: **Adaptive filter.** Schematic of an adaptive-frequency tracking filter, composed of (1) a time-varying band-pass filter, and (2) an adaptive mechanism to update the center frequency of the filter.

tracking algorithm has two parts as shown in Fig. 4.2, (1) a time-varying band-pass filter that extracts the sinusoidal component $s[n]$ present in the input signal $x[n]$, and (2) an adaptive mechanism that extracts the instantaneous frequency of $s[n]$, which is taken as the central frequency update of the time-varying band-pass filter. The output signal, $y[n]$, is obtained by filtering the input signal $x[n]$ with a bandpass filter whose transfer function is given by:

$$H(z, n) = \frac{1 - \beta}{2} \frac{1 - z^{-2}}{1 - \alpha[n](1 + \beta)z^{-1} + \beta z^{-2}} \quad (4.2)$$

The bandpass filter described by Eq. 4.2 has a time-varying center frequency, $\omega[n]$, determined by the time-varying parameter $\alpha[n] = \cos(\omega[n])$, and a fixed-bandwidth, determined by the parameter β , ($0 \ll \beta < 1$). The filter's frequency response is shown in Fig. 4.3, for three values of β and for a fixed central frequency of $\omega_0 = 0.5\pi$. The filter has unit gain and zero phase shift at ω_0 .

Then, to understand the cost function through which $\omega[n]$ is updated, consider that any sinusoid of the form $s[n] = A_0 \sin(\omega_0 n + \phi_0)$, as in Eq. 4.1 satisfies the real discrete oscillator equation, given below:

$$\begin{aligned} s[n] &= 2 \cos(\omega_0) s[n-1] - s[n-2] \\ &= 2\alpha_0 s[n-1] - s[n-2] \end{aligned} \quad (4.3)$$

From Eq. 4.3, it is therefore possible to recover the frequency ω_0 of a pure sinusoid with only

4 Spatiotemporal signal processing methods for 12-lead ECG

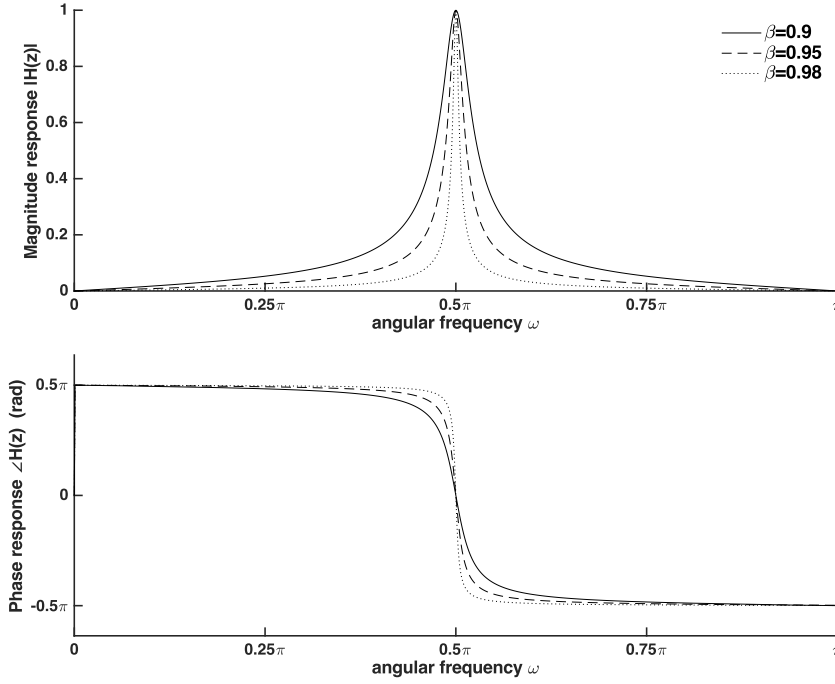


Figure 4.3: **Adaptive filter frequency response.** Frequency response of the adaptive band-pass filter described by Eq. 4.2, and whose cost function maximizes oscillatory behavior (Eq. 4.5), for three values of β and a fixed central frequency, $\omega_0 = 0.5\pi$.

three samples:

$$\alpha_0 = \frac{s[n] + s[n-2]}{2s[n-1]} \quad (4.4)$$

$$\omega_0 = \arccos \alpha_0$$

Therefore, if the goal is to maximize the “oscillatory” behavior of the output signal of the adaptive filter, the adaptive parameter of the cost function should minimize the difference between the current sample and its estimate given by the real discrete oscillator equation. For the output signal $y[n]$, the cost function is therefore given by:

$$J = E\{(y[n] - 2\alpha[n+1]y[n-1] + y[n-2])^2\} \quad (4.5)$$

The solution of $\frac{\delta J}{\delta \alpha[n+1]} = 0$ is given by

$$\alpha[n+1] = \frac{E\{y[n-1](y[n] + y[n-2])\}}{2E\{y^2[n-1]\}} \quad (4.6)$$

Since the expectations in the numerator and denominator of Eq. 4.6 cannot be computed, they are replaced by exponentially weighted averages of their real-time values, respectively

$Q[n]$ and $P[n]$, given by

$$\begin{aligned} Q[n] &= \delta Q[n-1] + (1-\delta)y[n-1](y[n] + y[n-2]) \\ P[n] &= \delta P[n-1] + (1-\delta)y^2[n-1] \end{aligned} \quad (4.7)$$

where δ , ($0 \ll \delta < 1$) is a forgetting factor that controls the convergence rate. The estimate of the new value of the adaptive parameter α is given by:

$$\alpha[n+1] = \frac{Q[n]}{2P[n]} \quad (4.8)$$

and the corresponding estimate of the instantaneous frequency is given by:

$$\begin{aligned} \omega[n+1] &= \arccos \alpha[n+1] \\ f[n+1] &= \frac{\omega[n+1]}{2\pi} \end{aligned} \quad (4.9)$$

Multi-signal frequency tracking

In the section above, an adaptive filtering method for extracting the instantaneous frequency of one signal was demonstrated. In this section, an extension for extracting the common oscillatory frequency of M signals will be presented.

To extract the common frequency of M correlated signals, individual bandpass filters of the form described in the previous section are used, and individual updates are computed as in the single-signal case. A central frequency is then calculated using a weighted sum of each of the individual update terms. The weights applied to each individual update are computed based on the minimization of the variance of the linear combination of the individual updates of the central frequency, as in (Prudat and Vesin, 2009). The idea is to weight most heavily the signals in which the oscillation accounts for the most variance. For each individual update given by $\alpha_m[n+1] = \frac{Q_m[n]}{2P_m[n]}$, and associated weights $W_m[n]$, $0 \leq W_m[n] \leq 1$, the central update $\alpha_c[n+1]$ is given by:

$$\alpha_c[n+1] = \sum_{m=1}^M W_m[n] \alpha_m[n+1] \quad (4.10)$$

In this work, both the single frequency tracker, and the multi-signal frequency tracker were tested, using ECG lead V_1 for the single frequency estimate, and ECG chest leads V_1 - V_{6b} as the input signals for the multi-signal frequency tracker. It was found that the variance in the instantaneous frequency estimate was significantly lower for the multi-signal frequency tracker than for the single frequency tracker, as shown in Fig. 4.4. The multi-signal frequency tracker was therefore used in this study to extract the common instantaneous frequency estimate of the signals recorded on ECG leads V_1 - V_{6b} .

4 Spatiotemporal signal processing methods for 12-lead ECG

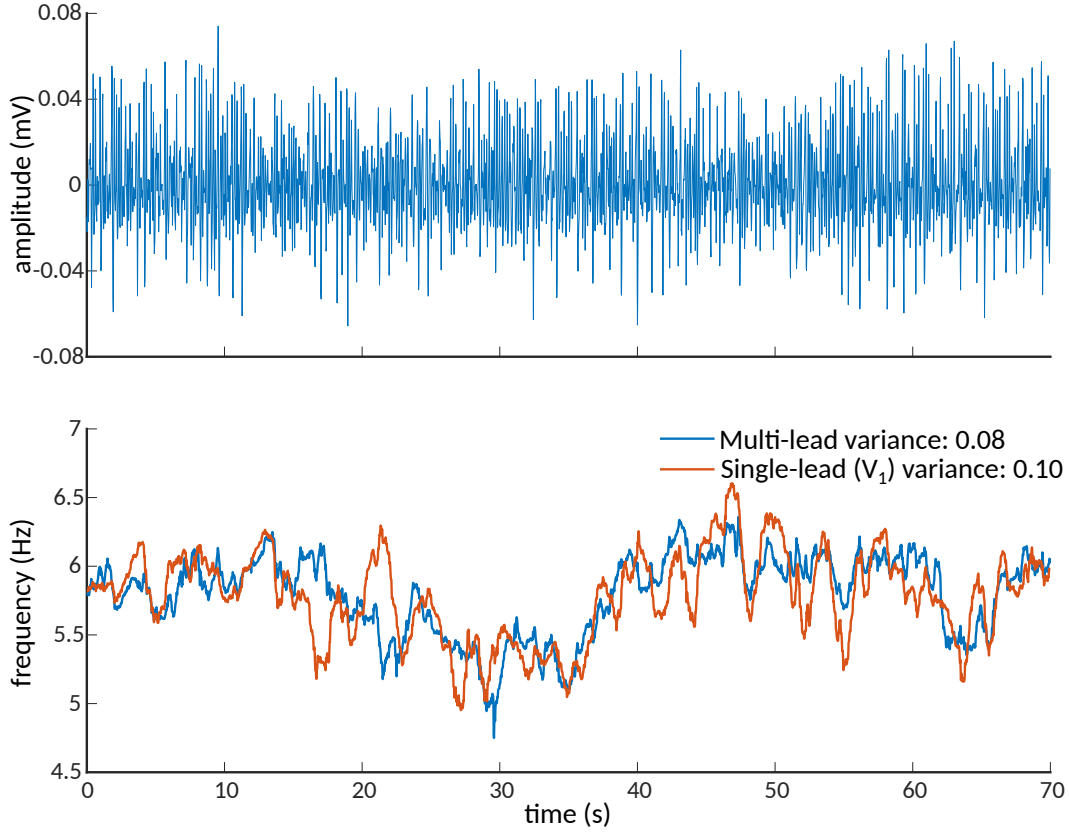


Figure 4.4: **Multiple frequency tracker advantage.** Illustrative example of multiple signal vs single adaptive frequency tracker for IF estimation. Top panel: Atrial ECG signal (lead V_1) with ventricular activity removed, on which the single frequency tracker was applied. Bottom panel: Multiple signal instantaneous frequency estimate in blue, single frequency tracker IF estimate. The variance of the single frequency tracker estimate is greater.

4.1.5 CALCULATION OF ECG-BASED ORGANIZATION INDICES

Following the f-wave extraction as outlined in Sec. 4.1.3, AF organization was quantified using frequency and time domain parameters. Frequency domain parameters included the instantaneous frequency (IF) and the adaptive organization index (AOI). The IF of the AF oscillations common to the signals recorded on all ECG chest leads (V_1 - V_{6b}) was extracted using the multi-signal frequency tracking extension outlined in Sec. 4.1.4. The AOI was defined as the ratio between the power of the extracted fundamental and harmonic frequency components, and the total power of the input signal. The AOI is thus bounded between zero and one, with a value close to one indicating that most of the signal power is concentrated in the fundamental and first harmonic frequency components. The AOI was computed individually for the signals recorded on ECG leads V_1 - V_{6b} . The algorithm bandwidth parameter β and forgetting factor δ were both set to 0.95, giving a filter convergence time of less than one second, at a sampling frequency of 50 Hz.

Time domain indices of AF organization were calculated separately for the atrial signals extracted from ECG leads V_1 - V_{6b} , including sample entropy (sampEn) (Alcaraz et al., 2010) and f-wave amplitude (FWA) (Meo et al., 2012). Sample entropy was calculated on the extracted atrial signals, using $m = 2$ samples within a tolerance of $r = 0.2$ applied to the signal standard deviation. The FWA was found by halving the difference of the upper and lower envelopes of the atrial signals obtained using local maxima and minima.

The IF and AOI signals were then divided into 10-s segments, and one mean value was recorded for each segment. For the time-domain measures (sampEn and FWA), the extracted atrial signals were divided into 10-s segments, and one sampEn and one mean FWA value were recorded for each segment. Therefore, one mean multi-lead IF estimate, six mean AOI, six sampEn, and six mean FWA values (one for each lead) were recorded for each 10-s signal segment, for each patient.

Finally, each epoch (and the associated calculated value of ECG-organization indices) was assigned one of the following three labels based on its temporal placement: (1) **pre-PVI**, if the epoch signal was recorded at baseline, prior to the start of ablation, (2) **dur-PVI** if signal segment was recorded during the PVI step of the ablation procedure, (3) **post-PVI** if the signal segment was recorded during the CFAE or linear ablation steps.

4.1.6 PATIENT GROUP COMPARISON AT EACH ABLATION STEP

We compared the values of the four ECG organization indices (IF, AOI, sampEn, FWA) at each ablation step (pre-PVI, dur-PVI, and post-PVI) described at the end of Sec 4.1.5 between the three patient groups (LTN, LTR, and NLT) outlined in Sec 4.1.2, to evaluate whether AF organization changes during catheter ablation were indicative of ablation outcome.

High DF and low OI values, as measured from surface ECG, have been shown to predict likelihood of arrhythmia recurrence following catheter ablation (Szilágyi et al., 2018). It was demonstrated that using adaptive versions of DF and OI, that account for the non-stationarity of ECG signals, increased predictive performance (Buttu et al., 2016). This finding provided the motivation to evaluate the evolution of the IF, AOI, sampEn, and FWA values across the three ablation procedure steps outlined at the end of Sec 4.1.5, and for the patient groups outlined in Sec 4.1.2. We calculated the values of these four ECG organization indices on all 10-s ECG signal segments, and then averaged the values calculated on all segments for each patient belonging to the same ablation step, to calculate one mean value for each patient at each procedure step (pre-PVI, dur-PVI, and post-PVI).

To investigate the finer-grained temporal evolution of the IF and the AOI throughout step-wise catheter ablation, we calculated the multi-lead IF estimate, and the AOI on lead V_1 only, as this lead has been shown to be strongly correlated with right atrial activity (Petrutiu et al., 2006), for all 10-s signal segments in the dur-PVI and post-PVI ablation steps. For each patient, we then calculated the mean IF and mean AOI of each 10-s segment, to create a time

4 Spatiotemporal signal processing methods for 12-lead ECG

sequence of the mean IF and mean AOI values found for each 10-s signal segment. To test for the presence of a possible transition in the mean of the sequences, we used a statistical approach based on the principle of minimum description length (MDL) (Rissanen, 1978). We compared the MDL values obtained when two different models were used to model the sequence: (1) a model with two parameters (one mean and one variance), and (2) a model with three parameters (two local means, and one variance). To estimate the second model, all sample indices, except the first and the last, were tested as candidates for the index of the transition, with the two means computed using respectively the samples preceding and following the candidate index. The index which resulted in the smallest residual variance was then retained as the transition index. The MDL was computed as below:

$$\text{MDL} = N \log \hat{\sigma}^2 + k \log N \quad (4.11)$$

with N the number of 10-s signal segments, $\hat{\sigma}^2$ the variance estimate, and k the number of parameters, i.e., $k = 2$ for the first model, and $k = 3$ for the second model. The MDL values obtained for the first and second models were compared, and if the MDL for the first model was smaller than that of the second, no mean transition was considered to have taken place. If the MDL for the second model was smaller than that of the first, a significant transition was considered to be present at the retained index. We quantified the significant transitions as follows:

$$\begin{aligned} \text{absolute change} &= y - x \\ \text{relative change} &= \frac{2(y - x)}{(y + x)} \end{aligned} \quad (4.12)$$

where y was the mean value of the signal segment IF and AOI values after the retained index, and x was the mean value before the retained index. An example of the test applied to two sequences, one found to have a transition and one without, is shown in Fig. 4.5.

Following the analysis of the temporal evolution of the IF and AOI parameters throughout stepwise catheter ablation, we examined the temporal evolution in the post-PVI procedure step only, to see whether different patterns could be found not only between the different patient groups, but also between the different types of atrial arrhythmia recurrence observed during the clinical follow-up period. For each available patient, we created temporal sequences of mean IF, AOI, sampEn, and FWA values of each 10-s signal segment, as was done for the IF and AOI above, but in this case only using signal segments labeled post-PVI. We applied the MDL statistical test described in Eq. 4.11, and placed the sequences separately into one of the following three categories, according to the type of transition reported by the MDL test: (i) **Type 1.** AF organization increases. For IF sequences, this is indicated by negative transitions, since decreasing frequency indicates an increase in AF cycle length, which indicates a more organized arrhythmia. For sampEn, this is also indicated by negative transitions, since lower sampEn values indicate less complexity and more regularity in time. For AOI and FWA sequences, this is indicated by positive transitions. (ii) **Type 2.** AF organization decreases. For IF sequences, this is indicated by positive transitions since increasing frequency indicates

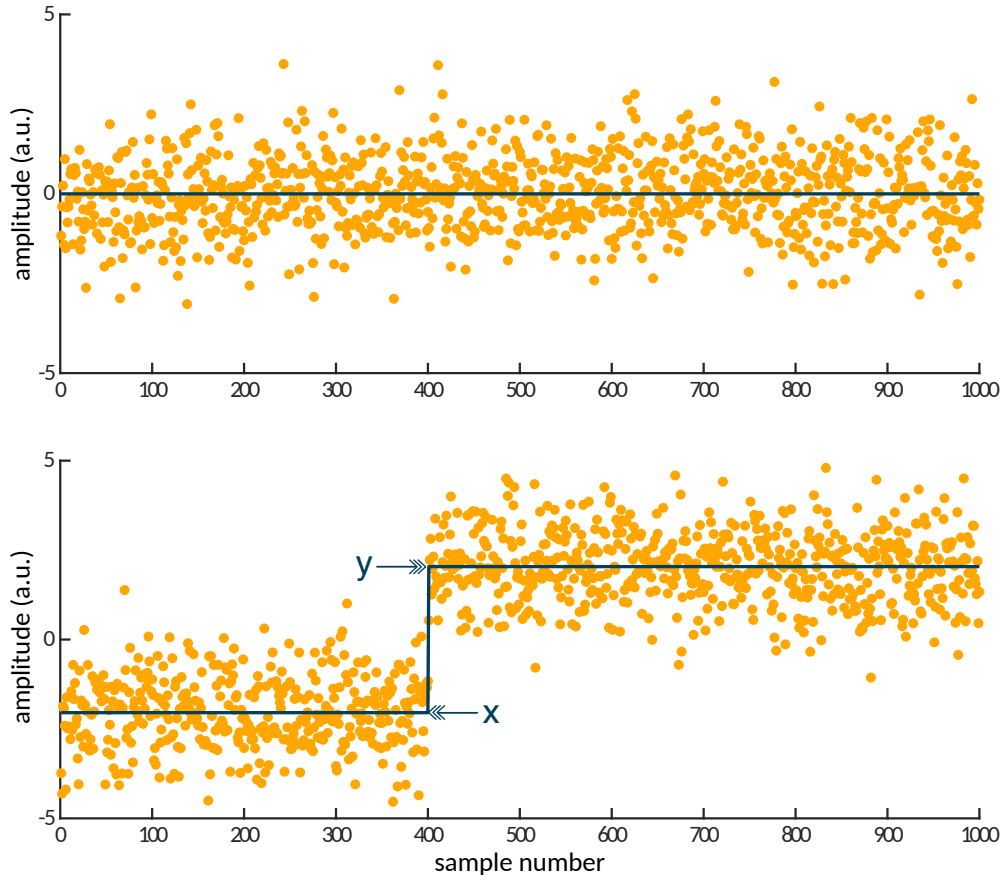


Figure 4.5: **Minimum description length.** Illustrative example of MDL test. Top panel: Sequence of random values in which the MDL test found no transition. Bottom panel: Sequence of random values, plus step function, in which the MDL test found a transition at the step index, with x the mean value before the transition, and y the mean value after the transition.

shorter AF cycle length. For sampEn, this is also indicated by positive transitions. For AOI and FWA sequences, this is indicated by negative transitions. (iii) **Type 3.** No changes in AF organization, indicated by no transitions in the sequences. The absolute and relative changes described in the previous section were also calculated for all sequences falling into the **Type 1** and **Type 2** categories.

4.1.7 STATISTICAL ANALYSIS

All numerical values are expressed as median and interquartile range (IQR). ECG-based organization index values described in Sec. 4.1.5 were compared across the three patient groups for all chest leads using the Kruskal-Wallis test. Amplitudes of post-PVI relative percent changes across the three patient groups (LTN, LTR, and NLT) as well as by type of recurrence (AT/AFL or AF) were also compared using the Kruskal-Wallis test. Statistical comparisons for categorical

4 Spatiotemporal signal processing methods for 12-lead ECG

variables measured using patient counts were performed using Fisher's exact test. Statistical significance was considered for $p < 0.05$.

4.2 RESULTS

4.2.1 STUDY POPULATION

A total of 40 patients with persistent AF were included in this study. Clinical characteristics for all patients are summarized in Table 4.1. The procedural endpoint was achieved in 28 patients (70%). AF was not terminated in the remaining 12 patients (NLT group), all of whom experienced an arrhythmia recurrence during follow-up. For patients in whom the procedural endpoint was reached, 8 (20%) remained in sinus rhythm (LTN group) throughout the follow-up period following a single procedure. Arrhythmia recurrence was observed in the remaining 20 patients (LTR group). In the LTR and NLT groups, recurrence occurred as AF ($n = 7$) and atrial tachycardia or atrial flutter ($n = 25$) on average 7 ± 10 months after the index procedure. Note that the sustained AF duration of the NLT group (median [IQR]: 22 [14; 39] months) was significantly longer than that of the LTN and LTR groups (20 [10; 24] and 13 [12; 24] months, respectively). The cumulative ablation time was also significantly different for each group, being the longest for the NLT group (76 [61; 81] min.), followed by the LTR group (55 [50; 60] min.). The mean follow-up duration for the study population was 32 ± 14 months, and at the end of the follow-up period, 34 (85%) patients were in sinus rhythm without (28/32, 82%) and with amiodarone (6/34, 18%), with a mean number of 2 ± 1 ablation procedures per patient.

4.2.2 ECG ORGANIZATION INDICES BEFORE AND DURING ABLATION

Figure 4.6 shows IF values for all patients at pre-PVI, dur-PVI, and post-PVI, and grouped as LTN, LTR, or NLT, to analyze both differences between patient groups and within the same patient group at different procedure steps. Figure 4.7 reports the same information for the AOI values calculated on leads V_1 , V_3 , V_4 , and V_{6b} . The values calculated on leads V_2 and V_5 did not show statistical significance. Median IF values observed in the LTN and LTR patient groups were significantly smaller ($p < 0.01$) than those observed in the NLT patient group at pre-PVI and dur-PVI. Significant differences at all steps were observed between the LTN and NLT patient groups only on lead V_1 . Other leads displayed varying significant differences between different combinations of groups and ablation steps. Significant differences between the LTN and NLT and the LTR and NLT groups in the same procedure step were observed only on V_{6b} , post-PVI. No significant differences were observed between the IF and AOI calculated at the pre-PVI, dur-PVI, and post-PVI ablation steps within a single patient group (LTN, LTR, or NLT). No significant differences could be observed between patient groups, nor within the same group between procedure steps for the sampEn and FWA indices. Together, these results suggest that patients in whom catheter ablation did not successfully terminate AF displayed significantly lower levels of AF organization both prior to and throughout the ablation procedure. In the

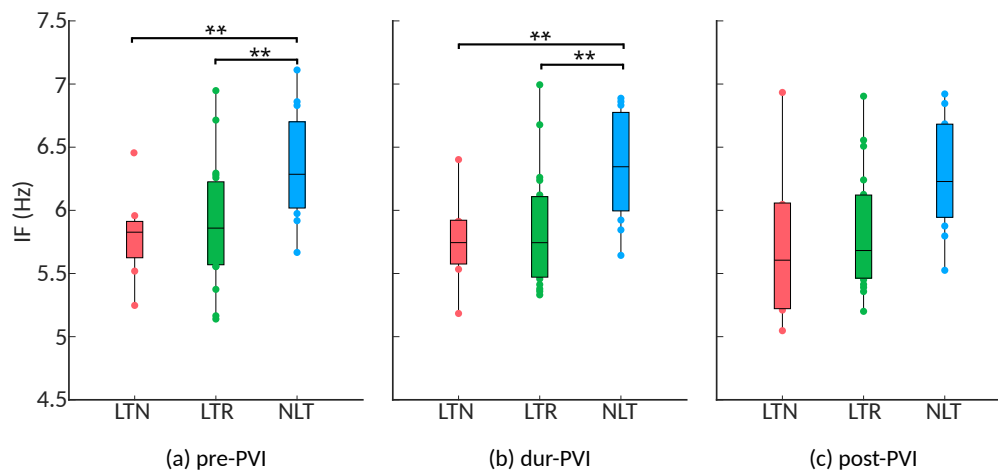


Figure 4.6: **Instantaneous frequency by group and step.** IF at (a) pre-PVI, (b) dur-PVI, and (c) post-PVI, for all patient groups. Significant differences between groups at each ablation step are indicated: ** $p < 0.01$.

following sections, the AOI, sampEn, and FWA indices will be reported only for lead V_1 , as this was the lead which displayed the most consistent significant differences between groups.

4.2.3 TEMPORAL IF AND AOI EVOLUTION THROUGHOUT STEPWISE CATHETER ABLATION

Several examples showing transitions, or lack thereof, in the means of segment sequences reported by the MDL test are shown in Fig. 4.8. Using the MDL statistical test, a transition in the mean of the sequence of the combined dur-PVI and post-PVI segment IF values was observed in 33 out of 40 patients. A transition was observed in 7/8 LTN patients, of which 2 in dur-PVI segments, and 5 in post-PVI segments. A transition was observed in 16/20 LTR patients, of which 6 dur-PVI and 10 post-PVI. Finally, a transition was observed in 10/12 NLT patients, of which only 1 dur-PVI and 9 post-PVI. These results suggest that stepwise catheter ablation led to changes in AF dynamics in most patients; however, no significant association was found between the timing of the change (dur-PVI or post-PVI) and the different patient groups.

4.2.4 TEMPORAL EVOLUTION OF AF ORGANIZATION POST-PVI

Atrial f-waves were not consistently observed in the post-PVI ECG signals of three patients. Since this precluded reliable f-wave extraction for a sufficient number of 10-s signal segments, the data from these patients were excluded from this part of the analysis. Additionally, two LTN patients reached the procedural endpoint dur-PVI; therefore, post-PVI analysis was not feasible. Figure 4.9 shows examples of the three types of AF organization outlined in Sec. 4.1.6 for IF and AOI (Type 1: increasing organization; Type 2: decreasing organization; Type 3: no change in organization). Tables 4.2 and 4.3 show relative percent changes in respectively IF

4 Spatiotemporal signal processing methods for 12-lead ECG

and AOI, and sampEn and FWA, post-PVI, according to ablation outcome. Ablation within the left atrium (CFAE and linear ablation) led to increases in AF organization in most patients [Type 1: decrease in IF, 24/35 (68%); increase in AOI, 25/35 (71%); decrease in sampEn, 21/35 (60%)]. Increases in FWA were observed in 16/35 (46%) of patients. However, no association between Type 1 transitions and ablation outcomes was found. No significant differences were observed in the relative percent changes in the IF, AOI, sampEn, and FWA epoch sequences between the LTN, LTR, and NLT patient groups.

Table 4.2: Relative changes in IF and AOI post-PVI, according to ablation outcomes, expressed as median with [25th; 75th] percentiles. Patient counts and percentages of total count are indicated for each type of transition.

	LTN (<i>n</i> =6)		LTR (<i>n</i> =18)		NLT (<i>n</i> =11)	
	IF	AOI	IF	AOI	IF	AOI
Rel. change %	-2 [-4; 16]	15 [11; 18]	-6 [-7; 0]	14 [0; 30]	-2 [-5; -1]	10 [2; 13]
Type 1	3 (50%)	5 (83%)	13 (72%)	12 (67%)	8 (73%)	8 (73%)
Type 2	2 (33%)	1 (17%)	3 (17%)	3 (17%)	1 (9.1%)	1 (9.1%)
Type 3	1 (17%)	0	2 (11%)	3 (17%)	2 (18%)	2 (18%)

Table 4.3: Relative changes in sampEn and FWA post-PVI, according to ablation outcomes, expressed as median with [25th; 75th] percentiles. Patient counts and percentages of total count are indicated for each type of transition.

	LTN (<i>n</i> =6)		LTR (<i>n</i> =18)		NLT (<i>n</i> =11)	
	sampEn	FWA	sampEn	FWA	sampEn	FWA
Rel. change %	-3.8 [-4.7; 0]	-0.21 [-16; 13]	-4.3 [-7.5; 0]	0 [-2.5; 14]	-2.1 [-3; 0]	3.7 [0; 5.7]
Type 1	4 (67%)	3 (50%)	11 (61%)	7 (39%)	6 (55%)	6 (55%)
Type 2	1 (17%)	3 (50%)	0	5 (28%)	0 (0%)	2 (18%)
Type 3	1 (17%)	0	7 (39%)	6 (33%)	5 (45%)	3 (27%)

Table 4.4 shows the distribution of the three categories of temporal evolution in the IF and AOI sequences, according to the form of recurrence observed during the follow-up period after a single ablation procedure. Increases in AF organization during ablation, as indicated by a decrease in IF and/or increase in AOI, were more frequent in patients whose arrhythmia recurred as atrial tachycardia or atrial flutter, than in patients whose arrhythmia recurred as AF [atrial tachycardia/atrial flutter vs AF, Type 1: decrease in IF, 19/23 (83%) vs. 2/6 (33%); increase in AOI, 18/23 (78%) vs 2/6 (33%); $p < 0.05$]. Median relative percent changes in IF and AOI showed significantly greater amplitudes in atrial tachycardia/atrial flutter recurrences than in AF recurrences (IF: -5 [-7; -2]% vs. 0 [-2; 0]%; AOI: 13 [5; 29]% vs 0 [-6; 8]%; $p < 0.05$). This suggests that if changes in AF organization occurred post-PVI, then recurrence occurred as an organized arrhythmia, such as atrial flutter or atrial tachycardia. However, little or no post-PVI changes in AF organization were associated with recurrence as a disorganized arrhythmia, i.e., AF. No results of statistical significance could be found between patient groups, nor between types of arrhythmia recurrences, for the sampEn and FWA variables.

Table 4.4: Relative changes in IF and AOI post-PVI, according to form of recurrence, expressed as median with [25th; 75th] percentiles. Patient counts and percentages of total count are indicated for each type of transition.

^aAT/AFL vs AF ($p < 0.05$).

^bType 1 transition associated with recurrence ($p < 0.05$).

	AT/AFL ($n = 23$)		AF ($n = 6$)	
	IF	AOI	IF	AOI
Rel. change %	-5 [-7; -2] ^a	13 [5; 29] ^a	0 [-2; 0] ^a	0 [-6; 8] ^a
Type 1	19 (83%) ^b	18 (78%)	2 (33%)	2 (33%)
Type 2	3 (13%)	2 (9%)	1 (17%)	2 (33%)
Type 3	1 (4%)	3 (13%)	3 (50%)	2 (33%)

4.3 DISCUSSION

The exploratory study presented in this chapter contains several findings, including: (i) patients in whom ablation failed to terminate AF and to restore long-term sinus rhythm displayed the lowest AF organization level as indicated by the highest IF and lowest AOI values, (ii) IF and AOI mean value transitions were more likely to occur post-PVI than dur-PVI, and (iii) AF reorganization during post-PVI was associated with organized arrhythmia recurrence as AT/AFL, while lack of AF reorganization was associated with disorganized arrhythmia recurrence as AF.

It has been suggested previously that high baseline DF and low OI values measured from the surface ECG are likely to predict arrhythmia recurrence after catheter ablation (Murase et al., 2020; Okumura et al., 2012; Szilágyi et al., 2018). In this study, an analysis of the median trends at each of the pre-PVI, dur-PVI, and post-PVI ablation steps confirmed higher IF and lower AOI

4 Spatiotemporal signal processing methods for 12-lead ECG

values in NLT patients at pre-PVI, for whom the stepwise catheter ablation procedure failed to terminate persistent AF. This analysis also revealed that the higher IF and lower AOI values persisted across the dur-PVI and post-PVI steps. However, we found that for any individual patient group (LTN, LTR, or NLT), the median IF and AOI values did not change significantly between the pre-PVI, dur-PVI, and post-PVI steps.

The temporal evolution of surface ECG and intracardiac EGM measures throughout catheter ablation has been previously studied. In (Forclaz et al., 2011), AF cycle length was observed to increase between progressive steps of post-PVI ablation in persistent AF patients, regardless of whether the stepwise catheter ablation procedure successfully terminated their AF. However, an increase in a temporal regularity index similar to the OI was found only in patients with AF termination. In addition, patients with the largest increases in the temporal regularity index more commonly experienced long-term freedom from arrhythmia during a follow-up period. A progressive increase in AF cycle length was observed at subsequent ablation steps in Calò et al. (2006), and a gradual increase in AF cycle length between ablation steps was associated with AF termination by ablation in O'Neill et al. (2006). Lankveld et al. (2016) investigated temporal changes in the values of DF estimated from 10-s ECG recordings obtained after each step performed in stepwise catheter ablation, for patients with persistent AF. An overall decrease in DF was found after each ablation step, with the highest values observed pre-ablation, decreasing following PVI, and further decreasing following left atrial ablation. The exact changes in the DF depended on whether left and/or right-sided ablation were performed. These findings are suggestive of a progressive increase in AF organization throughout ablation; however they do not reveal, at the level of surface ECG, which ablation steps may contribute most to this increase. Our study investigated this by extending the analysis to include many ECG epochs for each of the pre-PVI, dur-PVI, and post-PVI ablation steps, rather than only one segment after each procedure step as in Lankveld et al. (2016). In the present study, when the temporal evolution of AF complexity parameters dur-PVI and post-PVI was estimated statistically using a test for mean value transition based on the principle of MDL, IF and AOI mean transitions were observed in a large majority of patient epoch sequences. It was also observed that most of these transitions occurred in the post-PVI step. When mean value transitions were estimated on sequences composed of only post-PVI epoch means, most of them could be categorized as increasing AF organization, i.e., negative transitions in the IF sequences, indicative of a lengthening in the AF cycle length, and positive transitions in the AOI sequences. This suggests that it was CFAE and left atrial ablation, rather than PVI, that was associated with increasing AF organization, and therefore that AF substrate was more likely located in the left atrium, and not the pulmonary veins. The study performed in (Haïssaguerre et al., 2005) found that the largest increments in the gradual prolongation of the AF cycle length were observed after ablation of the pulmonary vein-left atrium junction, inferior left atrium/coronary sinus interface, and left atrial appendage. Our study suggests that this effect may be observed at the surface ECG level. The differences in the amplitudes of the transitions were not significantly linked to the LTN, LTR, and NLT patient groups. However, it was found that increases in AF organization post-PVI occurred more often in LTR and NLT patients who had a recurrence of

atrial tachycardia or atrial flutter, both organized arrhythmias. In contrast, when no changes in AF organization were observed post-PVI, disorganized arrhythmia recurrence as AF was more common. These findings suggest that ECG-based AF organization indices could help to assess the risk of later recurrence in the form of atrial tachycardia or atrial flutter or AF after a single stepwise catheter procedure.

The potential applications of analyzing the temporal evolution of ECG parameters throughout catheter ablation are manifold, including further insight into the interaction of catheter ablation with local substrate and the efficacy of an ongoing ablation. The small population size in this study may limit its predictive power. In addition, because this was a single-center study in which a single operator performed all ablation procedures, results may not extend to other centers. Importantly however, the study included consecutive patients undergoing radio-frequency ablation procedures for treatment of persistent AF; therefore, no selection bias was introduced. Also limiting our study was the recording of ECG signals only while patients were under general anesthesia, as this may have affected atrial activity dynamics. However, patient response to stepwise ablation was assessed using relative mean transitions in temporal ECG-based organization indices throughout ablation, reducing bias that could have been introduced by varying patient responses to general anesthesia. Importantly, our study was intended to identify (before and during ablation) ECG-based biomarkers to characterize the relationship of the AF substrate to procedural and clinical outcomes. Our study is however missing a comparative analysis of suitable measures designed for intracardiac electrograms that would strengthen our results. A final limitation was the definition of the clinical endpoint as a successful ablation after a single procedure, which might minimize the success rate of stepwise catheter ablation after multiple procedures (Scherr et al., 2015), especially for persistent AF patients. Since most recurrences occurred as atrial tachycardia or atrial flutter, using single-procedure ablation success as a clinical endpoint was aimed at lowering the bias due to repeat ablation procedures. The high recurrence as atrial tachycardia or atrial flutter may be a consequence of the extensive ablation in the index procedure, which included PVI, defragmentation, and lines. Any remaining gaps in these lesions may favor the emergence of atrial tachycardia or atrial flutter. Importantly, recurrence occurring as atrial tachycardia or atrial flutter may be an expression of both the ablation extent and the level of bi-atrial remodeling (Yang et al., 2017).

This study suggests that non-invasive ECG measures may be used pre-PVI to show the lowest levels of AF organization in NLT patients who do not respond well to stepwise catheter ablation. These measures are not however suitable for predicting which patients will experience an arrhythmia recurrence following a single ablation procedure.

Additionally, investigation of the temporal evolution of ECG-based indices during stepwise catheter ablation bears merit for consideration as a clinical tool to assess the progression of ongoing ablation procedures. Ablation following PVI within the left atrium (CFAEs and linear ablation) could be associated with increasing AF organization, particularly in those patients who may experience an arrhythmia recurrence as atrial tachycardia or atrial flutter rather

4 Spatiotemporal signal processing methods for 12-lead ECG

than AF. Patterns of temporal evolution in adaptive ECG measures could not be shown to distinguish persistent AF patients who did or did not experience an arrhythmia recurrence.

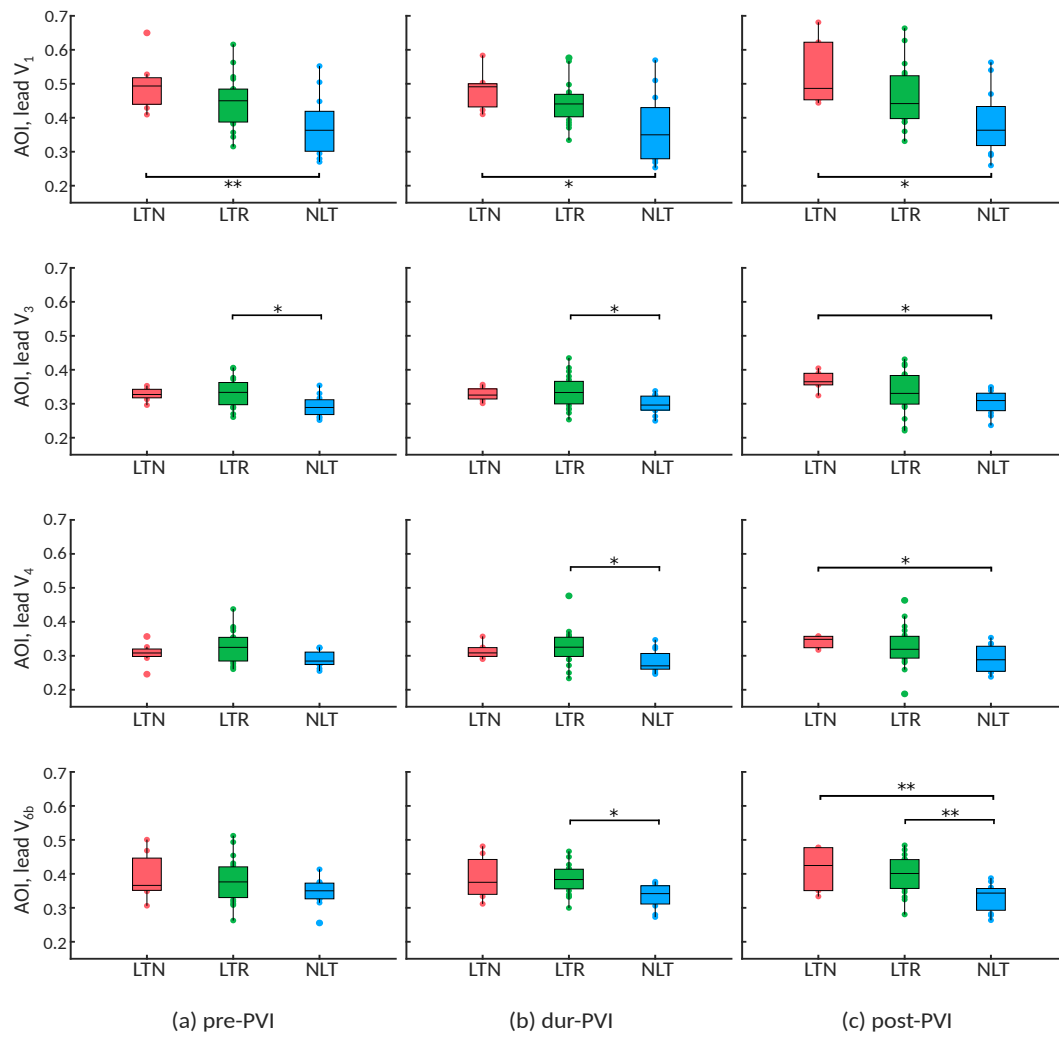


Figure 4.7: **Adaptive organization index by group and ablation step.** AOI calculated on leads V_1 , V_3 , V_4 , V_{6b} at (a) pre-PVI, (b) dur-PVI, (c) post-PVI for all patient groups. Significant differences between groups at each ablation step are displayed: * $p < 0.05$, ** $p < 0.01$. Leads V_2 and V_5 not shown, as results were not significant on these leads.

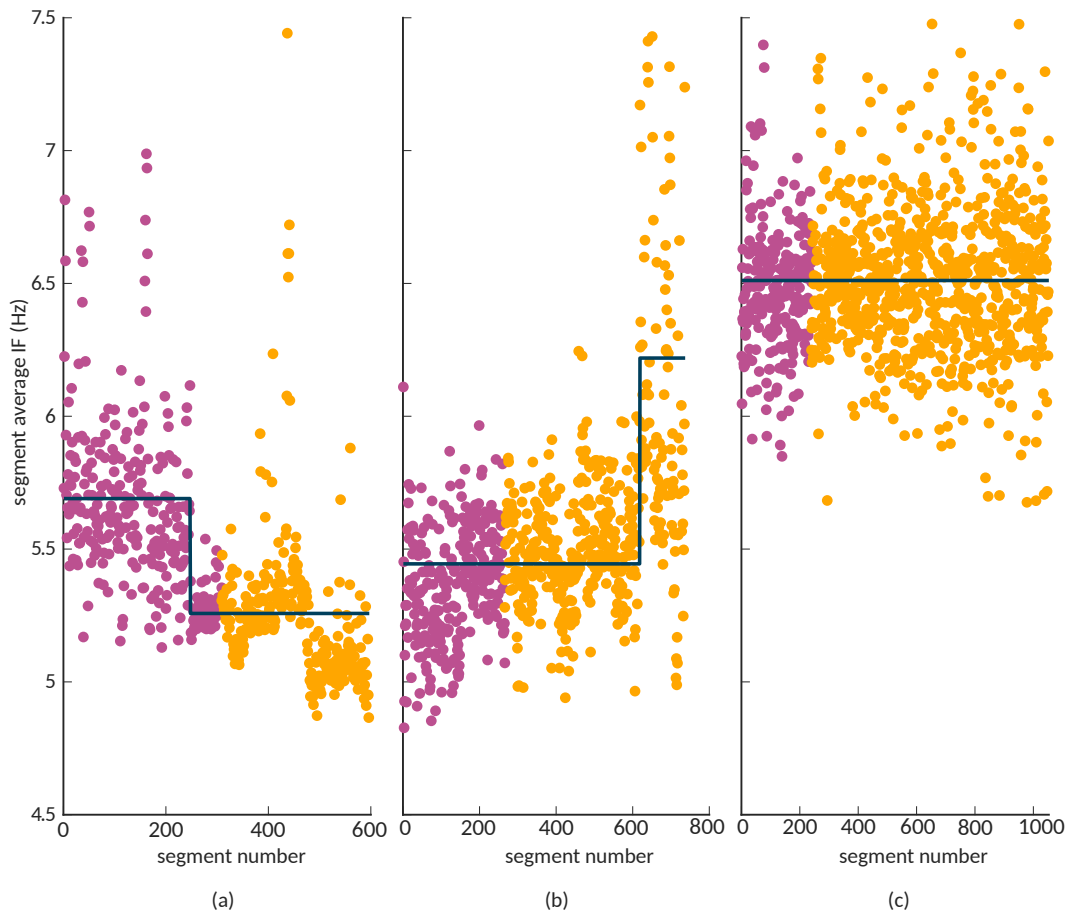


Figure 4.8: **Instantaneous frequency ablation intra-step transitions.** Sequences of the average 10-s ECG segment values of IF for three patients. (a) shows a negative transitions, with a relative change of -0.08%. (b) shows a positive transition, with a relative change of 0.13%. (c) shows a sequence where no transition in the mean value was observed.

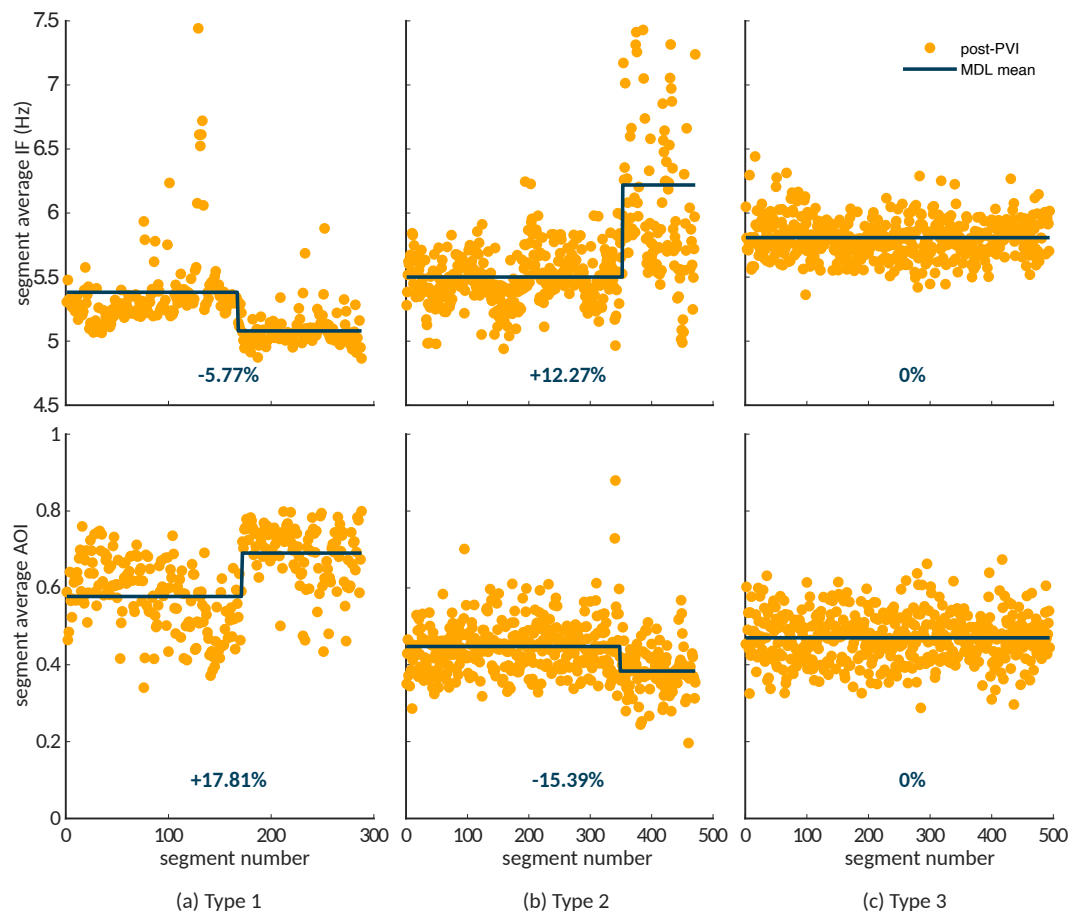


Figure 4.9: Three types of changes in AF organization. (a) Examples of Type 1, increasing AF organization, indicated by a negative IF transition in the first row, and a positive AOI transition in the second row. (b) Examples of Type 2, decreasing AF organization, indicated by a positive transition in the mean IF signal segment values, and a negative transition in the AOI segment sequence. (c) Examples of Type 3, no change in AF organization, indicated by no transitions in either sequence.

5

HEART RATE VARIABILITY ANALYSIS IN ATRIAL FIBRILLATION FOR ASSESS- ING RESPONSE TO CATHETER ABLA- TION

In healthy individuals, the heart rate (rate of ventricular activation) is a function of both the intrinsic rate of the sinus node and the influence of the autonomic nervous system.¹ The heart rate thus *varies* to respond to the body's physiological needs, slowing down at times of rest, and speeding up during times of physical exertion. Even when the body's physiological needs are stationary, the amount of time elapsed between successive heartbeats fluctuates slightly, and this fluctuation is referred to as heart rate variability (HRV). Heart rate variability can be quantified using RR-interval sequences, which show the times elapsed between successive R-waves of QRS complexes recorded on surface ECG. An example of an RR-interval sequence associated with a signal recorded during sinus rhythm is shown in Fig. 5.1a. Quantifying HRV (via RR-interval sequences), may be used to indicate various physiological measures of well-being, from sleep quality and level of fitness to diabetes and anxiety, with the complete absence of HRV indicating disease (Shaffer et al., 2014). In individuals with AF, ventricular activation, and thus the heart rate, is influenced largely by the ectopic activation of the atria (Cohen et al., 1983), rather than the intrinsic rate of activation of the sinus node.² An RR-interval sequence associated with an ECG signal recorded during atrial fibrillation is shown in Fig. 5.1b. It can be seen that the RR-interval sequence in AF looks much more random than the sequence in sinus rhythm.

The HRV in AF, quantified using RR-interval sequences, has been shown to be related to atrial fibrillatory rate (Corino et al., 2013). Importantly atrial fibrillatory rate has itself been associated with clinical outcomes and physiological characteristics in patients with AF, i.e., probability of spontaneous AF termination (Nilsson et al., 2006), AF termination by CA (Haïssaguerre et al., 2004), better response to antiarrhythmic drugs (Langberg et al., 1998) and to electrocardioversion (Holmqvist et al., 2006). However, determining the atrial fibrillatory rate noninvasively requires extraction of the atrial component from the ECG, which inevitably remains contaminated with artifacts from the ventricular response, and its

¹For a review of the relationship between sinoatrial node activation, autonomic nervous system, and heart rate, see Chapter 2.

²For a review of the origin of ventricular activation in AF, see Chapter 3.

5 Heart rate variability analysis in atrial fibrillation for assessing response to catheter ablation

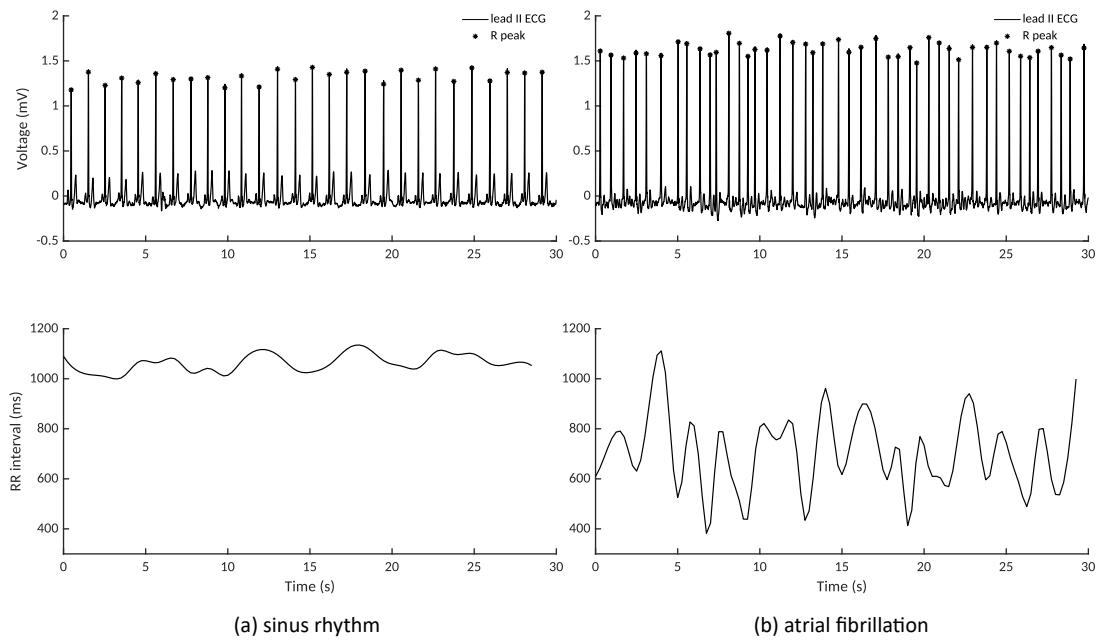


Figure 5.1: RR-intervals. Shown in the top row are ECG signals recorded on lead II, with annotated R peaks (*), and the resulting interpolated RR-interval sequences are shown in the bottom row, for (a) sinus rhythm, and (b) atrial fibrillation.

exact morphology depends widely on the chosen extraction algorithm (Langley et al., 2006; Sörnmo et al., 2018). Direct analysis of the ventricular response via RR-interval sequence analysis has the potential to be much more robust and consistent from a signal processing perspective, since RR-interval sequences can be easily and reliably extracted from even noisy ECGs. However, very few studies have quantified HRV in AF among different patient groups to investigate their relationship to response to catheter ablation treatment.³ Measuring HRV in AF does not however come without challenges, since RR-interval sequences recorded in AF often resemble white noise (Horan and Kistler, 1961) and therefore cannot be analyzed using traditional time and frequency domain methods like correlation, moving averages, or spectral analysis, i.e., methods that were explored in Chapter 4 for direct analysis of the atrial component of recorded ECG signals.

In the largest study to investigate the relationship between HRV and atrial fibrillatory rate, several HRV metrics, including the percentage of successive RR-intervals which differ by more than 20 or 50 ms (pNN20, pNN50), the standard deviation of normal RR-intervals in a sequence (SDNN), the root-mean-square of successive RR-interval differences (RMSSD), and approximate entropy were shown to be related to atrial fibrillatory rate, with the degree of correlation depending on whether patients were treated with anti-arrhythmic drugs (Corino et al., 2013). These results suggest that despite the random nature of the RR-interval sequences in AF, HRV metrics may be able to capture underlying trends in the atrial fibrillatory rate. Additionally, several cardiovascular physiology studies have shown success using nonlinear

³See Chapter 3 for an overview of catheter ablation and its role in treating AF.

dynamical analysis, and especially recurrence quantification analysis (RQA) for RR-interval sequences (Zbilut et al., 2002). While RQA was initially developed for analyzing dynamical systems demonstrating chaos, because it imposes no rigid constraints on data set size, stationarity, or statistical distribution, the technique may be suitable for physiological time series such as RR-intervals (Webber Jr and Zbilut, 1994) extracted from ECG recorded in AF, to reveal dynamical behaviors that are not obvious in the original time series, and not detectable by standard linear (time-domain and spectral) techniques.

This chapter presents a study in which a variety of HRV metrics, including the time-domain and entropy measures from Corino et al. (2013), and RQA, were computed for a persistent AF population, before and at the end of ablation, to (1) investigate whether changes in the ventricular response could be quantified before and at the end of catheter ablation procedures among patients grouped by CA outcome; (2) investigate whether HRV measured before ablation was associated with ablation outcome, and if so, to what extent it was predictive of procedural and clinical success, i.e., AF termination and long-term maintenance of sinus rhythm. This chapter therefore falls within the framework of providing noninvasive tools designed to characterize which patients are most likely to have successful catheter ablation procedures. An introduction to recurrence in dynamical systems will be given in Sec. 5.1. In Sec. 5.2, the preprocessing methods and HRV analysis will be presented. The results will be presented in Sec. 5.3, and their implications will be discussed in Sec. 5.4.

5.1 RECURRENCE IN A DYNAMICAL SYSTEM

Recurrence quantification analysis (RQA) is a method of nonlinear data analysis proposed to investigate dynamical systems. It is used to quantify the number and duration of recurrences of a phase space trajectory of a dynamical system. Recurrences of system trajectories in phase space can provide important clues about the systems from which they are derived. Recurrent plots (RP) provide a visual representation of recurrences, from which RQA can be performed to quantify the degree to which recurrences are present in the system. A brief introduction to this method of analysis, which does not make any assumptions about the linearity nor the stationarity of the data, will be given below.

5.1.1 DYNAMICAL SYSTEMS, PHASE SPACES AND THEIR TRAJECTORIES

The RR-interval sequence can be seen as an observable time series measurement resulting from a dynamical system, or a system whose *state* or *phase* evolves over time (Marwan et al., 2007). A *phase space trajectory* is a set of states compatible with starting from one particular initial condition. It is located in the full phase space, which represents the set of states compatible with starting from any initial condition. In a phase space, every *degree of freedom*, or dimension, represents an axis of a multidimensional space. Every possible state of the system (or allowed combination of values of the system's parameters) constitutes a *point* in the multi-dimensional phase space. Starting from a particular initial condition, the system's

evolving state over time traces a path, called a phase space trajectory through the multi-dimensional space. The phase space may be low dimensional, for example the trajectory in a one-dimensional system is called a *phase line*, and the trajectory in a two dimensional system is called a *phase plane*. An example of a two dimensional system would be the position and velocity of a pendulum. An example of a higher dimensional phase space would be one describing the motion of many molecules in a gas, with a separate dimension required for each particle's x, y, and z positions and momenta.

A dynamical system is given by (1) a phase space; (2) a continuous or discrete time; (3) a time-evolution law. For a d -dimensional system, the state of the system at a particular time t can be specified by d parameters, which form the vector $\mathbf{x}(t)$:

$$\mathbf{x}(t) = [x_1(t), x_2(t), \dots, x_d(t)]^T \quad (5.1)$$

in the d -dimensional phase space of the system. For example, in the case of a harmonic oscillator, the phase space would be two dimensions, consisting of the parameters position and velocity. The collection of vectors $\mathbf{x}(t)$ for $t = 1, \dots, N$ defines a phase space trajectory.

However, in experimental settings, it is rare for all parameters of the state vectors to be known or measurable. Instead, only a time-discrete measurement of one observable variable, such as the RR-interval sequence, is known, yielding a scalar and discrete time series:

$$u_i = u(i\Delta t), i = 1, \dots, N \quad (5.2)$$

and Δt is the sampling rate of the measurement. In this case, a phase space of an appropriate dimension must be *reconstructed*. The most commonly used method is time-delay embedding (Takens, 1981):

$$\mathbf{x}_i^m = \{u_i, \dots, u_{i+(m-1)\tau}\}_{i=1}^N \quad (5.3)$$

where m is the embedding dimension and τ is the time delay, which must be chosen appropriately. The reconstructed phase space trajectory composed of vectors $\{\mathbf{x}_i\}_{i=1}^N$ may be considered to represent the same dynamical system as the original, but unavailable trajectory, and therefore can be used to analyzed recurrences of a dynamical system represented by a univariate time series. For the remainder of the discussion, a fixed embedding dimension m and delay τ are assumed, therefore, these parameters will be dropped from definitions for simplicity.

5.1.2 RECURRENCE PLOT

The recurrence plot (RP) is a tool that measures recurrences of a trajectory $\mathbf{x}_i \in \mathbb{R}$ in phase space. Suppose we have a trajectory of the embedded vectors $\{\mathbf{x}_i\}_{i=1}^N$ of a system in its phase space. The components of the vectors of the trajectory could be the position and velocity of a pendulum, or quantities such as temperature, air pressure, and humidity, among others, for the atmosphere. The behavior of the dynamical system is described by a series of state vectors

5.1 Recurrence in a dynamical system

which make up a trajectory in an abstract mathematical space, with N discrete time steps. The corresponding recurrence plot, represented by the matrix $\mathbf{R}_{i,j}$, is given by the relation between the state vectors \mathbf{x}_i and \mathbf{x}_j of the trajectory at time steps i and j , for $i, j = 1, \dots, N$:

$$\mathbf{R}_{i,j}(\epsilon) = \Theta(\epsilon - \|\mathbf{x}_i - \mathbf{x}_j\|) \quad (5.4)$$

where N is the number of measured time steps, ϵ is a threshold distance, $\Theta(\cdot)$ is the Heaviside function, and $\|\cdot\|$ is a norm (L_1, L_2, L_∞). An equivalent representation is the following:

$$\mathbf{R}_{i,j}(\epsilon) = \begin{cases} 1 & \text{if } \mathbf{x}_i \approx \mathbf{x}_j \\ 0 & \text{if } \mathbf{x}_i \not\approx \mathbf{x}_j \end{cases} \quad i, j = 1, \dots, N \quad (5.5)$$

where $\mathbf{x}_i \approx \mathbf{x}_j$ means equality according to the chosen norm up to an error ϵ . Some minimum error value ϵ is necessary because real dynamical systems do not recur exactly to a formerly visited state, but only approximately. The matrix $\mathbf{R}_{i,j}$ compares state vectors of the system at times i and j , revealing when similar states of the underlying system occur. Looking at these patterns of recurrence allows studying dynamical systems and their trajectories.

The recurrence plot is obtained by plotting the recurrence matrix (Eq. 5.4 and Eq. 5.5), using different colors to correspond to its binary entries, usually using black dots at the coordinates (i, j) if $\mathbf{R}_{i,j} = 1$, and a white dot if $\mathbf{R}_{i,j} = 0$. The axes of the recurrence plot are time axes, and their directionality is rightwards and upwards, by convention. Since $\mathbf{R}_{i,i} = 1 \mid_{i=1}^N$ by definition, the recurrence plot always has an upward right black diagonal line, called the line of identity. Additionally, the recurrence plot is symmetric with respect to the main diagonal, $\mathbf{R}_{i,j} = \mathbf{R}_{j,i}$.

Finally, the threshold parameter ϵ must be chosen appropriately. If it is too small, almost no points would be considered to recur, and nothing could be learned from the recurrence structure of the underlying system. If ϵ is chosen too large, too many points are included. Several guidelines for selecting an appropriate ϵ value have been proposed, specifically that it should be a few percent, but not exceed 10% of the phase space diameter (Zbilut and Webber Jr, 1992), often estimated as the standard deviation of the time series to be embedded.

Recurrence plots are used to visualize trajectories in phase space, which is especially advantageous for high dimensional systems. They can be used to gain insight regarding the time evolution of the phase space trajectories, since typical patterns in a recurrence plot can often be linked back to specific behavior of the system. Several large scale patterns (typology) can be observed in recurrence plots; some of the most common ones are demonstrated in Fig 5.2. Homogeneous recurrence plots (Fig. 5.2a) are associated with stationary random time series, displaying few and scattered recurrences, compared to the time spanned by the recurrence plot. Periodic (Fig. 5.2b) and quasi-periodic recurrence plots have diagonal lines off the main diagonal, representing an underlying periodic dynamic, as the trajectory revisits the same part of the phase space repeatedly. Drift (Fig. 5.2c) occurs in a system with slowly varying parameters, i.e. non-stationary systems. Very little recurrence is visible far from the line of identity. Disrupted (Fig. 5.2d) or abrupt changes in the dynamics of a system can cause white

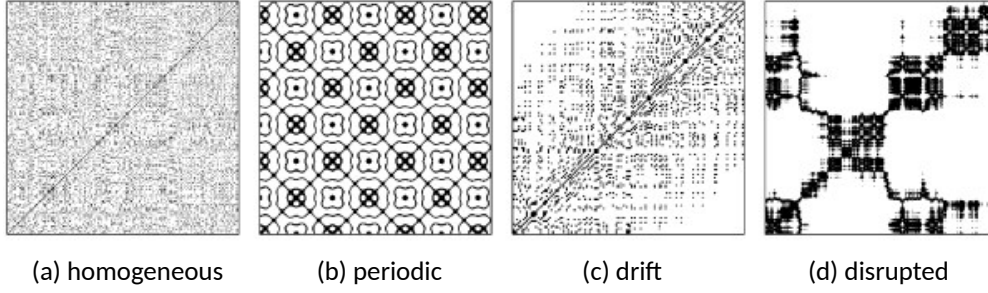


Figure 5.2: **Recurrence plot patterns.** (a) homogeneous (uniformly distributed white noise). (b) periodic (super-positioned harmonic oscillations). (c) drift (logistic map corrupted with linearly increasing term). (d) disrupted (Brownian motion). Figure adapted from Marwan et al. (2007).

areas or bands in the recurrence plot. Additionally, smaller scale structures, including single dots, and the formation of diagonal, vertical and horizontal, and bowed lines give indications about recurrence behaviour of dynamical systems. Single, isolated recurrence points occur if states are rare, or if they persist for only a short amount of time. Diagonal lines occur when a segment of the trajectory runs almost in parallel to another segment for l consecutive time units (periodicity). Vertical (or horizontal) lines indicate consecutive time steps when the state does not change very much, since consecutive states remain close to some initial state, i.e., $\{\mathbf{x}_i \approx \mathbf{x}_j, \mathbf{x}_i \approx \mathbf{x}_{j+1}, \dots, \mathbf{x}_i \approx \mathbf{x}_{j+v-1}\}$.

5.1.3 RECURRENCE QUANTIFICATION ANALYSIS

Recurrence in a dynamical system refers to points at which the phase space trajectory of the dynamical system visits the same small region of the phase space. While the large-scale and small-scale structures of recurrence plots can often be seen visually, several measures have been proposed to quantify recurrence plot patterns like recurrence point density, and presence of diagonal and vertical lines. Such measures can be used to more precisely quantify the degree to which constructed recurrence plots exhibit homogeneous, periodic, drift, or disrupted properties. These measures, collectively called recurrence quantification analysis (RQA), can also be used to detect transitions in the dynamics of the system, for example chaos-order (Trulla et al., 1996), or even chaos-chaos transitions (Marwan et al., 2002). Several common RQA metrics will be described below. Note that these metrics depend on the parameters used to construct the recurrence plot. However, in their definitions, it is assumed that the recurrence plot was calculated using a fixed threshold ϵ , and fixed time delay embedding parameters m and τ .

The simplest RQA metric is the recurrence rate, or percent recurrence, called REC in this study. It is simply a measure of the density of points which are considered recurrence points

in the recurrence plot, but does not give any clues as to the structure of the recurrence points:

$$\text{REC} = \frac{1}{N^2} \sum_{i,j=1}^N \mathbf{R}_{i,j} \quad (5.6)$$

In the limit $N \rightarrow \infty$, REC corresponds to the probability that a state recurs to its ϵ -neighborhood in phase space. Several other RQA measures are based on a histogram, $P(l)$ of diagonal line lengths l in the recurrence plot:

$$P(l) = \sum_{i,j=1}^N ((1 - \mathbf{R}_{i-1,j-1})(1 - \mathbf{R}_{i+1,j+1})) \prod_{k=0}^{l-1} \mathbf{R}_{i+k,j+k} \quad (5.7)$$

Dynamic processes with uncorrelated, or weakly correlated, stochastic or chaotic behavior result in only single isolated recurrence points, whereas deterministic systems displaying periodicity result in longer diagonals in the recurrence plot. Therefore, a measure called determinism (DET) quantifies the ratio of recurrence points that form diagonal lines of at least length l_{\min} to all recurrence points:

$$\text{DET} = \frac{\sum_{l=l_{\min}}^N lP(l)}{\sum_{l=1}^N lP(l)} \quad (5.8)$$

The threshold l_{\min} in Eq. 5.8 excludes diagonal lines which are formed by the tangential motion of the phase space trajectory (since for $l_{\min} = 1$, $\text{DET} = 1$). Diagonally adjacent points for which $\mathbf{R}_{i,j} = 1$ form line segments; therefore, a diagonal line segment is distinct from individual recurrence points, indicating that the phase space trajectory recurs to the same state at least l_{\min} consecutive times, i.e., the state of the trajectory at times $i, i+1$ is repeated at times $j, j+1$. The determinism measure, as suggested by its name, indicates how predictable the system is. The length of the diagonal lines in the recurrence plot is related to how long states of the trajectory remain similar, therefore the reciprocal of the maximal diagonal line length L_{\max} (excluding the line of identity), called the divergence (DIV), is also a measure recurrence in the system:

$$\text{DIV} = \frac{1}{L_{\max}} \quad (5.9)$$

5.2 METHODS

The study population, stepwise ablation procedure, and ECG acquisition and basic preprocessing steps for the analyses presented in this chapter were as described in Sec. 4.1. For this study, patients were split into four groups, based on observed procedural and clinical ablation outcomes. For the procedural outcomes, the groups were as follows: (1) left-terminated (LT, $n = 28$), patients in whom AF terminated within the left atrium into sinus rhythm or atrial tachycardia during the ablation; (2) not terminated (NT, $n = 12$), patients in whom stepwise catheter ablation failed to terminate AF. For the clinical outcomes following ablation, the

5 Heart rate variability analysis in atrial fibrillation for assessing response to catheter ablation

groups were as follows: (1) sinus rhythm (SR, $n = 8$), patients who remained in sinus rhythm for the duration of the follow-up period; (2) arrhythmia recurrence (AR, $n = 32$), patients who experienced an arrhythmia recurrence during the follow-up period.

In the remainder of this section, the methods used for RR-interval sequence extraction and subsequent analysis will be described. Additionally, the statistical methods used to compare RR-interval sequences between patient groups, between BL and endABL steps within the same patient group will be presented.

5.2.1 RR-INTERVAL SEQUENCE EXTRACTION

To analyze (1) the degree to which HRV was associated with refractoriness to catheter ablation treatment, and (2) whether changes in HRV from BL to endABL could be observed using traditional and/or recurrence analysis methods, RR-interval sequences were required. The sequences were extracted from ECG signals recorded prior to and throughout the catheter ablation procedures. Two five-minute ECG signals were kept for each patient, one recorded at baseline (BL - prior to ablation), and one at the end of the ablation (endABL), recorded just prior to either AF termination (for LT patients) or cardioversion (for NT patients). Each five-minute ECG signal was divided into five segments of a length one-minute, to increase the number of data points on which to calculate HRV metrics. To extract the RR-intervals, R-peaks were detected from the ECG segments recorded on lead II, since this lead views the wave of electrical activation travelling from the right shoulder to the left leg,⁴ giving the best view of ventricular activation.

An R-peak detection algorithm was applied to the one-minute BL and endABL signal segments recorded on ECG lead II. The algorithm, called “Relative Energy,” was developed for impulse-like event detection in biomedical signals (Yazdani et al., 2017). The algorithm compares the mean energies in a narrow time interval and in a wide time interval centered on the same part of the signal. When an impulse like “event,” such as an R-peak of a QRS complex, occurs, the mean energy of the signal in the narrow time interval is greater than the mean energy in the wide time interval, allowing the detection of R-peaks in the signal. This method was chosen for its demonstrated performance in detecting R-peaks in ECG signals recorded during AF.

The Relative Energy algorithm was applied to the 10 one-minute ECG signal segments (BL and endABL) available for each patient. Therefore, 10 corresponding RR-interval sequences were extracted for each of the 40 patients, providing 400 RR-interval sequences in total, 200 at BL and 200 at endABL. Since the RR-interval sequence is not regularly sampled, resampling was performed at a sampling rate of 4 Hz. Once the BL and endABL RR-interval sequences were extracted, HRV analysis was performed, which will be discussed below.

⁴See Chapter 2 for an overview of ECG leads.

5.2.2 HRV ANALYSIS

Time-domain HRV analysis

Time-domain metrics of HRV were calculated on each of the BL and endABL RR-interval sequences, including: pNN20 (percentage of successive RR-intervals that differ by more than 20 ms), pNN50 (percentage of successive RR-intervals that differ by more than 50 ms), SDNN (standard deviation of RR-intervals), RMSSD (root mean-square of successive RR-interval differences). These metrics are standard for HRV quantification (Shaffer and Ginsberg, 2017), and were shown to be related to atrial fibrillatory rate in AF patients not treated with antiarrhythmic drugs (Corino et al., 2013).

Recurrence HRV analysis

While not as common for HRV analysis, nonlinear recurrence quantification analysis (RQA) has been suggested as more suitable for analyzing RR-sequences in AF, since it does not make any assumptions regarding sequence stationarity or number of available samples. This analysis involved (1) reconstruction of a system phase space, (2) recurrence plot construction, (3) RQA.

To reconstruct the phase space for a sequence of RR-intervals, embedded vectors were created as in Eq. 5.3. The i^{th} embedded vector therefore is a sequence $\mathbf{x}_i = \{RR_i, RR_{i+\tau}, \dots, RR_{i+(m-1)\tau}\}$, for embedding dimension m and sample delay, τ .

To create the recurrence plot, each of its points $\mathbf{R}_{i,j}$ was filled with a black or white dot according to Eq. 5.4, using embedded vectors \mathbf{x}_i and \mathbf{x}_j . The L_2 norm was chosen for this work, and the embedding parameters were set as follows: $m = 2$, $\tau = 1$, and $\epsilon = 0.1$, in line with suggestions that the threshold be set at a small percentage of the maximum phase space diameter, here estimated separately as the standard deviation of each RR-interval sequence (Marwan et al., 2007; Zbilut and Webber Jr, 1992). Therefore, measurements on time series with different amplitudes could be compared. Recurrence plots were then calculated for the embedded vectors from each BL and endABL RR-interval sequence, for a total of 400 recurrence plots.

Finally, RQA was performed for each constructed recurrence plot by calculating the REC, DET, and DIV metrics described by Eq. 5.6, Eq. 5.8, and Eq. 5.9 respectively, with $l_{\min} = 2$.

Entropy-based HRV analysis

Approximate entropy (ApEn) was found by Corino et al. (2013) to be related to atrial fibrillatory rate in AF patients, regardless of whether or not patients were taking antiarrhythmic drugs. However, ApEn is known to depend on data sequence length, and since the RR-interval sequences used in this study were shorter than those used in Corino et al. (2013), sample entropy (sampEn) was preferred. sampEn was introduced as an alternative to ApEn for

estimating the regularity of physiological time series when only noisy or short time series are available (Richman and Moorman, 2000), and it was shown to be less dependent on time sequence length than ApEn. Lower sampEn values indicate less complexity and more regularity in time series. For an RR-interval sequence which contains repeating patterns, the sampEn value should be lower.

For a given embedding dimension m , tolerance r , and number of data points N , $\text{sampEn}(m, r, N)$ is the negative natural logarithm of the conditional probability that two sequences similar for m points, within a tolerance determined by r , remain similar at the next point. For embedded vectors \mathbf{x}_i^m and \mathbf{x}_j^m as defined in Eq. 5.3, let $B_i^m(r)$ be $(N - m - 1)^{-1}$ times the number of vectors $\mathbf{x}_m(j)$ similar within r to $\mathbf{x}_m(i)$, $j = 1 \dots N - 1$, $j \neq i$ to exclude counting self-similarity. Then

$$B^m(r) = \frac{\sum_{i=1}^{N-m} B_i^m(r)}{N - m} \quad (5.10)$$

is the probability that two embedded vectors will be similar for m points. Similarly, let $A_i^m(r)$ be $(N - m - 1)^{-1}$ times the number of vectors $\mathbf{x}_{m+1}(j)$ similar within r of $\mathbf{x}_{m+1}(i)$, $j = 1 \dots N - 1$, $j \neq i$ to exclude self matches. Then

$$A^m(r) = \frac{\sum_{i=1}^{N-m} A_i^m(r)}{N - m} \quad (5.11)$$

is the probability that two embedded vectors will be similar for $m + 1$ points. Then sampEn is defined as:

$$\text{sampEn} = -\ln \frac{A^m(r)}{B^m(r)} \quad (5.12)$$

and note that for known r and m , given B the total number of similar vectors of length m and A the total number of similar vectors of length $m + 1$, $\frac{A}{B} = \frac{A^m(r)}{B^m(r)}$ and $\text{sampEn}(m, r, N) = -\ln \frac{A}{B}$. Therefore, $A < B$ and $\text{sampEn}(m, r, N) \geq 0$. Smaller values of sampEn indicate more self-similarity in the data sequence, or less noise. The sampEn metric was calculated using embedded vectors created from each of the BL and endABL RR-interval sequences, with $m = 2$, and r was calculated using the same $\epsilon = 0.1$ multiplier of the standard deviation of the RR-interval sequence as was used for RQA.

5.2.3 STATISTICAL ANALYSIS

The purpose of this section is to describe how the HRV metrics described in Sec. 5.2.2 were compared: (1) within the same patient group (LT, NT, SR, or AR), between BL and endABL, and (2) for different patient groups, at either BL or endABL (LT vs NT, or SR vs AR). The purpose was to compare the relationship between the metrics and catheter ablation procedural and clinical outcomes.

Calculated values of continuous parameters are expressed as mean \pm standard deviation. Statistical inter-group, or inter-step (BL vs endABL) differences were calculated as mean p -values across 3-folds, with 20% of the parameter values left out of each fold. One-way analysis of variance (ANOVA) was calculated on the data included in each fold to test for differences

in the group or ablation step means. Statistical tests were performed on multiple folds of the data to reduce the likelihood of chance group differences due to a small data set; statistical significance was considered for p -values less than 0.05. To quantify the association between CA outcome and the HRV metrics, we checked for statistical differences between these metrics calculated on BL and endABL RR-interval sequences associated with (1) LT vs NT groups for procedural outcome, and (2) SR vs AR groups for single-procedure clinical outcome.

For metrics displaying statistically significant differences between patient groups at BL, univariate logistic regression classifiers were used to test their predictive power for procedural and clinical ablation outcome. We used 3-fold cross validation (CV), with an 80/20 train-test split for each fold, and group-wise CV used to ensure that metrics calculated from RR-interval sequences of the same patient were assigned only to either the train or test set for each fold. Classifiers were trained on the train data of each fold, and then used to perform predictions on the test data of each fold. The resulting receiver operating curves (ROC) were analyzed to obtain area under the curve (AUC) to compare the predictive power of each HRV metric. We reported the AUC as mean \pm standard deviation over all CV folds, and the sensitivity and specificity were reported for the optimal classification threshold determined through using the mean ROC curve. The sensitivity and specificity were the fraction of true positive and true negative cases correctly identified, where NT/AR were considered positive cases, and LT/SR were considered negative cases, respectively.

5.3 RESULTS

5.3.1 CHANGE IN HRV METRICS FROM BL TO ENDABL

Table 5.1 shows HRV metric values calculated from sequences extracted at BL and endABL for patients grouped by single-procedure ablation outcome (LT vs NT). The same information is shown in Table 5.2 for patients grouped by clinical outcome (SR vs AR). Statistically significant differences in mean value from BL to endABL are indicated for each patient group, with the p -values calculated across three-folds of the data, as described in Sec. 5.2.3. A graphical representation of the HRV metric values is demonstrated in Fig. 5.3 for patients grouped by single procedure outcomes and Fig. 5.4 grouped by clinical outcomes following ablation. It can be seen that mean values of metrics which quantify regularity (REC and DET) were greater at endABL than at BL, while metrics which quantify variability (DIV, sampEn, pNN20, pNN50, SDNN, and RMSSD) were less at endABL than at BL, for all patient groups. The difference was statistically significant for all metrics for the LT patient group, and for all metrics except sampEn for the SR patient group. For the NT patient group, the difference was statistically significant for sampEn, pNN20, pNN50, SDNN, and RMSSD, while for the AR patient group, the difference was statistically significant for all metrics except DET.

Shown in Fig. 5.5 is an illustrative example of changes in the RR-interval sequence recurrence plot dynamics associated with an LT patient at BL and endABL. Note the increased REC

5 Heart rate variability analysis in atrial fibrillation for assessing response to catheter ablation

Table 5.1: **HRV metrics by ablation step, for procedural outcomes.** HRV metrics grouped by ablation step, i.e. baseline (BL), before ablation, and end of ablation (endABL), expressed as mean \pm standard deviation. p -values indicate statistical significance between the mean values at the BL and endABL steps, calculated for both the LT and NT patient groups.

	LT			NT		
	BL	endABL	p -value	BL	endABL	p -value
REC	0.009 \pm 0.005	0.0218 \pm 0.04	0.0007	0.007 \pm 0.005	0.008 \pm 0.004	0.522
DET	0.166 \pm 0.11	0.26 \pm 0.19	0.0001	0.123 \pm 0.12	0.141 \pm 0.1	0.29
DIV	0.56 \pm 0.24	0.41 \pm 0.21	0.0001	0.66 \pm 0.28	0.56 \pm 0.24	0.11
sampEn	4.13 \pm 2.6	2.98 \pm 2.21	0.016	5.45 \pm 2.77	4.24 \pm 2.6	0.072
pNN20	0.44 \pm 0.06	0.387 \pm 0.06	0.0001	0.465 \pm 0.04	0.435 \pm 0.04	0.003
pNN50	0.379 \pm 0.07	0.294 \pm 0.08	0.0001	0.416 \pm 0.04	0.361 \pm 0.05	0.001
SDNN	171 \pm 47	114 \pm 51	0.0001	213 \pm 51	127 \pm 30	0.001
RMSSD	242 \pm 73	155 \pm 70	0.0001	305 \pm 75	175 \pm 42	0.001

Table 5.2: **HRV metrics by ablation step, for clinical outcomes.** HRV metrics grouped by ablation step, i.e. baseline (BL), before ablation, and end of ablation (endABL), expressed as mean \pm standard deviation. p -values indicate statistical significance between the mean values at the BL and endABL steps, calculated for both the SR and AR patient groups.

	SR			AR		
	BL	endABL	p -value	BL	endABL	p -value
REC	0.008 \pm 0.003	0.045 \pm 0.07	0.03	0.009 \pm 0.005	0.011 \pm 0.008	0.022
DET	0.14 \pm 0.11	0.36 \pm 0.27	0.0007	0.16 \pm 0.12	0.19 \pm 0.12	0.051
DIV	0.59 \pm 0.23	0.17 \pm 0.12	0.0009	0.59 \pm 0.26	0.49 \pm 0.23	0.0025
sampEn	4.4 \pm 2.6	2.7 \pm 2.5	0.064	4.56 \pm 2.7	3.52 \pm 2.35	0.0017
pNN20	0.44 \pm 0.06	0.37 \pm 0.06	0.0005	0.45 \pm 0.05	0.4 \pm 0.06	0.0001
pNN50	0.376 \pm 0.07	0.29 \pm 0.07	0.0004	0.39 \pm 0.06	0.32 \pm 0.08	0.0001
SDNN	162 \pm 33	116 \pm 53	0.0003	189 \pm 54	119 \pm 44	0.0001
RMSSD	227 \pm 52	162 \pm 80	0.0003	270 \pm 82	161 \pm 59	0.0001

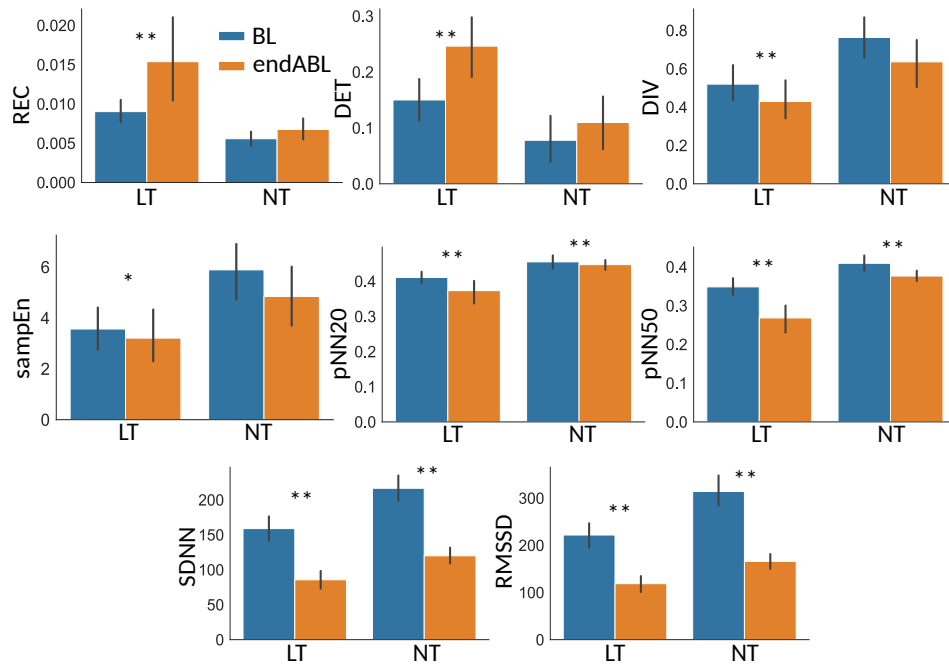


Figure 5.3: **Change in HRV metrics from BL to endABL, by procedural outcome..** HRV metrics at baseline (BL - before ablation) and at the end of ablation (endABL) are shown, grouped according to single-procedure ablation outcome (LT=left terminated, NT=not terminated). Significant differences in mean value at BL and endABL are indicated with asterisks, * $p<0.05$, ** $p<0.01$.

and DET, as well as increased structure, observed in the endABL recurrence plot (Fig. 5.5b) compared to the BL recurrence plot (Fig. 5.5a). Fig. 5.6 shows the same information for an NT patient, for whom the increased regularity observed in the LT patient was absent; no differences were discernible in the recurrence plot dynamics for the NT patient.

5.3.2 ASSOCIATION BETWEEN HRV METRICS AND ABLATION OUTCOME

Table 5.3 shows HRV metrics calculated separately for LT and NT procedural outcomes grouped by ablation step, at baseline (BL) and at end of ablation (endABL). The p -values indicate significant differences in mean LT vs NT values, at either BL or endABL. The same information is shown in Table 5.4 for clinical outcomes (SR vs AR). A graphical representation of the differences in HRV metric values between the LT and NT patient groups, at both the BL and endABL steps is demonstrated in Fig. 5.7. The same information is shown in Fig. 5.8 for differences between the SR and AR patient groups. It can be seen that mean values of metrics which quantify regularity (REC and DET) were greater for the LT and SR patient groups than for the NT and AR patient groups, while metrics which quantify variability (DIV, sampEn, pNN20, pNN50, SDNN, and RMSSD) were less for the LT and SR patient groups than for the NT and AR patient groups. The difference between the LT and NT patient groups at BL was significant only for the pNN20, pNN50, SDNN, and RMSSD metrics, while at endABL, the

5 Heart rate variability analysis in atrial fibrillation for assessing response to catheter ablation

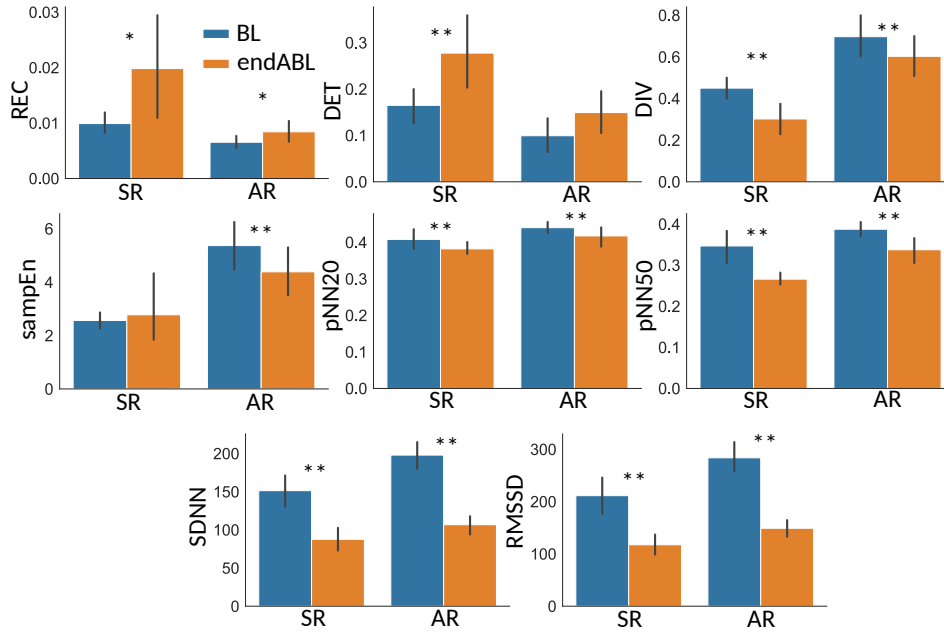


Figure 5.4: **Change in HRV metrics from BL to endABL, by clinical outcome.** HRV metrics from BL (BL - before ablation) and at the end of ablation (endABL) are shown, grouped according to clinical outcome during the follow-up period after catheter ablation (SR=sinus rhythm, AR=arrhythmia recurrence). Significant differences in mean value at BL and endABL are indicated with asterisks, * $p<0.05$, ** $p<0.01$.

difference showed statistical significance for all metrics. The difference between the SR and AR patient groups at BL was statistically significant only for the SDNN and RMSSD metrics, while at endABL only the REC, DET, and DIV metrics had statistically significant different values in the means between the patient groups.

5.3.3 PREDICTIVE POWER OF HRV METRICS FOR ABLATION OUTCOME

A summary of the ROC analysis for the pNN20, pNN50, SDNN, and RMSSD metrics, which displayed statistically significantly different values in the mean between the LT and NT patient groups at BL, for predicting procedural catheter ablation outcome is shown in Table 5.5. A summary of the ROC analysis for the SDNN and RMSSD metrics, which displayed statically significantly different values in the mean between the SR and AR patient groups at BL, for predicting clinical ablation outcome throughout the follow up period described in Sec. 5.1.2, is shown in Table 5.6. The sensitivity and specificity values are shown for RR-interval sequence-wise classification. The ROC curves associated with procedural outcome prediction are shown in Fig. 5.9, while those for clinical outcome prediction are shown in Fig. 5.10. It can be seen that for prediction of arrhythmia termination by catheter ablation, SDNN and RMSSD perform the best, with the least variation across cross-validation folds (AUC: 0.93 ± 0.06 , 0.91 ± 0.04 respectively). These two variables do not quite perform as well for prediction of arrhythmia recurrence, or equivalently sinus rhythm maintenance during the follow-up period (AUC:

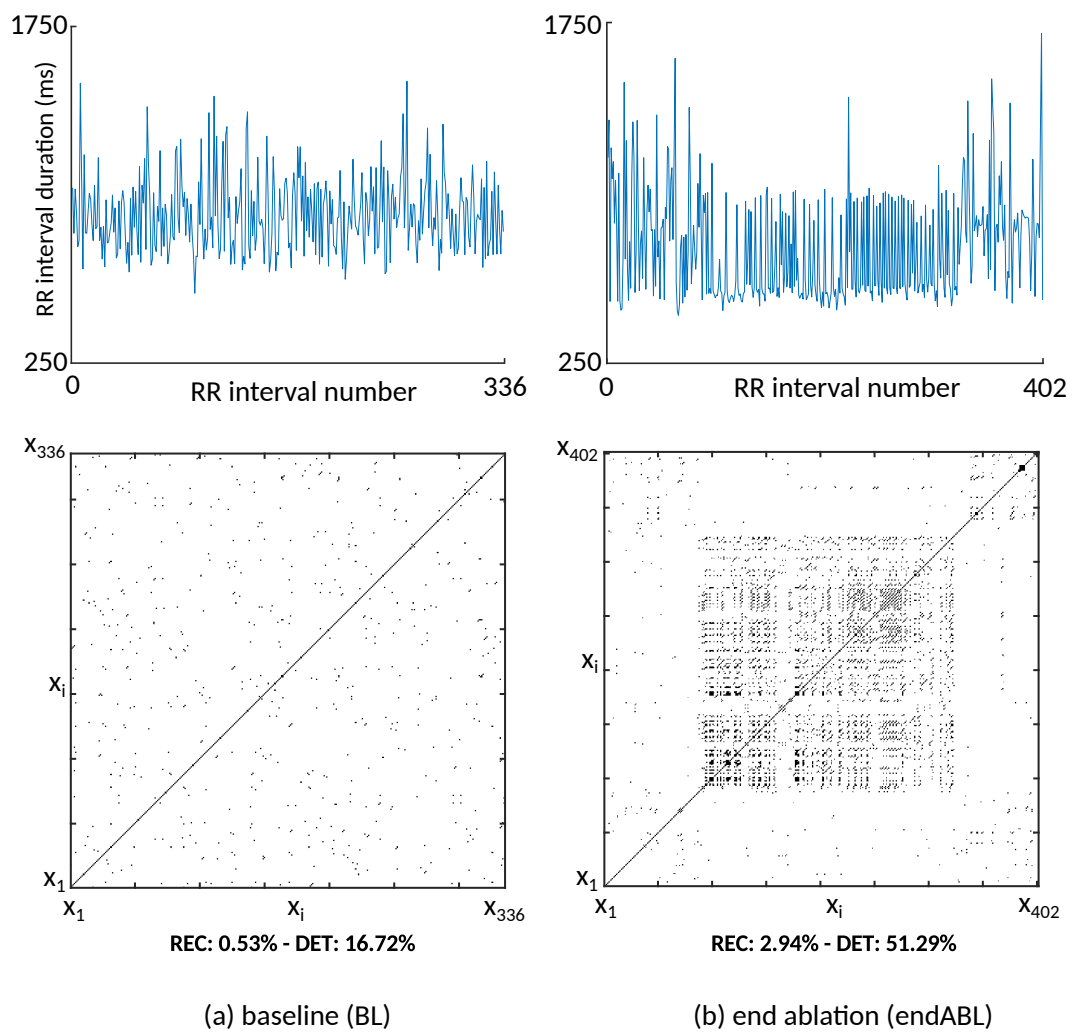


Figure 5.5: **RR-interval recurrence plot dynamics at BL and endABL for an LT patient.** (a) Top panel: RR-intervals extracted from a 5-minute baseline (pre-ablation) ECG segment. Bottom panel: Recurrence plot constructed using embedded vectors from baseline RR-interval sequence. (b) Top panel: RR-intervals extracted from a 5-minute ECG segment recorded at the end of ablation, just before spontaneous AF termination. Lower panel: Corresponding recurrence plot, constructed using embedded vectors from endABL RR-interval sequence.

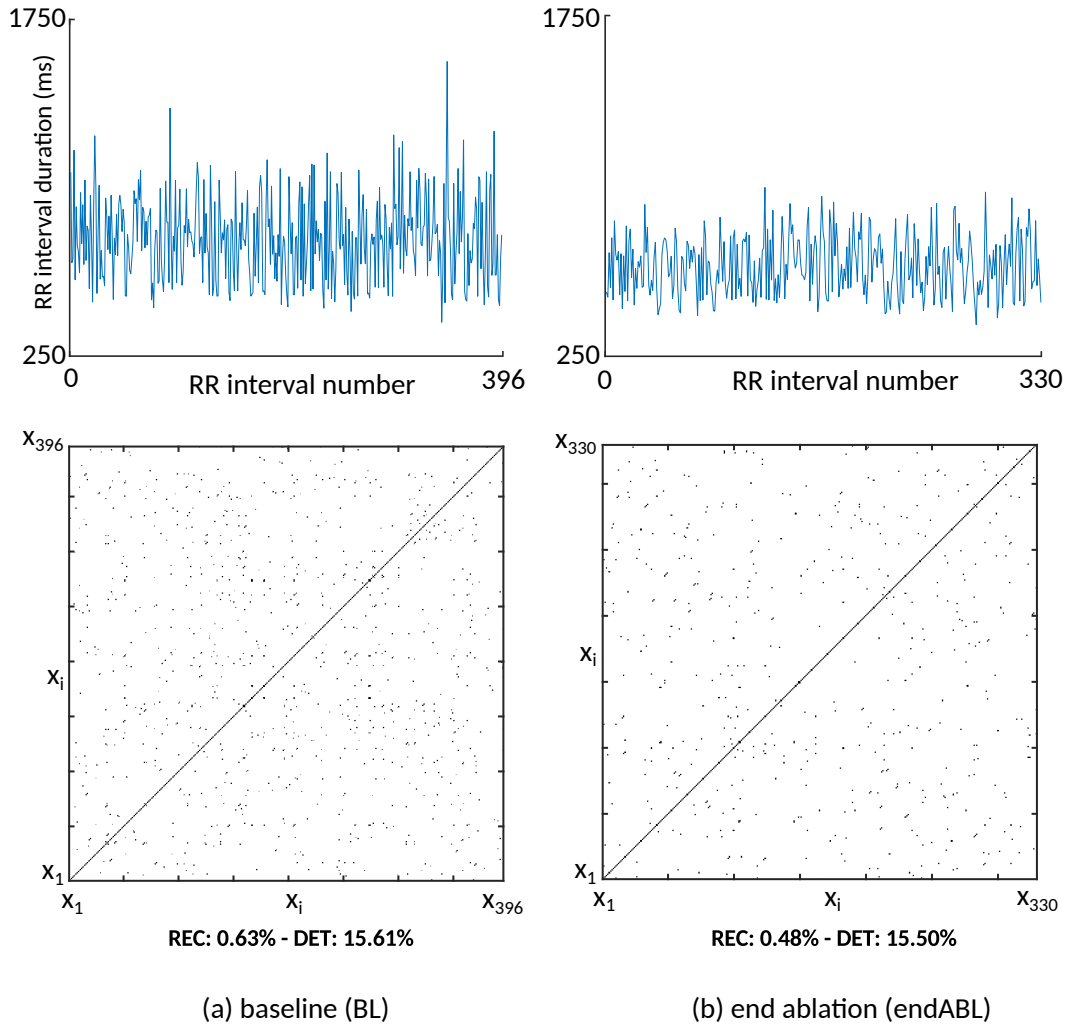


Figure 5.6: RR-interval recurrence plot dynamics at BL and endABL for an NT patient. (a) Top panel: RR-intervals extracted from a 5-minute baseline (pre-ablation) ECG segment. Bottom panel: Recurrence plot constructed using embedded vectors from baseline RR-interval sequence. (b) Top panel: RR-intervals extracted from a 5-minute ECG segment recorded at the end of ablation, just before electrocardioversion. Lower panel: Corresponding recurrence plot, constructed using embedded vectors from endABL RR-interval sequence.

Table 5.3: **HRV metrics by ablation procedural outcome.** HRV metrics grouped by procedural outcome of catheter ablation, expressed as mean \pm standard deviation. p -values indicate statistical significance between the mean values of the LT and NT patient groups for each metric, calculated both at baseline (BL) and end of ablation (endABL).

	BL			endABL		
	LT	NT	p -value	LT	NT	p -value
REC	0.009 \pm 0.005	0.007 \pm 0.005	0.139	0.0218 \pm 0.04	0.008 \pm 0.004	0.02
DET	0.166 \pm 0.11	0.123 \pm 0.12	0.176	0.26 \pm 0.19	0.141 \pm 0.1	0.0001
DIV	0.56 \pm 0.24	0.66 \pm 0.28	0.138	0.41 \pm 0.21	0.56 \pm 0.24	0.0001
sampEn	4.13 \pm 2.6	5.45 \pm 2.77	0.054	2.98 \pm 2.21	4.24 \pm 2.6	0.001
pNN20	0.44 \pm 0.06	0.465 \pm 0.04	0.029	0.387 \pm 0.06	0.435 \pm 0.04	0.0001
pNN50	0.379 \pm 0.07	0.416 \pm 0.04	0.006	0.294 \pm 0.08	0.361 \pm 0.05	0.0001
SDNN	171 \pm 47	213 \pm 51	0.0001	114 \pm 51	127 \pm 30	0.022
RMSSD	242 \pm 73	305 \pm 75	0.0001	155 \pm 70	175 \pm 42	0.017

Table 5.4: **HRV metrics by ablation clinical outcome.** HRV metrics grouped by clinical outcome following catheter ablation, expressed as mean \pm standard deviation. p -values indicate statistical significance between the mean values of the SR and AR patient groups for each metric, calculated both at baseline (BL) and end of ablation (endABL).

	BL			endABL		
	SR	AR	p -value	SR	AR	p -value
REC	0.008 \pm 0.003	0.009 \pm 0.005	0.375	0.045 \pm 0.07	0.011 \pm 0.008	0.0001
DET	0.14 \pm 0.11	0.16 \pm 0.12	0.339	0.36 \pm 0.27	0.19 \pm 0.12	0.0001
DIV	0.59 \pm 0.23	0.59 \pm 0.26	0.397	0.17 \pm 0.12	0.49 \pm 0.23	0.0001
sampEn	4.4 \pm 2.6	4.56 \pm 2.7	0.338	2.7 \pm 2.5	3.52 \pm 2.35	0.114
pNN20	0.44 \pm 0.06	0.45 \pm 0.05	0.241	0.37 \pm 0.06	0.4 \pm 0.06	0.017
pNN50	0.376 \pm 0.07	0.39 \pm 0.06	0.226	0.29 \pm 0.07	0.32 \pm 0.08	0.105
SDNN	162 \pm 33	189 \pm 54	0.032	116 \pm 53	119 \pm 44	0.358
RMSSD	227 \pm 52	270 \pm 82	0.028	162 \pm 80	161 \pm 59	0.24

5 Heart rate variability analysis in atrial fibrillation for assessing response to catheter ablation

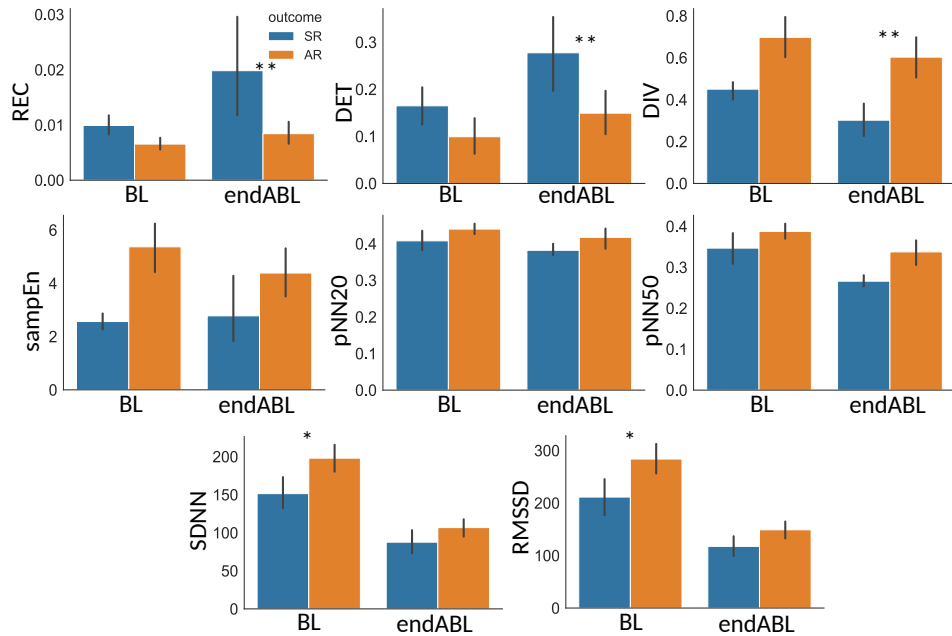
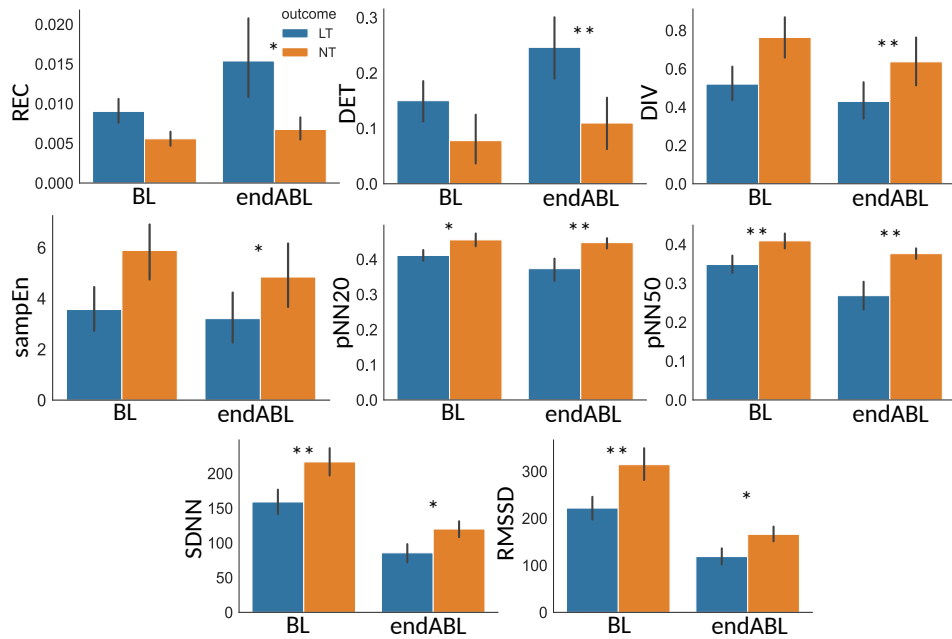


Figure 5.8: **RR-interval metrics at BL and endABL by procedural outcome of catheter ablation.** Mean values of all HRV metrics are shown at BL and endABL, for SR vs AR patient groups. (SR=sinus rhythm, AR=arrhythmia recurrence at follow-up), * $p<0.05$, ** $p<0.01$.

0.78±0.17, 0.77±0.17, respectively).

Table 5.5: **Predictive power of HRV metrics for ablation procedural outcome.** Area under the curve (AUC) values expressed as mean ± standard deviation for metrics showing statistically significant different mean values between LT and NT patient groups at baseline (BL). Sensitivity and specificity indicate the rate of detection of arrhythmia persistence and arrhythmia termination at the end of ablation, respectively.

	AUC (mean ± std)	Sensitivity (%)	Specificity (%)
pNN20	0.69±0.15	82.7	53.5
pNN50	0.71±0.18	92	46.5
SDNN	0.93±0.06	88	79.8
RMSSD	0.91±0.04	90.7	79.8

Table 5.6: **Predictive power of HRV metrics for ablation clinical outcome.** Area under the curve (AUC) values expressed as mean ± standard deviation for metrics showing statistically significant different mean values between SR and AR patient groups at baseline. Sensitivity and specificity indicate the rate of detection of arrhythmia recurrence and sinus rhythm maintenance throughout the follow-up period, respectively.

	AUC (mean ± std)	Sensitivity (%)	Specificity (%)
SDNN	0.78±0.17	69.4	99
RMSSD	0.77±0.17	69	99

5.4 DISCUSSION

Atrial fibrillatory activity is known to influence the irregular ventricular response seen in AF (Cohen et al., 1983; Corino et al., 2013), and several studies have suggested that quantifiable measures of the ventricular response can be linked with AF complexity and disease progression. In this chapter, the usefulness of quantifying the ventricular response in persistent AF for determining patient response to catheter ablation treatment was investigated. Specifically, RR-interval sequences were extracted from ECG signals recorded prior to and at the end of catheter ablation, just before either AF termination or electrocardioversion. A variety of metrics quantifying HRV were then computed, to investigate whether time-domain, entropy, and recurrence measures introduced for the analysis of dynamical time-series would reveal differences in the ventricular response of patients whose arrhythmia was terminated by catheter ablation and those in whom it was not, both prior to and at the end of ablation. We also investigated whether HRV as measured by these metrics prior to ablation was associated with procedural and clinical catheter ablation outcomes. Finally, the predictive power of HRV metrics shown to be significantly associated with catheter ablation outcomes was tested. We

5 Heart rate variability analysis in atrial fibrillation for assessing response to catheter ablation

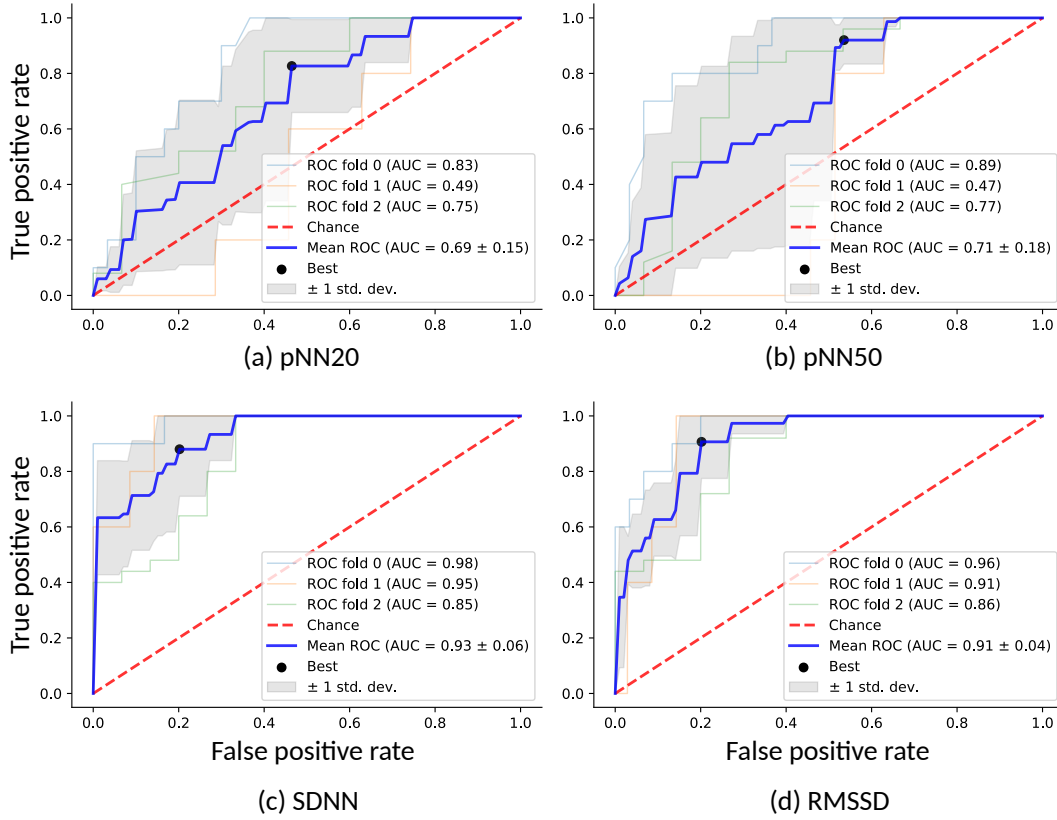


Figure 5.9: ROC analysis for predicting arrhythmia termination by catheter ablation. Univariate predictive performance of (a) pNN20, (b) pNN50, (c) SDNN, and (d) RMSSD for classification of left terminated arrhythmia (LT) at the end of ablation, or not terminated (NT), using the HRV metric values calculated at baseline (BL), prior to ablation.

found promising results for prediction of both procedural and clinical ablation outcomes, with the time-domain SDNN metric performing best. To our knowledge, this is the first time changes in HRV of persistent AF patients following catheter ablation procedures have been reported, as well as quantification of the ventricular response for predicting catheter ablation outcome.

5.4.1 CHANGE IN HRV BEFORE AND AT THE END OF ABLATION

It has been suggested that despite the irregular and apparently random nature of RR-intervals in AF, some structure can be quantified. For example, in a study by Rawles and Rowland (1986), it was shown that while most (70%) RR-interval sequences of patients in AF were estimated to be random using autocorrelation-based approaches, some sequences did demonstrate significant correlation between consecutive RR-intervals (30%). This suggests that patients in AF can have patterns of detectable regularity in their ventricular response. Therefore, in this study the aim was to investigate whether changes in HRV could be measured between prior to ablation (at baseline - BL) and at the end of ablation (endABL). Importantly, these differences

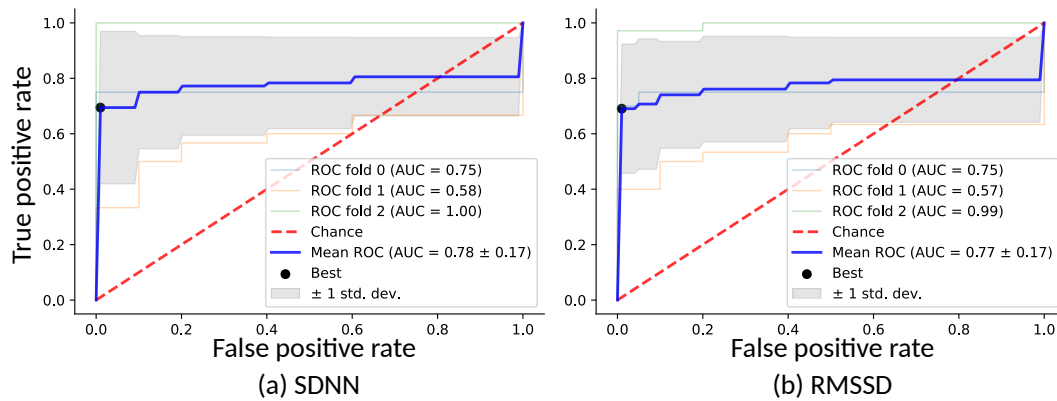


Figure 5.10: **ROC analysis for predicting clinical outcome following catheter ablation.** Performance of (a) SDNN and (b) RMSSD for univariate prediction of sinus rhythm maintenance throughout the follow-up period following catheter ablation, with metric values calculated using RR-sequences recorded at baseline (BL), prior to ablation.

were investigated separately for LT/SR patients and NT/AR patients, to see whether changes in HRV at the start and end of ablation could be associated with likelihood of arrhythmia termination by catheter ablation.

The results presented in Sec 5.3.1 demonstrated that while all HRV metrics measured increased between BL and endABL among LT patients, only time-domain HRV metrics (pNN20, pNN50, SDNN, RMSSD) showed significant differences between BL and endABL for NT patients. This indicates more repeatability in the RR-interval sequence recorded at endABL compared to that at BL, and thus a more regular ventricular response in LT patients just prior to AF termination. This suggests that sinus rhythm restoration by catheter ablation is more likely in patients who, as a group, showed increasing regularity in their RR-interval sequences, but only when measured using the recurrence metrics presented in Sec. 5.1.3, as well as the sampEn metric. The changes in the time-domain metrics (pNN20, pNN50, SDNN, RMSSD) would therefore appear to be due more to general effects of ablation on the ventricular response, since they occurred in all patients, regardless of ablation outcome. The increasing REC and DET values observed in the LT group between BL and endABL were suggestive of increasing organization and regularity in the ventricular response, while the decreasing DIV and sampEn indicated a potential reduction in the complexity of the atrial fibrillatory activity on the ventricular response just prior to AF termination, since the decreased value was not significantly present in NT patients. The exact electrophysiological mechanisms responsible for the presence or lack of increasing organization, and why it arose only in LT patients, could not however be explained without access to simultaneously recorded intracardiac electrogram data.

Less information could be gleaned about changes in HRV between BL and endABL for SR and AR patients, as in both patient groups, nearly all the HRV metrics displayed significantly greater values at endABL than BL. This could be because many of the patients in the AR group

5 Heart rate variability analysis in atrial fibrillation for assessing response to catheter ablation

had increased organization in their atrial fibrillatory activity and thus ventricular response leading up to arrhythmia termination. It was only later, during the follow-up period, that many of them experienced a recurrence in their ablation, suggesting that the change alone from BL to endABL was not indicative of likelihood of sinus rhythm maintenance or arrhythmia recurrence during the follow-up period.

5.4.2 ASSOCIATION BETWEEN HRV AND ABLATION OUTCOME

It has been shown that RR-interval regularity was linked with sinus rhythm restoration in patients with AF who underwent cardioversion (Van Den Berg et al., 2004). Specifically, clustering was applied to RR-intervals, and in patients in whom clear clusters were found, sinus rhythm restoration was achieved in 94% of cases, while in patients for whom no clustering of RR-intervals could be found, only 71% of patients experienced sinus rhythm restoration. Therefore, this study also investigated whether more regularity would be quantifiable in LT patients compared to NT patients (and SR patients compared to AR patients) at BL, to investigate the ability of HRV metrics to predict AF termination by catheter ablation (procedural outcomes), and long-term maintenance of sinus rhythm following catheter ablation (clinical outcomes).

The results presented in Sec 5.3.2 demonstrated that time-domain measures of HRV (pNN20, pNN50, SDNN, and RMSSD) displayed significantly lower mean values at BL among the LT patient group than NT patient group. Only pNN20 and pNN50 displayed significantly lower mean values at BL for the SR patient group than AR patient group. These results suggest that increased regularity in the ventricular response prior to ablation was associated with both greater likelihood of AF termination by catheter ablation, and greater likelihood of sinus rhythm maintenance throughout the follow-up period. The recurrence metrics and sampEn did not display significant differences between the two patient groups at baseline, suggesting that they were more useful with regard to their association to change in atrial activity organization over the course of the catheter ablation procedure, as discussed in 5.4.1 above. These results appear contrary to those reported by (Akyürek et al., 2003), in which SDNN, RMSSD, and pNN50 were all found to be significantly lower in patients with AF recurrence than in those with sinus rhythm maintenance following cardioversion. However, in their study, RR-interval sequences were quantified after cardioversion for patients in sinus rhythm. Therefore, their results could be reflective of the role of the autonomic nervous system in recurrence after cardioversion. In the study reported in this chapter, the ventricular response in AF was quantified, therefore, the role of the autonomic nervous system was not investigated.

5.4.3 HRV PREDICTIVE POWER FOR ABLATION OUTCOME

For HRV metrics which had significant differences in mean value between LT and NT, and SR and AR patient groups at BL, we tested their classification performance for predicting AF

termination by catheter ablation, and sinus rhythm maintenance during the follow-up period, respectively. This step was important to test not only the association between these metrics and CA outcome, but also their potential clinical impact as noninvasive electrocardiographic biomarkers of suitability for catheter ablation.

Specifically, classification performance was tested using univariate logistic regression classifiers for pNN20, pNN50, SDNN, and RMSSD for predicting AF termination by catheter ablation, and SDNN and RMSSD for predicting sinus rhythm maintenance during the follow up period. These metrics were chosen since they displayed significant differences between the LT and NT, and SR and AR patient groups, respectively, at BL. Importantly, group-wise CV was used for the HRV metrics computed on RR-interval sequences extracted from the same patient, which were included only in either the train or test set for each fold. The mean and standard deviation of the AUC across folds were also reported for each metric's classifier to indicate the outcome prediction model variance. These steps were important considering the small size of our data set.

For procedural outcome prediction, all metrics tested displayed good univariate predictive performance (AUC - pNN20: 0.69 ± 0.15 , pNN50: 0.71 ± 0.18 , SDNN: 0.93 ± 0.06 , and RMSSD: 0.91 ± 0.04). SDNN and RMSSD in particular had high AUCs with low variance across data folds. The finding that SDNN and RMSSD both displayed high AUC values with low variability across cross-validation folds was indicative of the potential of these measures to act as noninvasive electrocardiographic biomarkers for likelihood of successful catheter ablation procedures to terminate AF in persistent AF patients.

For clinical outcome prediction, both metrics tested also displayed good univariate predictive performance (AUC - SDNN: 0.78 ± 0.17 , RMSSD: 0.77 ± 0.17), though not as good as the best performance for procedural outcome prediction. The finding that these metrics also displayed relatively high AUC values and low variability for predicting long-term sinus rhythm maintenance throughout the follow-up period was suggestive of the suitability of these metrics to predict not only successful procedural outcomes of catheter ablation, but also sinus rhythm maintenance thereafter. To our knowledge, this is the first study to test predictive performance of HRV metrics for AF termination by procedural catheter ablation and long-term maintenance of sinus rhythm thereafter.

Comparison with other surface ECG predictive biomarkers for CA outcome prediction

Many studies have extracted surface ECG based indices thought to be associated with AF complexity in an attempt to associate them with procedural and clinical outcomes following CA. These indices most often rely on extraction of the atrial component of the surface ECG, through either extraction of f-waves in TQ segments, or ventricular activity (QRST complex) cancellation. For example, Meo et al. (2012) proposed a an f-wave amplitude based metric that computed a “global” atrial amplitude using weighted contributions from each independent lead of the 12-lead ECG calculated using principle component analysis (PCA). The proposed

metric achieved good predictive power, with AUC ranging from 0.65-0.95 depending on the number of leads included on their database of 28 persistent AF patients using leave-one-out CV. Matsuo et al. (2009) evaluated the ability of pre-procedural clinical and surface ECG variables to predict procedural and clinical outcomes of CA in patients with persistent AF, and found that surface ECG AF cycle length was the only independent predictor of procedural AF termination, with an AUC of 0.88. Additionally, AF cycle length and AF duration were both found to be independent predictors of clinical ablation outcome with high AUCs. However, AF cycle length was manually computed, from 10 unambiguous fibrillatory waves. This process is time intensive, and unambiguous fibrillatory waves can be difficult to obtain, especially for persistent AF patients, and if only short recordings are available. Lankveld et al. (2016) computed a variety of surface ECG parameters thought to be associated with AF complexity and found that f-wave amplitude had the best predictive performance for procedural and clinical outcomes (AUC: 0.76 ± 0.15 , 0.69 ± 0.13 , respectively), with comparable scores on their validation set. However, their f-wave amplitude computation required QRST cancellation. Di Marco et al. (2014) calculated recurrence plot indices, including REC and DET, on the atrial component of surface ECG recorded in both paroxysmal and nonparoxysmal AF, and found that higher REC was associated with a decreased risk of AF recurrence at follow-up. Their study additionally reported that DET was a significant predictor of 6-month post-ablation outcome (AUC=0.67). Similarly, a drawback of this study was the need to use TQ segments to obtain the atrial waveform, which is often very difficult in persistent AF patients who have high heart rates. While these studies all showed promising results and have been useful for testing noninvasive surface ECG indices for their association with AF outcomes, their clinical implementation would necessitate time-consuming calculations. The HRV metrics tested in this study are much simpler to calculate, and much easier for future studies to reproduce. Comparing our results with these studies serves only to underline the ability of the HRV metrics tested in this study to reproduce similar results on an in-house data set for predicting CA outcome using a metric computed on surface ECG prior to CA procedures. Clearly, the respective databases and metrics cannot be directly compared.

Comparison with clinical scoring systems for CA outcome prediction

Several clinical scoring systems have been proposed and tested for predicting CA outcome. These scoring systems use clinical parameters thought to be associated with AF complexity such as patient age, type of AF (e.g., paroxysmal, persistent), sex, as well as physiological parameters quantifying left atrium enlargement to compute a score. Examples include AP-PLE (Kornej et al., 2015), MB-LATER (Mujović et al., 2017), and ATLAS (Mesquita et al., 2018). These studies have obtained high AUCs, 0.634, 0.782, and 0.75, respectively. However, some of the clinical parameters require knowledge of the full patient clinical history, and obtaining left-atrium parameters may require pre-procedural imaging and sophisticated electrophysiological mapping software, making the clinical implementation of these scores less practical, as CT imaging prior to PVI is performed routinely in 59% of electrophysiology centers (Calkins et al., 2018).

Finding definitive measures to select patients with high likelihoods of successful catheter ablation outcomes remains elusive. However, the results presented in this chapter demonstrate that changes in HRV metrics indicative of increasing organization in the ventricular response are associated with better catheter ablation procedural outcomes. This work has also demonstrated the feasibility of quantifying the ventricular response using HRV analysis for investigating suitability for catheter ablation procedures. HRV analysis is easier to perform in a consistent manner than direct analysis of the atrial component of ECG signals, and should therefore be considered for the noninvasive quantification of atrial fibrillation disease complexity.

Since AF ablation and follow-up strategies, as well as patient cohorts differ considerably among electrophysiology centers, future studies are needed to prospectively validate and compare CA outcome prediction scores in independent external cohorts in order to determine their relative predictive ability for post-CA recurrence, and establish their applicability in everyday clinical practice.

6 SPATIOTEMPORAL SIGNAL PROCESSING METHODS FOR BSPM

6.1 INTRODUCTION

In contrast to the many studies that have analyzed the 12-lead electrocardiogram (ECG) for the study of atrial fibrillation (AF), relatively few have developed AF analysis tools for body-surface potential map (BSPM) signals. Despite the development of these 12-lead ECG based indices, to our knowledge, the use of ECG for AF in clinical practice is still limited to its diagnosis (Lankveld et al., 2014). The traditional 12-lead ECG was designed to capture mainly ventricular activity (VA), therefore, BSPM signals could harbor additional information from the atrial activity (AA) relevant for AF analysis.

Various studies have performed analyses of BSPM data for the study of AF. For example, (Bonizzi et al., 2010) applied principal component analysis (PCA) to BSPM data and proposed two novel parameters derived from the resulting PCA mixing matrices to quantify complexity and stationarity in BSPM recordings, finding a significant inverse correlation between the two. It was additionally found that these parameters formed clusters for organized vs. disorganized AF, but no further clinical application was proposed by the authors. The study in (Di Marco et al., 2012) proposed four parameters to quantify spatial organization, variability, spectral concentration, and spectral variability of BSPM signals. They found that greater spatial organization was associated with reduced variability of spatial organization over time, and that lower spectral variability was associated with increased spectral concentration. However, the clinical impact of the parameters was not assessed. Later, (Meo et al., 2018) proposed the non-dipolar component index (NDI), which was calculated as the residual variance not accounted for by the first three principal components (PCs) of concatenated TQ segments of BSPM signals. It was found that the NDI correlated with AF complexity and AF termination at the end of catheter ablation (CA) procedures. However, correlation with clinical CA outcome was not reported, and the NDI leaves unexploited the temporal variability of BSPM signals found to be indicative of AF organization in (Bonizzi et al., 2010; Di Marco et al., 2012). These parameters do however show promise for capturing information from BSPM signals relevant for the computational analysis of AF signals. Additionally, they are all linked in that they use PCA in the computation of their indices. However, insufficient attention has been paid to the temporal aspect of the data, with most of the parameters using concatenated TQ segments. While this method has merit as it eliminates the possibility of interfering VA, it precludes a temporal analysis, and we aim to address this with our novel indices.

6 Spatiotemporal signal processing methods for BSPM

Despite the above research, the use of BSPM for persistent AF treatment remains limited in clinical practice, and there are not many tools available for its efficient analysis. Apart from its use in electrocardiographic imaging (ECGI), the clinical advantage of BSPM over 12-lead ECG signal analysis for AF remains unclear. In this study, we draw on the above research to propose two novel indices also employing PCA: error ratio, normalized root-mean square error (ER_{NRMSE}) and error ratio, mean absolute error (ER_{ABSE}), which exploit spatiotemporal information in BSPM recordings. The indices make use of the full set of BSPM electrodes by measuring how well only a subset of electrodes can represent AA on all BSPM electrodes compared to the optimal PCA-representation. The indices also encapsulate the temporal variability of the AA using long-duration BSPM recordings. We hypothesized that when subsets can represent AA nearly as well as the optimal PCA-representation, the AF is more organized and stable with time, and thus more likely to respond well to CA treatment. When the optimal PCA representation is much better than the electrode subset representation, we hypothesized that this could be indicative of a disorganized AF that is more variable over time, manifested as greater spatial variability in the recorded AA on the BSPM vest. In this way, we aim to provide additional tools which efficiently utilize the large amount of data incurred when working with BSPM recordings and show their clinical relevance for persistent AF disease quantification through correlation with and prediction of single-procedure CA outcome. We first discuss the study population and BSPM signal acquisition and pre-processing. An overview of the novel indices and BSPM vest electrode subset selection required for their calculation is then given. The statistical cross-validation protocol used to evaluate their clinical relevance is then presented. Finally, the results, implications, and limitations of the study are discussed.

6.2 METHODS

6.2.1 STUDY POPULATION

We studied a total of 13 patients admitted for CA of drug-refractory persistent AF. Their baseline characteristics are reported in Table 6.1. The CA endpoint was complete pulmonary vein isolation (PVI). Electrical cardioversion was performed on patients still in AF after PVI completion to restore sinus rhythm (SR). Patients were then monitored throughout a follow up period and divided into two groups: (1) SR and arrhythmia recurrence (AR), according to whether they experienced an AR within 6 months, but at least 2 months after undergoing CA. The study protocol was approved by the Lausanne University Hospital Human Research Ethics Committee, and all patients provided written informed consent.

6.2.2 BSPM SIGNAL ACQUISITION AND PREPROCESSING

BSPMs were recorded with a 252-lead vest (CardioInsight™, Medtronic, MN, USA) at a sampling frequency of 1 kHz in persistent AF patients the day before undergoing CA at Lausanne University Hospital in Switzerland. A schematic of the vest is shown in Fig. 6.1. Mean signal

Table 6.1: Study population baseline characteristics.

Characteristic	<i>n</i> = 13
Sex (M/F)	8/5
Age, mean \pm std, years	63 \pm 8
Hypertension, <i>n</i>	6
Coronary artery disease, <i>n</i>	2
Heart Failure, <i>n</i>	3
Valvular Disease, <i>n</i>	3
Diabetes, <i>n</i>	2
Left ventricular ejection fraction, mean \pm std, %	51 \pm 13
Sustained AF duration, mean \pm std, months	11 \pm 13
<i>std, standard deviation</i>	

recording duration was 17 ± 4 minutes. Electrode contact and signal quality varied considerably over the course of the recording duration. Recordings were therefore visually inspected, and one-minute segments with good signal quality were extracted from the long duration recordings for further analysis. Remaining leads with poor signal quality were removed (up to 30 leads), and signals from high quality leads were used to estimate BSPM signals at the removed locations using interpolation. Recordings were then processed for removing baseline drift and high frequency noise (bandpass filter 1-30 Hz). R-peaks were detected and QRST delineation was performed in each lead using an open source ECG delineation toolbox (Pilia et al., 2021). In order to evaluate BSPM signals free of ventricular interference and enable a temporal analysis, the spatiotemporal method for QRST cancellation was applied (Stridh and Sornmo, 2001), described in detail in Appendix A. This method, which operates on a single-beat, multi-lead basis, was chosen due to its exploitation of multiple leads and its tested performance (Langley et al., 2006). Clustering was applied to QRST complexes across all leads, so that the complexes used in each ensemble average had similar shapes. The extracted one-minute atrial activity BSPM segments (AA-BSPM) devoid of VA were then further normalized to have zero mean and unit variance, and low-pass filtered by a 10th order Butterworth filter with a cutoff frequency of 30 Hz to eliminate signal discontinuities introduced by spatiotemporal VA cancellation. An example of a BSPM signal before and after AA extraction is shown in Fig. 6.2. The power spectral densities (PSD) of all AA-BSPM segments were computed using a Welch periodogram (2-second Hamming window with a 4096 Fast Fourier transform per window and 50% window overlap) to determine the body surface distribution of the atrial DF. The DF was defined as the highest peak in the power spectrum.

6 Spatiotemporal signal processing methods for BSPM



Figure 6.1: **BSPM vest.** CardioInsight™ BSPM vest with 252 unipolar electrodes. The reference electrode is not shown. **(A)** Anterior part of vest with 126 electrodes. **(B)** Posterior part of vest with 126 electrodes.

6.2.3 AA-BSPM RECONSTRUCTION USING A SUBSET OF BSPM ELECTRODES

The purpose of this section is to describe how only a subset of vest electrode signals may be used to reconstruct the signals on all vest electrodes, as this is an important concept in the development of the novel indices ER_{NRMSE} and ER_{ABSE} (elaborated in Sec. 6.2.5). Each AA-BSPM segment may be represented by a matrix $X \in \mathbb{R}^{m \times n}$, with m consecutive samples in the rows, and n synchronously recorded signals in the columns, one from each BSPM vest electrode. Given an arbitrary subset of signals recorded on k vest electrodes, $S \in \mathbb{R}^{m \times k}$, $k < n$, the minimum least-squares transformation of the subset matrix S to approximate the full BSPM signal matrix X is given by:

$$\underset{A}{\operatorname{argmin}} \|X - SA\|_F^2 \quad (6.1)$$

whose known solution is $A = S^+ X$, where $(\cdot)^+$ and $\|\cdot\|_F$ denote the Moore-Penrose pseudoinverse and the Frobenius norm of a matrix, respectively. Then, to represent the full BSPM signal matrix X as accurately as possible, one should aim to find a subset S of vest electrode signals such that the AA-BSPM segment X is best represented by S , most commonly in terms of the Frobenius norm:

$$\underset{S}{\operatorname{argmin}} \|X - SS^+ X\|_F^2 \quad (6.2)$$

Finding the subset S is thought to be an NP-hard problem, with $\binom{n}{k}$ solutions, (Altschuler et al., 2016; Civril, 2014). Therefore, finding the optimal solution would involve searching the $\binom{n}{k}$ solutions, which for n and k of reasonable size is not feasible. The goal for electrode subset selection is then to find good, but not necessarily optimal subsets, and this will be discussed in the next section. An upper limit on the performance of a subset of k electrode

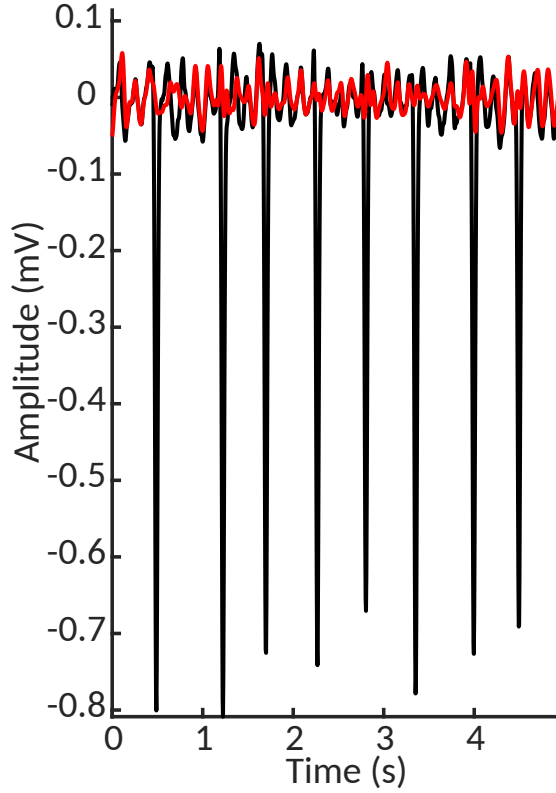


Figure 6.2: **Atrial activity extraction on BSPM** In black, the original recorded signal on vest lead 56, which corresponds to lead V_1 of the standard 12-lead ECG configuration. In red, the signal after spatiotemporal QRST cancellation.

signals for reconstructing the signals on all n electrodes is given by reconstruction using the first k principal components (PCs), since the explicit goal of PCA is to minimize the Frobenius reconstruction criterion. The PCs may be obtained efficiently by singular value decomposition (SVD) of X , $X = U\Sigma V^T$. The first k PCs are the columns of the matrix $U_k\Sigma_k$, where U_k contains the first k columns of U , and Σ_k contains the $k \times k$ upper-left portion of Σ . The corresponding rank- k reconstruction of X is given by:

$$X_k = U_k\Sigma_k V_k^T \quad (6.3)$$

where V_k contains the first k columns of V . Then the minimum approximation error $\|X - Q\|_F^2$ which can be attained by an arbitrary rank- k matrix is achieved when $Q = X_k$. Note that each PC is a linear combination of the signals on all n electrodes of X . Therefore, the rank- k PCA solution X_k is distinct from reconstruction using a subset S of k vest electrode signals and serves only as an upper bound to compare how well a given S captures the information on all BSPM electrodes.

6.2.4 ELECTRODE SUBSET SELECTION AND COMPARISON

The purpose of this section is to describe the different subsets of vest electrodes we used for the calculation of the novel indices ER_{NRMSE} and ER_{ABSE} , which will be elaborated in the next section. We also describe the characterization of the vest electrode subsets in terms of their capacity to accurately represent AA-BSPM signal information on all vest electrodes and compare this to the optimal PCA representation, as this is an important concept for the understanding of the novel indices.

(1) **Sequential** This algorithm was first proposed by (Lux et al., 1978) and later used by (Guillem et al., 2008, 2009) for selecting electrode subsets from a wider array of body vest electrodes. As its name suggests, this sequential approach greedily chooses electrodes one after the other, at each step picking the column containing the electrode signal which minimizes the reconstruction error, i.e., Eq. 6.2. This algorithm is in no way guaranteed to be optimal, since at each step it only considers that one additional electrode must be selected, rather than considering the entire subset. However, it can be relatively efficient (Altschuler et al., 2016; Farahat et al., 2011) and in general has had good performance for electrode selection. Therefore, it was chosen for use in this study. We call SEQ_k the subset of k vest electrodes (columns) chosen sequentially from the BSPM signal matrix X , for $k = 8 : 30$ electrodes. The lower limit of $k = 8$ electrodes was chosen to equal the number of independent leads used in the standard ECG, and the upper limit of $k = 30$ electrodes was chosen as a result of suggestions that roughly 30 electrodes are necessary to accurately represent AA in AF (Guillem et al., 2009).

(2) **Standard ECG** A subset of BSPM vest electrodes closest to the positions of the six precordial leads plus two limb leads used in the standard 12-lead ECG was extracted. We refer to this subset, which contains 8 electrodes, as ECG_8 .

(3) **Augmented ECG** Additionally, there have been suggestions that posterior electrodes may be desirable to better capture left atrial activity in AF. Therefore, a subset of vest electrodes closest to the augmented ECG suggested in (Petruțiu et al., 2009) consisting of the eight electrodes in the ECG_8 subset plus 3 posterior electrodes, V_8 , V_9 , and V_{10} in the same horizontal plane as V_6 , was tested. We refer to this subset, which contains 11 electrodes, as ECG_{11} .

Subsets were compared regarding how well they could represent the full BSPM signal matrix as follows. $SEQ_{8:30}$, ECG_8 , ECG_{11} , and $PCA_{8:30}$ subset reconstructions were calculated for five-second windows of each AA-BSPM segment. Given \hat{X} the reconstruction (Eq. 6.2) and X the full BSPM signal matrix for a window, two error measures were calculated and averaged over all windows in a segment. The first was the normalized root-mean square reconstruction error (NRMSE), given by:

$$\text{NRMSE} = \frac{\|X - \hat{X}\|_F}{\|X\|_F} \quad (6.4)$$

The second was the mean absolute difference (ABSE) across all electrodes between the atrial DF on each vest electrode signal of X and \hat{X} , where the DF was obtained as described at the

end of the previous section:

$$\text{ABSE} = \frac{1}{L} \sum_{l=1}^{L=L} |\text{DF}(X(:, l)) - \text{DF}(\hat{X}(:, l))| \quad (6.5)$$

where $L = 252$ vest electrodes in our case. The above measures were calculated on five-second windows of the one-minute AA-BSPM segments extracted from each patient and then averaged over all windows, for \hat{X} found for the ECG₈, ECG₁₁, and SEQ_{8:30} subsets determined for each window. Finally, for comparison, the above measures were calculated for $\hat{X} = X_k$, the rank- k PCA reconstruction as described in Eq. 6.3 for $k = 8 : 30$.

6.2.5 NOVEL SPATIOTEMPORAL INDICES ER_{NRMSE} , ER_{ABSE}

The purpose of this section is to combine the concepts discussed in Secs. 6.2.3 and 6.2.4 to introduce the novel indices ER_{NRMSE} and ER_{ABSE} . These indices quantify the capacity of a subset of BSPM vest electrodes to accurately represent the AA, and the atrial DF, respectively, on all BSPM electrodes over time, compared to the optimal PCA representation of the same rank as the electrode subset.

For the calculation of the indices, the one-minute AA-BSPM segments were divided into windows of five-seconds as in Sec. 6.2.4. The SEQ₈ and SEQ₁₁ subsets were obtained for the first window, and reconstructions were obtained on subsequent windows using these subsets and the corresponding matrices A from Eq. 6.1 determined for the first window. Concretely, for the first five-second window, the solution to Eq. 6.1 is $A^1 = S_k^1 X^1$, where X^1 is the full BSPM signal matrix for the first window, and S_k^1 contains the signals on a subset of k vest electrodes. The reconstruction for the i^{th} window X^i is given by $\hat{X}^i = S_k^i A^1$, where S_k^i contains the signals of X^i on the SEQ_{8,11} subset electrodes determined for the first five-second window X^1 , or the ECG₈/ECG₁₁ subset electrodes. In addition, the optimal rank- k ($k = 8, 11$) PCA reconstruction for each window, X_k^i , was determined as previously described, using the first k PCs, which we refer to as PCA _{k} . Then, the first index, ER_{NRMSE} , is given by the ratio of the reconstruction error obtained using SEQ₈, SEQ₁₁, ECG₈, or ECG₁₁, and the optimal same-rank reconstruction obtained with PCA₈ or PCA₁₁:

$$\text{ER}_{\text{NRMSE},i} = \frac{\|X^i - \hat{X}^i\|_F}{\|X^i - X_k^i\|_F} \quad (6.6)$$

The second index, ER_{ABSE} , is given by the ratio of the mean-absolute error between the atrial DFs extracted on each electrode of the subset vs PCA reconstructions:

$$\text{ER}_{\text{ABSE},i} = \frac{\sum_{l=1}^{L=L} |\text{DF}(X^i(:, l)) - \text{DF}(\hat{X}^i(:, l))|}{\sum_{l=1}^{L=L} |\text{DF}(X^i(:, l)) - \text{DF}(X_k^i(:, l))|} \quad (6.7)$$

The above indices were calculated on each five-second window following the first window of the one-minute AA-BSPM segments, then averaged across all windows, for one value per one-minute AA-BSPM segment. We chose to calculate these indices for the SEQ₈ and SEQ₁₁

6 Spatiotemporal signal processing methods for BSPM

subsets to allow a direct comparison with the standard and augmented ECG subsets, ECG₈ and ECG₁₁.

We hypothesized more organized, easier to treat forms of AF should have lower error ratios (ER), indicating stability in the AF dynamics between windows. This is because for lower ERs, the subset of electrodes chosen for the first window and A^1 permit a reconstruction of the i^{th} window that is closer to the optimal PCA reconstruction of the same rank. As a comparison to another BSPM index utilizing PCA for AF analysis, we calculated the NDI proposed by (Meo et al., 2018), which was found to be useful for quantifying AF complexity, choosing patients eligible for AF ablation and assessing therapy impact. The NDI was calculated as the residual variance not accounted for by the first three PCs of each AA-BSPM window. Note also that this index uses only PCA and therefore is not dependent on any particular subset of electrodes.

6.2.6 PERFORMANCE METRICS AND STATISTICAL ANALYSIS

The purpose of this section is to describe how the different electrode subsets introduced in Sec. 6.2.4 were compared in terms of their capacity to accurately represent AA-BSPM signal information on all vest electrodes compared to the optimal PCA representation. We also describe the methods used to quantify the relationship between the indices ER_{NRMSE}, ER_{ABSE} and NDI, and single-procedure CA success rate.

Calculated values of continuous parameters are expressed as mean \pm standard deviation. The statistical distributions of all parameters were checked using a Lilliefors test. Statistical inter-group differences were calculated as mean p -values across 3-folds, with 20% of the parameter values left out of each fold. One-way analysis of variance (ANOVA) was used for normally distributed data, or Wilcoxon's rank sum test was used for non-normally distributed data. Statistical tests were performed across folds to reduce the likelihood of chance group differences due to a small data set, and statistical significance was considered for p -values less than 0.05. For comparing the different electrode subsets in terms of their capacity to accurately represent AA-BSPM segments, we checked for statistical differences of the NRMSE and ABSE parameters calculated using the different electrode subsets (SEQ _{k} , ECG₈, ECG₁₁), or using the corresponding number of PCs (PCA _{k}). For comparing the relationships between single-procedure CA outcome and ER_{NRMSE}, ER_{ABSE}, and NDI, we checked for statistical differences between these indices calculated for AA-BSPM segments associated with AR and SR outcome groups.

For indices ER_{NRMSE}, ER_{ABSE}, and NDI displaying statistically significant differences between groups, univariate logistic regression classifiers were used to test their predictive power for single-procedure CA outcome. We used group-wise 3-fold cross-validation (CV) to ensure that indices calculated from different AA-BSPM segments of the same patient were only assigned to either the train or test set (80/20) for each fold. The resulting receiver operating curves (ROC) were analyzed to obtain area under the curve (AUC) to compare the predictive power of each index. We reported the AUC for AA-BSPM segment-wise classification as mean

\pm standard deviation over all CV folds, and the sensitivity and specificity were reported for the optimal classification threshold value determined through ROC analysis. The sensitivity and specificity were the fraction of true positive and true negative cases correctly identified, respectively, where AR was considered a positive case, and SR was considered a negative case.

6.3 RESULTS

6.3.1 STUDY POPULATION

At the time of this study, clinical outcome information was available for 11 patients, 6 of whom experienced an AR (55%) (3.4 ± 0.9 months post-CA). Therefore, only BSPM data from 11 patients were available for the part of the study associating the novel indices to CA outcome. Patients experiencing an AR were offered repeat procedures, however, in this study, only signals recorded prior to the first procedure and associated clinical outcomes were analyzed. Seven high quality one-minute AA-BSPM segments were extracted from the long duration BSPM recordings of each patient. Therefore, 91 one-minute AA-BSPM segments were available for the analysis with results described in Sec. 6.3.2, and 77 AA-BSPM segments for the results described in Secs. 6.3.3, 6.3.4, with each segment associated with an SR or AR outcome.

6.3.2 AA-BSPM RECONSTRUCTION WITH BSPM ELECTRODE SUBSETS

A representation of the spatial distributions of the SEQ_8 , SEQ_{11} , ECG_8 , and ECG_{11} subsets used for AA-BSPM reconstruction is shown in Fig. 6.3. For each subset type, the color of each electrode represents its occurrence in all the subsets used to calculate NRMSE and ABSE, that is, in what ratio of the tested subsets the electrode was included. It can be seen in Fig. 6.3a, b, that for SEQ subsets, both anterior and posterior electrodes were included in the subsets, with certain torso regions (upper and lower) being less represented in the subsets, while the mid-section regions were in general more represented. For the ECG subsets, the same subset of electrodes was applied to each five-second window of AA-BSPM data, as seen in Figs. 6.3c, d.

The similarity between reconstructed and original BSPM signals is shown in Fig. 6.4. A five-second window of a signal recorded on vest lead 57, close to the position of precordial lead V_1 , as well as its optimal least-squares reconstructions using the ECG_8 and SEQ_8 subsets associated with the window and its PCA_8 reconstruction are demonstrated in Fig. 6.4a. It can be seen that morphological characteristics of the signal were mostly captured in the reconstructed signals. However, the amplitude of the recorded signal was not perfectly reconstructed. The power spectral densities of the original and reconstructed signals are shown in Fig. 6.4b. It can be seen that the DF was correctly captured on this electrode. The NRMSE and ABSE as a function of number of electrodes included in the subsets are shown in Figs. 6.4c, d, taken as a mean across all patients, with error bars representing the 95% confidence interval. In addition, the PCA_k reconstruction obtained for k PCs equaling the number of electrodes is shown. As

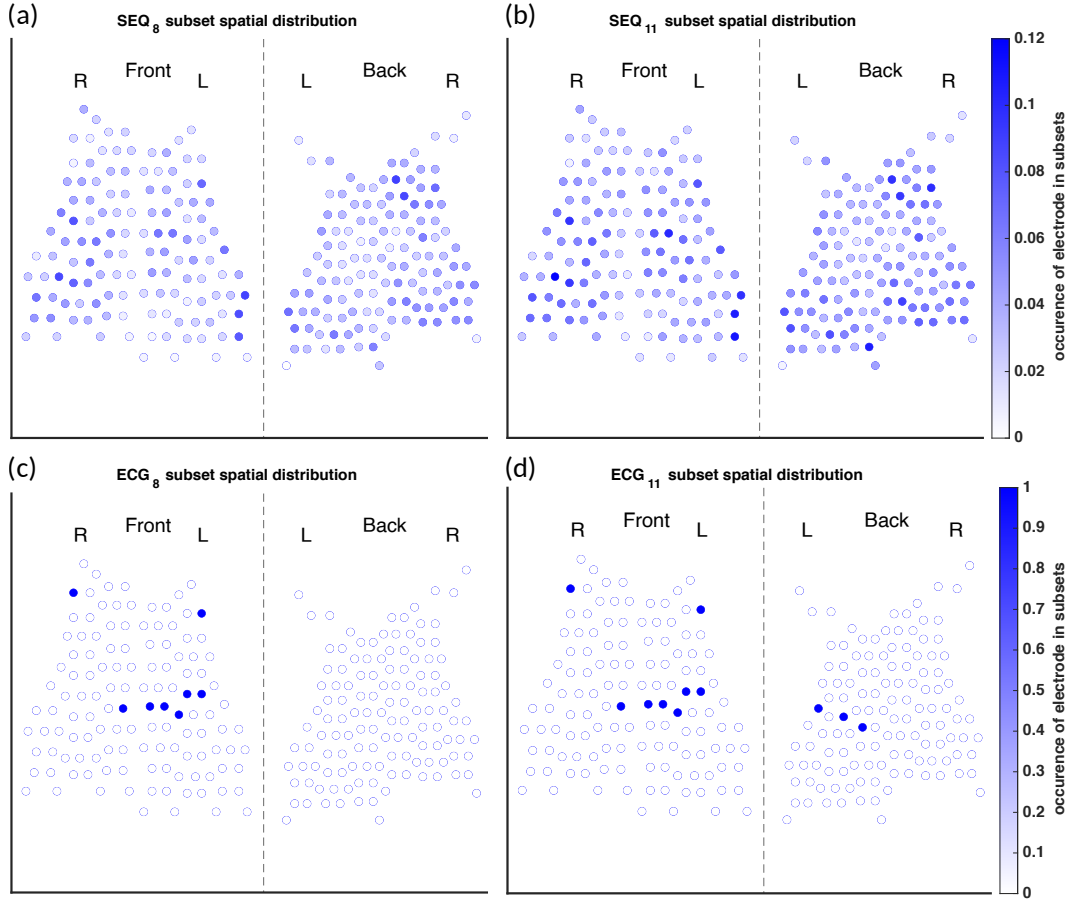


Figure 6.3: **Subset electrode occurrence.** Occurrence of each electrode in the (a) SEQ₈, (b) SEQ₁₁, (c) ECG₈, and (d) ECG₁₁ subsets. The color of each electrode indicates its occurrence in all of the subsets used to calculate reconstruction performance measures, where, for example, 1 indicates the electrode was present in every subset tested, and 0.1 indicates the electrode was present in 10% of subsets.

expected, reconstructions using ECG₈ and ECG₁₁ subsets had higher NRMSE and ABSE values than reconstructions using SEQ₈ and SEQ₁₁, and this difference was statistically significant ($p < 0.01$). In addition, it can be seen that PCA_k reconstruction consistently performed better than SEQ_k reconstruction, and this difference was also statistically significant for $k = 8 : 30$, ($p < 0.01$).

6.3.3 BSPM AF SPATIOTEMPORAL INDICES AND CA OUTCOME

For the analysis of ER_{NRMSE} and ER_{ABSE}, only the indices calculated using SEQ₈, SEQ₁₁, PCA₈, and PCA₁₁ were used, to allow for comparison with ECG₈ and ECG₁₁. Shown in Fig. 6.5 are the (a) ER_{NRMSE}, (b) ER_{ABSE}, and (c) NDI values according to CA outcome. The associated mean \pm standard deviation values of the indices are shown in Table 6.2. There was a statistically significant difference in the NDI value between the SR and AR groups, with NDI greater in the

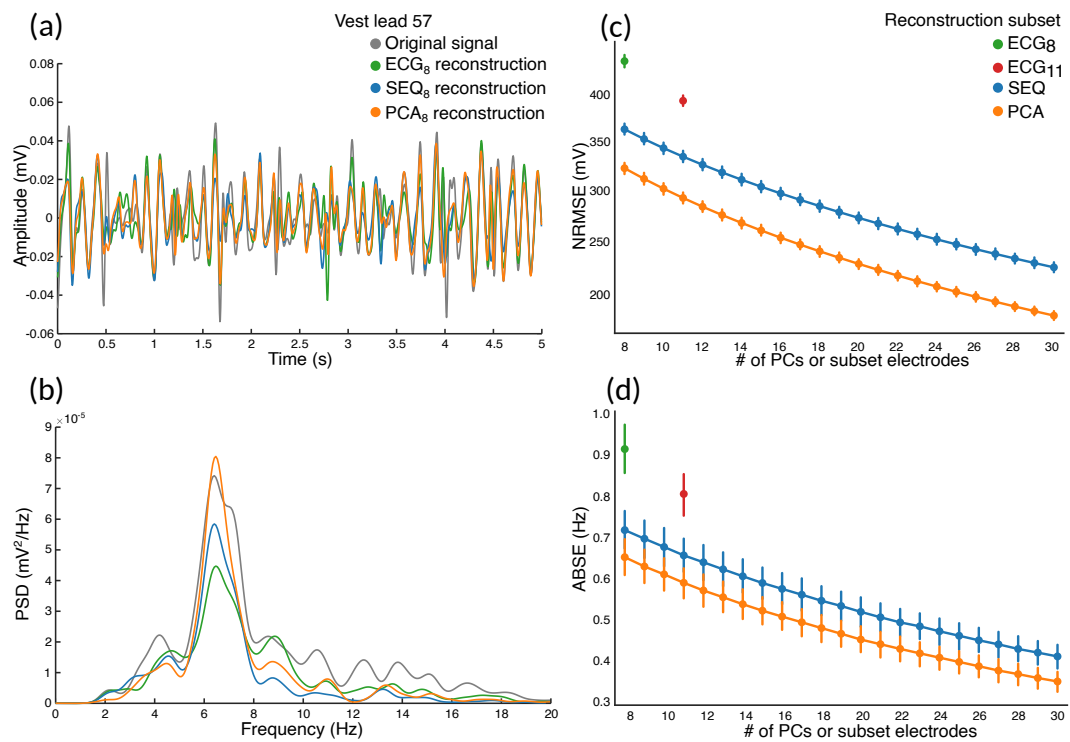


Figure 6.4: Atrial activity reconstruction. (a) A five-second window of the original recorded (in grey) and reconstructed signals, for vest electrode 57, close to V_1 . Reconstruction with the ECG₈ subset (green), SEQ₈ subset (blue), and PCA₈ (orange). (b) The corresponding power spectral densities (PSD) of the original recorded and reconstructed signals. (c) Normalized root-mean square reconstruction error (NRMSE), and (d) mean absolute error (ABSE), as a function of number of principal components or vest electrodes used in subset for reconstruction.

6 Spatiotemporal signal processing methods for BSPM

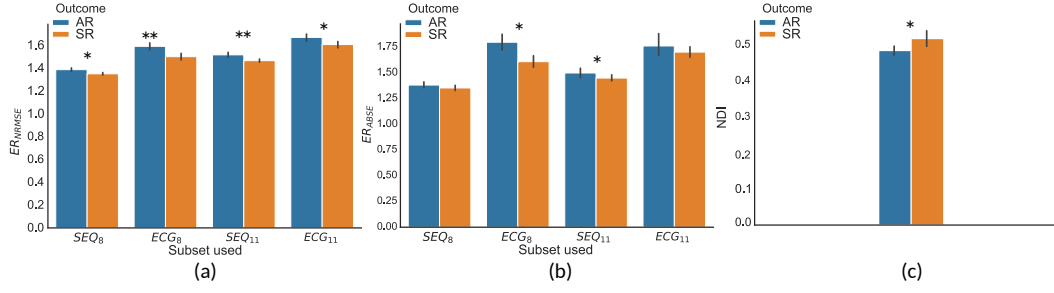


Figure 6.5: **BSPM indices by ablation outcome.** BSPM analysis indices, grouped according to clinical outcome. (a) Error ratio NRMSE to PCA (ER_{NRMSE}); (b) Error ratio ABSE to PCA (ER_{ABSE}); (c) Non-dipolar component index (NDI). Significant differences between AR and SR outcome means are indicated by asterisks. (* $p < 0.05$, ** $p < 0.01$.)

SR group. Greater ER_{NRMSE} values were associated with AR following single-procedure CA, while lower ER_{NRMSE} values were associated with SR, for all electrode subsets tested. Finally, for ER_{ABSE} , greater values were again observed for AR than SR, with statistical significance only for the ECG₈ and SEQ₁₁ subsets.

Table 6.2: **ER_{NRMSE} , ER_{ABSE} , and NDI values by vest electrode subset.** ER_{NRMSE} , ER_{ABSE} , and NDI values by vest electrode subset (not applicable for NDI) and single procedure CA outcome, expressed as mean \pm standard deviation. p -values were computed as means across three folds of data, in which a p -value for the statistical significance between index values by outcome was computed using 80% of the AA-BSPM segments in each fold.

	ER_{NRMSE}			ER_{ABSE}		
	SR	AR	p -value	SR	AR	p -value
SEQ ₈	1.349 \pm 0.034	1.385 \pm 0.053	0.01	1.352 \pm 0.078	1.38 \pm 0.096	0.294
ECG ₈	1.499 \pm 0.091	1.589 \pm 0.102	0.008	1.607 \pm 0.171	1.796 \pm 0.253	0.045
SEQ ₁₁	1.464 \pm 0.041	1.515 \pm 0.075	0.002	1.448 \pm 0.093	1.497 \pm 0.159	0.033
ECG ₁₁	1.605 \pm 0.082	1.667 \pm 0.100	0.037	1.7 \pm 0.15	1.76 \pm 0.351	0.107
NDI						
	SR	AR	p -value			
	0.517 \pm 0.07	0.484 \pm 0.041	0.018			

6.3.4 PREDICTIVE POWER OF SPATIOTEMPORAL INDICES FOR OUTCOME CLASSIFICATION

A summary of the ROC analysis of the NDI, ER_{NRMSE} , and ER_{ABSE} parameters for prediction of CA outcome is shown in Table 6.3. Note that sensitivity and specificity values are shown for segment-wise classification. It can be seen that ER_{NRMSE} displayed the most consistent performance across folds and electrode subsets, with AUC = 0.77 \pm 0.08, sensitivity = 76.2%,

and specificity = 84.8% for ER_{NRMSE} calculated with the SEQ_{11} electrode subset. Despite the associations between NDI and ER_{ABSE} and CA outcome, the predictive performances of these indices were not as consistent as for ER_{NRMSE} . The ROC curves associated with ER_{NRMSE} calculated for each subset are shown in Fig. 6.6. The ROC curves associated with NDI and ER_{ABSE} are not shown due to their lower performance; refer to Table 6.3 for the results associated with these indices.

Table 6.3: **Predictive power of BSPM indices for CA outcome.** Predictive power of BSPM indices for CA outcome for each of the tested subsets. Sensitivity and specificity indicate the rate of detection of arrhythmia recurrence and sinus rhythm 6 months post single-procedure CA, respectively. AUC, area under the curve

	AUC (mean \pm std)	Sensitivity (%)	Specificity (%)
ER_{NRMSE}			
SEQ_8	0.72 \pm 0.09	61.9	84.8
ECG_8	0.81 \pm 0.26	64.3	98.9
SEQ_{11}	0.77 \pm 0.08	76.2	84.8
ECG_{11}	0.69 \pm 0.28	57.1	84.8
ER_{ABSE}			
ECG_8	0.76 \pm 0.23	57.1	98.9
SEQ_{11}	0.52 \pm 0.29	28.6	98.9
NDI			
	0.37 \pm 0.45	33	98.9

To further test the efficacy of ER_{NRMSE} , we repeated the statistical comparison and predictive performance analysis for SEQ subsets with 8 to 30 electrodes, to see whether performance changed for different numbers of electrodes included in the SEQ subset. The results are shown in Figs. 6.7 and 6.8. It can be seen in Fig. 6.7a that the ER_{NRMSE} was greater in the AR group than SR group when calculated with all $SEQ_{8:30}$ subsets. However, this difference was only statistically significant for ER_{NRMSE} calculated with $SEQ_{8:24}$ subsets, as shown in Fig. 6.7b, with the p -values from significance testing transformed as $\frac{-\log_{10}(p)}{\max(-\log_{10}(p))}$ to allow for a graphical representation. In Fig. 6.8 are shown AUC values associated with the ROC analysis of the ER_{NRMSE} calculated with $SEQ_{8:30}$ subsets. It can be seen that the AUC increased, and variance of the AUC decreased, for up to 15 electrodes included in the SEQ subset. For more than 15 electrodes, the AUC generally decreased, and variance of the AUC increased.

6.4 DISCUSSION

In this study, we developed two novel, fully spatiotemporal indices for the efficient processing of long-duration BSPM signals collected from patients with persistent AF. The use of spa-

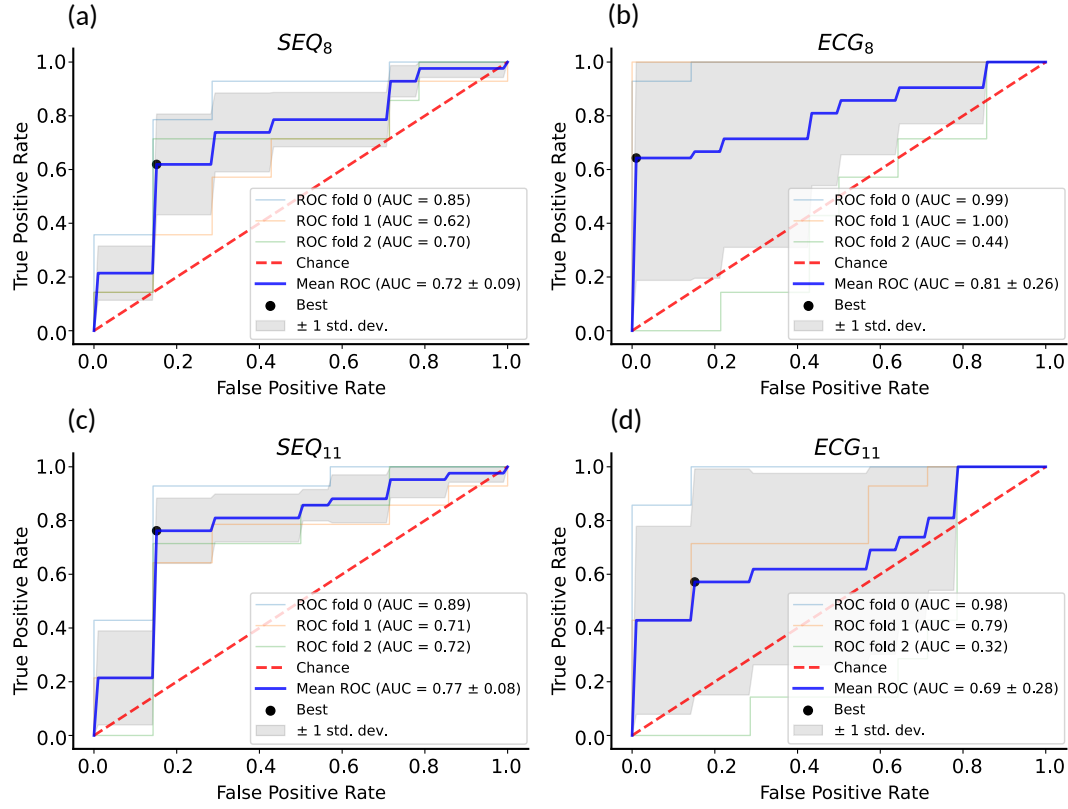


Figure 6.6: **ER_{NRMSE} ROC analysis.** ROC analysis for ER_{NRMSE} for predicting CA outcome calculated with (a) SEQ_8 ; (b) ECG_8 ; (c) SEQ_{11} ; and (d) ECG_{11} vest electrode subsets. The optimal tradeoff between true positive rate and false positive rate is indicated by a black dot.

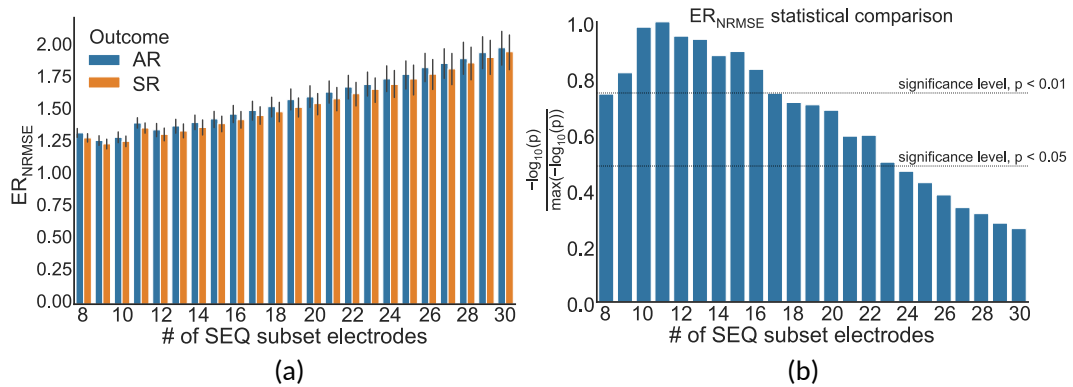


Figure 6.7: **Statistical significance by number of subset electrodes.** (a) Representation of p values associated with statistical comparison of ER_{NRMSE} mean values for AR and SR patient groups. The $p = 0.05$ and $p = 0.01$ significance levels are indicated by dashed lines; (b) ER_{NRMSE} values grouped according to clinical outcome, calculated with $SEQ_{8:30}$ subsets.

tiotemporal ventricular activity cancellation rather than short, nonconsecutive TQ segments allowed the incorporation of a temporal component in the analysis. By combining PCA and the temporal component, a true spatiotemporal characterization was achieved. To the best of our knowledge, this is the first study to propose indices exploiting temporal irregularity in long-duration BSPM recordings for persistent AF analysis, with a view to predicting AR following single procedure CA. The selection of which electrodes to use for the calculation of the novel indices can be automatically performed using the sequential subset selection method, or can be adapted for different subsets of electrodes, such as the standard or augmented ECG lead configurations. Finally, in our study, we have investigated the relationship between the proposed novel indices and their correlation with and predictive power for CA outcome. We found that a mean AUC of up to 0.8 may be achieved for predicting arrhythmia recurrence in persistent AF patients who underwent single-procedure CA for the novel index ER_{NRMSE} .

6.4.1 ELECTRODE SUBSET CAPACITY TO REPRESENT AA-BSPM

PCA-based indices have been used extensively in ECG signal processing (Castells et al., 2007), with applications including extraction of atrial fibrillatory waves, quantification of AF spatial complexity and organization, and efficient analysis of BSPM data. In this study, we have included a framework for understanding how PCA-based reconstruction of AA-BSPM signals compares to reconstruction using a subset of vest electrode signals. The use of vest electrode reconstruction was based on previous studies, which have demonstrated that the full BSPM signal matrix may be projected onto a smaller matrix containing only a subset of BSPM vest electrode signals (Lux et al., 1978; Guillem et al., 2008, 2009; Feng et al., 2019). The resulting reconstruction error between the original and projected matrices has been shown to depend on the number of electrodes included in the subset, as well as the type of BSPM signals. For example, Guillem et al. (2009) found that with the same number of electrodes, reconstruction error was lower for ventricular than atrial activity. In our study, as the number of electrodes

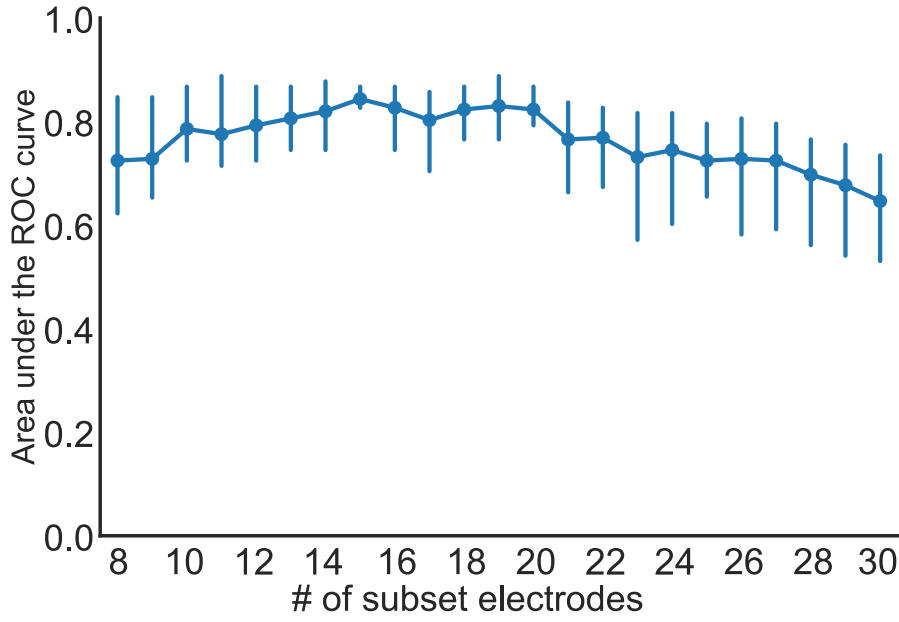


Figure 6.8: **ER_{NRMSE} predictive performance.** Mean and standard deviation of the area under the ROC curve (AUC) computed using three cross-validation folds, for ER_{NRMSE} performance for predicting CA outcome when calculated with SEQ_{8:30} electrodes.

included in the ECG or SEQ subsets increased, the NRMSE and ABSE both decreased, in line with results from Guillem et al. (2009). We also showed for the first time in our study the same trend for optimal PCA reconstruction. It can be noted that for all numbers of electrodes tested, there was a greater overlap between the ABSE values than NRMSE values between the different subset types. This could be because the reconstruction method used optimized for NRMSE, and not ABSE.

Regarding the comparison of different BSPM electrode subsets, it was found that SEQ subsets more accurately represented BSPM signal data than standard and augmented ECG subsets in both signal domains, manifested through lower NRMSE and ABSE values for both $k = 8$ and $k = 11$ electrodes included in the vest subset. This reinforces the idea that standard ECG electrode configurations are not optimal in terms of accurately representing the full BSPM signal matrix. Since results from previous works have suggested that the addition of posterior electrodes may be useful to better reflect left atrial activity in AF (Ihara et al., 2007; Petrutiu et al., 2009; Buttu et al., 2013; Guillem et al., 2013), we did include the augmented ECG₁₁ subset. Interestingly, it was found that the decrease in reconstruction error between the ECG₈ and ECG₁₁ subsets was greater than the decrease in error between the SEQ₈ and SEQ₁₁ subsets, lending support to the argument that the addition of carefully positioned posterior electrodes may indeed be beneficial for representing AA-BSPM data. Additionally, it was found that PCA-based reconstruction performed better than electrode subset based reconstruction, in both the temporal and frequency domains. This is to be expected, since PCA explicitly optimizes for the reconstruction criterion. However, this remains an important result since

to our knowledge, the gap between electrode subset and PCA reconstruction had not been previously investigated.

6.4.2 STATISTICAL COMPARISON OF NOVEL INDICES

The finding in our study that ER_{NRMSE} , ER_{ABSE} , and NDI all showed statistically significant differences between AA-BSPM segments associated with AR or SR outcomes demonstrates that each of these indices shows some potential to be used as computational tools for AF disease management. Since calculation of ER_{NRMSE} and ER_{ABSE} required selection of a subset of vest electrodes, these indices were calculated for standard and augmented ECG subsets (ECG_8 and ECG_{11} , respectively), as well as for sequentially chosen subsets (SEQ_8 and SEQ_{11}), which differed between AA-BSPM segments, to test the robustness of the indices with respect to both which and how many electrodes were included in the subsets.

Many previous studies have investigated capturing AF information using surface recorded ECG signals, however, most often using a single or limited number of leads. This prevents the exploitation of the spatial diversity of multi-lead ECGs and is dependent on the available electrode signal containing information representative of the underlying AF. Since electrode placement cannot be exact, and patient anatomy varies widely, this is not always guaranteed. Further, it has already been shown that inclusion of multiple leads is beneficial, leading to greater correlation between calculated 12-lead ECG indices and AF complexity and outcomes (Meo et al., 2013; Zarzoso et al., 2016). The idea in this study was therefore to add to the limited number of BSPM indices for AF analysis, integrating both temporal and spatial information.

Bonizzi et al. (2010) showed that reconstruction error using the PCA rank-3 approximation of TQ segments of BSPM signals recorded during AF was capable of separating AA signals into clusters based on levels of AF organization, with greater reconstruction error corresponding to higher AF complexity and lower stationarity. Later, Di Marco et al. (2012), using PCA-based indices, found that higher spatial organization, indicating easier to treat forms of AF, was correlated with more temporally stable atrial activation patterns. We hypothesized that lower ER_{NRMSE} values would therefore be observed among SR patients, indicating more stability in the AF dynamics between BSPM windows, and this was indeed the case. The finding that ER_{NRMSE} displayed greater values in AR AA-BSPM segments than SR segments for all four electrode subsets lends support to its use as a robust index for predicting single-procedure AF outcome. Further, Di Marco et al. (2012) also found that greater temporal variability was associated with lower spectral concentration. Therefore, we hypothesized again that lower ER_{ABSE} values would be observed for SR patients. While the ER_{ABSE} calculated for AR patients was greater than that for SR patients, this difference was only statistically significant for two of the electrode subsets tested, potentially making it less robust than ER_{NRMSE} . This lower robustness could relate to the finding discussed above that there was a greater overlap in ABSE values calculated for subset vs. PCA reconstruction.

6 Spatiotemporal signal processing methods for BSPM

The NDI was unexpectedly found to be greater for SR segments than AR segments, meaning that the remaining variance unexplained by the first three PCs of the BSPM signal data was on average greater for SR segments than AR segments. This is contrary to the results of Meo et al. (2018), who found smaller NDI values in concatenated TQ segments of BSPM data collected from patients with successful procedural CA outcome. Several key differences in our study could explain the contradictory results, including our use of longer duration AA-BSPM segments rather than concatenated TQ segments. Additionally, the study by Meo et al. (2018) compared NDI values calculated for procedural outcomes, while in this study we used single-procedure clinical outcomes. Future studies testing the NDI may shed light on this discrepancy.

6.4.3 ASSESSMENT OF CLINICAL IMPACT OF NOVEL INDICES

The clinical impact of the indices tested in this study depends not only on their association with CA outcomes but also their ability to predict CA outcomes. Therefore, we tested classification performance of univariate logistic regression classifiers for ER_{NRMSE} , ER_{ABSE} , and NDI. The use of group-wise CV was important to ensure AA-BSPM segments extracted from the same patient were included only in either the train or test set of each fold. Reporting both mean and standard deviation values of the AUC for each classifier also gave an indication of the CA outcome prediction model variance for different folds of the data. These were important features of our methodology considering the small-size of our data set.

Importantly, only ER_{NRMSE} displayed consistent results in predictive power across tested vest electrode subsets. The AUCs for this index calculated with each subset (SEQ_8 : 0.72 ± 0.09 , ECG_8 : 0.81 ± 0.26 , SEQ_{11} : 0.77 ± 0.08 , ECG_{11} : 0.69 ± 0.28) were as good or better than the AUC associated with NDI (0.69), found by Meo et al. (2018), and the model variance was not reported in their study. Additionally, the study by Meo et al. (2018) also tested prediction performance for NDI combined with clinical parameters, achieving an AUC of 0.7. Our results were also as good or better than those described by Lankveld et al. (2016), in which predictive performance varied from $AUC=0.76 \pm 0.15$ for 12-lead ECG derived complexity parameters alone to $AUC=0.79 \pm 0.13$ for ECG plus clinical parameters. Additionally, the results were in line with those obtained by Zeemering et al. (2018), for which an AUC of 0.66, 95% confidence interval [0.64-0.67] was obtained for the best ECG parameter studied (dominant atrial frequency in lead II). The study also reported better performance when several ECG parameters were combined (AUC 0.78 [0.76-0.79]), and best performance for combining ECG plus clinical parameters ($AUC=0.81$ [0.79-0.82]). It is important to note that the variance across CV folds was less for ER_{NRMSE} calculated with SEQ subsets compared to ECG subsets, and in general lower than model variances reported in other studies. This result was also found to be true in our additional analysis calculating ER_{NRMSE} with $SEQ_{8:30}$ electrodes, finding high predictive performance for nearly all numbers of electrodes included in the subset. That ER_{NRMSE} showed the best results and lowest variance when calculated with SEQ electrode subsets could indicate that when working with BSPM signals, an informed patient or segment specific selection of

subset electrodes may be useful, for example using the sequential algorithm. This is logical given the nonstationary nature of BSPM recordings in AF. This was further supported by the lack of a clear pattern of specific electrodes included in the SEQ subsets as seen in Fig. 6.3; rather, certain regions of the vest contain electrodes picked by the sequential algorithm more often than other regions. The finding that specificity was generally higher than sensitivity across all indices tested could indicate that this index would be more useful for selecting which patients would be most likely to benefit from CA, as opposed to selecting those least likely to benefit. Note that specificity was also higher than sensitivity for the NDI in the original study (Meo et al., 2018). The other two indices appear less robust to predict CA outcome, with low AUC and sensitivity values for NDI. For ER_{ABSE} , the results appear more promising, but still displaying relatively low sensitivity and more variable AUC values across CV folds than ER_{NRMSE} .

These results all point towards the potential value of ER_{NRMSE} as a clinically useful tool that could be used to analyze BSPM data in persistent AF. If confirmed by future studies, the use of ER_{NRMSE} could be important in assisting in prediction of successful CA outcomes, which would be useful for improving informed decision-making regarding treatment for persistent AF. This would be particularly important given the low success rate of CA for treating persistent AF. Finally, the added clinical value of using BSPM data in AF remains unclear, as evidenced by its being largely limited to research use (Salinet et al., 2021). However, if indices calculated using BSPM data, such as ER_{NRMSE} , could be shown to be consistently associated with and good predictors of CA outcomes, this could confirm the validity of using BSPM data for AF analysis.

6.4.4 LIMITATIONS

The study population, at 13 patients, and 11 patients with clinical outcome data, was small; however, the effort in obtaining BSPM recordings is considerable, due to the high number of electrodes which must be used. The use of group-wise CV on segments of data extracted from each patient did however permit a robust analysis using this data set. In addition, the randomized inclusion criteria enhances our conclusions on BSPM AF characterization, though this may not be representative of the general characteristics of a wider population. Given the variation in experimental set up and parameters used, comparing with parameters from previous studies was challenging, and a more systematic study would be required for integration of the contributions of this work into clinical practice. Further, the small size of the population precluded the analysis of correlation with clinical indices, or whether the proposed indices could be combined with clinical indices for predicting CA outcome, as it has been shown previously in several studies that combining ECG-based indices with clinical parameters yields the best clinical performance (Lankveld et al., 2016; Zeemering et al., 2018; Meo et al., 2018). Additionally, the follow-up duration was relatively limited, and again due to the small study size, the impact of anti-arrhythmic medications could not be assessed since these were used by most patients. Finally, while we have shown the usefulness of the proposed

6 Spatiotemporal signal processing methods for BSPM

indices for predicting CA outcome, we were unable to examine these indices for quantifying AF complexity due to a lack of available simultaneous intracardiac recordings.

7 CONCLUSION

Atrial fibrillation treatment is subpar, especially for persistent AF patients whose quality of life suffers the most. Decades of research have resulted in a better understanding of AF, but the exact molecular mechanisms behind its genesis and progression remain unknown. Numerous ECG and clinical biomarkers have been proposed through either direct or indirect correlation with AF disease organization, complexity, disease dynamics and progression. Many of these biomarkers have been tested for their association with AF outcome, and their performance as independent predictors of AF termination by CA, and long-term maintenance of sinus rhythm thereafter, has also been assessed. Using these results, several studies have built pre-ablation predictive models consisting of several ECG biomarkers, several clinical biomarkers, or a combination of both.

In this thesis, we collected ECG data in two persistent AF patient cohorts. In one cohort, 12-lead ECG was recorded, while in the other, BSPM ECG consisting of 252 leads was recorded. Using this data, we calculated ECG biomarkers before and during catheter ablation, to evaluate their utility as tools which could be used by clinicians to track progress while performing ablation. We tested and validated ECG biomarkers correlated with AF disease complexity for their association with and predictive power for AF termination by catheter ablation, and long-term maintenance of sinus rhythm thereafter, showing in particular that HRV metrics show promise as predictive ECG biomarkers for catheter ablation outcomes. Inspired by signal processing techniques which exploit the spatial diversity of multi-lead ECG, we also proposed two novel BSPM ECG biomarkers for the prediction of sinus rhythm maintenance after catheter ablation. The work described in the main chapters of this thesis is summarized below.

7.1 MAIN FINDINGS

In **Chapter 4**, we showed that two spatiotemporal electrocardiographic biomarkers, instantaneous frequency (IF) and adaptive organization index (AOI) measured noninvasively pre-ablation indicated lower levels of AF organization in patients whose arrhythmia was not terminated by ablation (NLT patients). These biomarkers were not however found to be associated with AF recurrence in the follow-up period post-ablation. In other words, they were not found to differ significantly between LTN and LTR patients. Additionally, we found that the value of the biomarkers evolved over the course of CA, indicative of increased AF organization, especially in patients with AF termination and long-term maintenance of sinus rhythm. These results indicate that the IF and AOI measures could be used by clinicians to track ablation

7 Conclusion

progress.

In **Chapter 5**, we showed that commonly used HRV metrics have the potential to be used as ECG biomarkers for predicting AF outcomes. Changes in HRV metrics from pre-ablation to the end of ablation indicative of increasing organization in the ventricular response were associated with AF termination by CA; this was especially the case for recurrence measures. In addition, we showed that lower HRV measured pre-ablation was not only associated with, but also predictive of AF termination and long-term maintenance of sinus rhythm, finding that SDNN performed especially well on our patient population. HRV analysis is much easier to perform in a consistent manner than direct analysis of the atrial component of ECG signals. Therefore, we believe it should be seriously considered in combination with clinical biomarkers for the noninvasive quantification of AF refractoriness to CA.

Finally, in **Chapter 6**, drawing inspiration from biomarkers quantifying spatial and temporal variability in the 12-lead ECG signal, we developed two novel ECG biomarkers, ER_{NRMSE} and ER_{ABSE} for the efficient processing of BSPM data recorded in AF. We tested these biomarkers for their association with and predictive power for post-ablation AF recurrence. We compared the performance of these biomarkers to another recently proposed BSPM biomarker, finding superior performance in our novel biomarkers when tested on our patient population.

7.2 CONTRIBUTIONS

The main contributions of this thesis can be summarized as follows:

ECG biomarkers associated with AF complexity evolve over the course of catheter ablation, indicative of increased AF organization, especially in patients with arrhythmia termination and long-term maintenance of sinus rhythm.

ECG biomarkers associated with AF complexity indicate higher levels of AF organization pre-ablation in patients who, as a group, have their AF terminated by ablation and have long-term sinus rhythm thereafter.

ECG biomarkers based on HRV analysis showed greater HRV, and lower heart rate regularity, in patients who did not have their AF terminated.

The proposal of two novel BSPM biomarkers, which were shown to be associated with and predictive of post-ablation AF recurrence.

7.3 GENERAL DISCUSSION AND PERSPECTIVES

Guidelines and research for AF treatment are constantly evolving. Forward looking approaches to AF treatment focus on adapting to the needs and physiological presentation of each patient. A recent publication (Noubiap et al., 2021) summarizing data on the association between

key AF biomarkers and incident AF and adverse clinical events, i.e., stroke, in AF patients highlighted the importance of genetic and molecular biomarkers in managing AF. The authors described that these biomarkers are indicative of inflammation and oxidative stress, which are thought to be key factors for AF incidence, progression, and response to treatment. The authors suggest that these biomarkers could be used to improve early identification of AF type (paroxysmal vs persistent), to aid in clinical AF risk stratification, and to predict outcomes of rhythm-control therapies like catheter ablation. Specific clinical use cases described by the authors include biomarkers guiding patient selection for extended ECG recordings and implantation of a cardiac monitor for high risk patients.

Another review from 2013 describing treatment in 2033 (Gillis et al., 2013) noted that the approach to AF management is general and focuses on stroke risk assessment and prevention, arrhythmia management, and treating underlying causes. The authors of this study argued that resulting AF management is based largely on intermittent snapshots of the presentation of each patient's arrhythmia, and that such an approach discounts the fact that AF is often asymptomatic. They mention that a combination of ECG, clinical, and genomic biomarkers would be required to take AF treatment from its current trial and error approach to a targeted, individualized strategy. Additionally, to quote one of the largest studies to compare rate and rhythm control strategies for AF from 2002, "AF is the most common sustained cardiac arrhythmia, yet the optimal strategy for its management remains uncertain" (AFFIRM Investigators, 2002). Twenty years later, an AF review paper (Brundel et al., 2022) reads, "AF is the most common cardiac arrhythmia despite substantial efforts to understand the pathophysiology of the condition and develop improved treatments. Identifying the underlying causative mechanisms of in individual patients is difficult and the efficacy of current therapies is suboptimal." Therefore, while great strides have been made in understanding the molecular mechanisms behind AF, the complicated nature of the disease, and the degree of inter-patient variability observed impede the development of targeted and effective therapeutic strategies.

To our knowledge, biomarkers, ECG, clinical, genomic or otherwise, are still not used for AF risk stratification and guiding AF treatment. It stands to be observed that for AF biomarkers to be used in clinical practice, future studies to compare the most promising proposed biomarkers in independent and external patient cohorts are needed. Only then could their true predictive performance for AF termination by catheter ablation and sinus rhythm maintenance thereafter be objectively validated. It is our hope that such studies will be undertaken, and that biomarkers, or combinations of them, that are the most performant for guiding individualized AF therapy will become common in clinical settings.

APPENDIX

A ATRIAL ACTIVITY EXTRACTION

Surface ECG signals are a reflection of the global activity of the heart, so they include both ventricular and atrial components (see Chapter 2). However, the ventricles are much larger than the atria, so the amplitude of the ventricular component is much greater than that of the atrial component. Additionally, the heart rate is often very high in AF, meaning that intervals in which only atrial activity is present, that is, the TQ intervals between consecutive QRST complexes are very short. These two factors combine to make pure analysis of the atrial component of the ECG in AF a difficult problem, as the frequency content of the atrial and ventricular components overlap, so linear filtering is not an option for removing the ventricular component.

Many algorithms have been developed for extracting the atrial component. Atrial activity extraction, f-wave extraction, and ventricular activity cancellation are common terms assigned to these algorithms. Here, we will use the term f-wave extraction to emphasize that we aim to extract f-waves, which are characteristic of AF, in the presence of ventricular activity.

There are several factors to consider when designing and choosing an algorithm for f-wave extraction (Sörnmo et al., 2018). For example, the number of leads used to record the ECG signals, the level of noise and artifacts present in the signal, the length of the ECG recordings, and the relative presence of ventricular premature beats (VPB), whether the algorithm needs to work in real-time or with limited computational power, are all factors that should be considered when choosing an algorithm. As a result, numerous f-wave extraction algorithms have been developed, each having its own strengths and limitations.

Most f-wave extraction algorithms rely on some form of beat averaging to remove the QRST complex. The idea is to compute an average QRST complex, obtained from an ensemble of beats with similar morphology, and subtract the resulting average from each beat of the original ECG. Other algorithms use nonlinear Kalman or adaptive filtering techniques, and still others use variants of principal components analysis (PCA), independent components analysis (ICA), or blind-source separation to extract an “atrial source,” assumed to be separable from the “ventricular source.” The performance of each algorithm depends on the specific application and operating conditions under which it was tested; however, a study (Langley et al., 2006) which compared the performance of three algorithms (spatiotemporal QRST cancellation, PCA, ICA) did not find significant differences between the three, noting only that the PCA and ICA algorithms did occasionally extract f-waves with a notable residual from the ventricular activity.

The purpose of this appendix is to describe in detail the two f-wave extraction methods used in this thesis, (1) single-beat (SB), for the standard 12-lead ECG signals analyzed in Chapters 4 and 5 of this thesis, (2) spatiotemporal QRST cancellation (STC), for the BSPM signals analyzed in Chapter 6. Because the single-beat algorithm is an extension of the spatiotemporal algorithm, we will start with describing the spatiotemporal algorithm.

A.1 SPATIOTEMPORAL QRST CANCELLATION TECHNIQUE

The purpose of this section is to describe the f-wave extraction algorithm proposed by Stridh and Sornmo (2001), and applied to the BSPM ECG signals analyzed in Chapter 6 of this thesis. The authors refer to this algorithm as spatiotemporal QRST cancellation, which extends the average beat subtraction (ABS) (Slocum et al., 1992) method by introducing multi-lead information.

The ABS approach exploits the fact that ventricular and atrial activity are uncoupled in AF, therefore, an average of all the beats in the recorded ECG signal is subtracted from the ECG to extract a residual f-wave signal. However, the average beat is not an accurate representation of each individual beat due to changes in consecutive QRST morphology caused by slight temporal variations in the electrical axis of the heart, notably because of respiration. These axis variations can lead to QRST related artifacts in the extracted f-wave signal. Therefore, Stridh and Sornmo (2001) created the spatiotemporal QRST cancellation technique which uses multi-lead information and alignment of the template with each individual beat to achieve superior f-wave extraction performance.

A.1.1 METHODS

Observation model

One cardiac cycle in the ECG can be represented by a matrix $Y \in \mathbb{R}^{N \times L}$, where N is the number of samples making up the cardiac cycle recorded on L ECG leads:

$$Y = [y_1 \cdots y_L] \quad (\text{A.1})$$

where each column contains the samples of the l^{th} lead. The beat of each cardiac cycle may be modeled as the sum of atrial activity (Y_A), ventricular activity (Y_V), and additive noise (W'). The ventricular activity may be represented by an averaged beat $X \in \mathbb{R}^{(N+2\Delta) \times L}$, and a spatial alignment matrix $S \in \mathbb{R}^{L \times L}$ is defined. The matrix S introduces the following properties in the f-wave extraction process: (1) the possibility to share information between leads to allow for electrical axis variations, (2) the possibility to scale to allow for variations in tissue conductivity and heart position which could affect amplitude differently in different leads.

The matrix S is defined as the product of two matrices, $S = DQ$, where D is a diagonal amplitude scaling matrix with positive diagonal elements d_l and M rotation matrix. In addition,

A.1 Spatiotemporal QRST Cancellation Technique

a time-shift matrix J_τ is introduced to correct for temporal misalignment between the observed and average template beat:

$$J_\tau = [\mathbf{0}_{N \times (\Delta + \tau)} \mathbf{I}_{N \times N} \mathbf{0}_{N \times (\Delta - \tau)}] \quad (\text{A.2})$$

The purpose of this matrix is to select the N samples of the average template beat that best fit the observed beat Y , with the maximum temporal alignment shift given by Δ . The resulting model of the ventricular activity is therefore:

$$Y_V = J_\tau X S \quad (\text{A.3})$$

Then the goal is to estimate the parameters of Q , D and τ and subtract Y_V from Y . The amount of noise W' in the signal affects how well the quantity $J_\tau X S$ fits Y_V , therefore, an intermediate estimate \tilde{Y}_A is used that is subtracted from the observed signal before estimating the cancellation parameters:

$$Z - J_\tau X S = W' + Y_A - \tilde{Y}_A = W \quad (\text{A.4})$$

where $Z = Y - \tilde{Y}_A$. This is referred to as AF reduction.

QRST cancellation parameter estimation

The estimation of the QRST cancellation parameters is performed by solving the following minimization problem:

$$\epsilon_{\min}^2 = \min_{D, Q, \tau} \|Z - J_\tau X D Q\|_F^2 \quad (\text{A.5})$$

Minimizing with respect to Q and D independently cannot be performed, therefore finding a closed form solution is not trivial. Therefore, an iterative approach is used, where the error ϵ^2 is minimized with respect to Q by maximizing the last term, assuming D is known.

$$\epsilon^2 = \text{tr}(Z Z^T) + \text{tr}(J_\tau X D D^T X^T J_\tau^T) - 2 \text{tr}(D^T X^T J_\tau^T Z Q^T) \quad (\text{A.6})$$

The maximization can be done using SVD, which decomposes a matrix T into two orthonormal matrices U and V and a diagonal matrix Σ containing the singular values along the diagonal: $T = U \Sigma V^T$. By setting $T = D^T X^T J_\tau^T Z$, the last term in the equation above can be expressed as $2 \text{tr}(T Q^T)$, which is maximized when $\hat{Q} = U V^T$. After estimating Q , Eq. A.6 may be written as

$$\epsilon^2 = \text{tr} \left[(Z Q^{-1} - J_\tau X D) Q Q^T (Z Q^{-1} - J_\tau X D)^T \right] \quad (\text{A.7})$$

which can be simplified using $Z' = Z Q^{-1}$:

$$\epsilon^2 = \text{tr} \left[(Z' - J_\tau X D) (Z' - J_\tau X D)^T \right] \quad (\text{A.8})$$

which when expanded yields:

$$\epsilon^2 = \text{tr}(Z' Z'^T) + \text{tr}(D D^T X^T J_\tau^T J_\tau X) - 2 \text{tr}(D^T X^T J_\tau^T Z') \quad (\text{A.9})$$

A Atrial activity extraction

Equation A.9 can be minimized by setting its derivative with respect to the diagonal entries of D equal to zero, since D is a diagonal matrix. The diagonal entries in D may be estimated by:

$$\hat{d}_l = ([J_\tau X]_l^T)^{-1} ([J_\tau X]_l^T [Z']_l), i = 1, \dots, L \quad (\text{A.10})$$

for a given Q . An improved estimate of Q is then obtained using the updated scale factor estimates \hat{d}_l . The matrix D is initialized to the identity matrix, since a solution close to $Q = D = I$ is desirable. The rotation matrix at update k is estimated using D_{k-1} , and since

$$\|Z - J_\tau X D_{k-1} Q_k\|_F \leq \|Z - J_\tau X D_{k-1} Q_{k-1}\|_F \quad (\text{A.11})$$

the error is necessarily less than or equal to that of the previous step. Once Q_k is known, D_k may be calculated, and

$$\|Z - J_\tau X D_k Q_k\|_F \leq \|Z - J_\tau X D_{k-1} Q_k\|_F \quad (\text{A.12})$$

The above iteration is repeated until the difference in error between two successive iterations is sufficiently small. Finally, minimization with respect to τ is solved by a grid search of τ in the interval $[-\Delta, \Delta]$, with estimates of Q and D required for all values of τ tested.

A.2 SINGLE-BEAT METHOD

The single-beat method, described in (Lemay et al., 2007), is an extension of the spatiotemporal QRST cancellation algorithm described in the section above, in which not only each cardiac cycle, but also ventricular depolarization (QRS complexes) and repolarization (T and U waves) are treated separately. The motivation for using two templates is that T wave duration changes with heart rate, while QRS duration does not. Additionally, using two templates, separate amplitude scaling and rotation scaling matrices can be applied in the two intervals. This purpose of this section is to describe the single-beat algorithm for f-wave extraction.

Using the single beat method, the average template beat X is partitioned into two submatrices:

$$X = [X_1 X_2] \quad (\text{A.13})$$

where X_1 and X_2 contain the ensemble averaged samples of the QRS and the JQ interval, respectively. The two intervals are processed differently with respect to how the two templates are fitted to the observed signal. While spatiotemporal optimization using the scaling, rotation, and time-alignment techniques are performed for the QRS interval, only time alignment is performed in the JQ interval because the SNR is often quite low.

Analysis of the component of the ECG signal of atrial origin is complicated by the fact that the atrial fibrillatory waves present in AF, called f-waves, are of much smaller amplitude than QRST complexes. It is possible to algorithmically detect the deflections, or *fiducial points* of the QRST complex, and to analyze only the portions of the ECG, the TQ segments, which are known to be of atrial origin. However, if temporal or spectral analysis are desired, then it is

preferable to have a longer duration continuous signal, as the TQ segments, especially in AF, are short, often less than half a second. Therefore, several algorithms for atrial activity extraction, also called f-wave extraction or ventricular activity cancellation, have been developed, to allow for more robust and accurate temporal and spectral analysis on a longer-duration signal. The purpose of this appendix is to describe in detail the two atrial activity extraction methods used in this thesis, which are related to one another.

However, analysis of the component of the ECG signal of atrial origin is complicated by the fact that the atrial fibrillatory waves present in AF, called f-waves and shown in Fig. 3.3, are of much smaller amplitude than QRST complexes. Therefore, it is necessary to apply signal processing techniques to reduce and ideally eliminate the QRST complexes to obtain a signal of purely atrial origin. These techniques, referred to as atrial activity extraction, f-wave extraction, or ventricular activity cancellation, are described below.

It is possible to algorithmically detect the deflections, or *fiducial points* of the QRST complex, and to analyze only the portions of the ECG which are known to be of atrial origin, the TQ segments. However, TQ segments, especially in AF, are short, often less than half a second. Therefore, if temporal or spectral analysis is desired, it is preferable to have a longer duration, continuous signal available for analysis. Several algorithms have thus been developed for atrial activity extraction, to allow for more robust and accurate temporal and spectral analyses on longer-duration signals of atrial origin.

B THE CONCEPT OF INSTANTANEOUS FREQUENCY

A signal's frequency describes the number of cycles per unit time; $f = \frac{1}{T}$, where T is the period of time required to complete one cycle. For non-stationary signals, this frequency can change with time, therefore it is natural to consider how to describe a signal's *instantaneous frequency*. To do so, instantaneous frequency must be defined in some way, and the exact interpretation and definition of what instantaneous frequency means are not without controversy.

For complex-valued frequency modulated signals, the concept of instantaneous frequency is rather straightforward. Given a frequency modulated signal of constant amplitude $s(t) = A \cos \phi(t)$, the instantaneous angular frequency is given by the instantaneous rate of change of the phase angle, $\omega_i(t) = \frac{d\phi(t)}{dt}$. Therefore, the instantaneous frequency is given by:

$$f_i = \frac{1}{2\pi} \frac{d\phi(t)}{dt} \quad (\text{B.1})$$

However, when only a real signal is available, the above definition is not applicable. However, Gabor (1946) introduced the concept of an analytic signal, which allows the creation of a complex-valued signal from a real one. For a real-valued signal $x(t)$, the analytical signal is given by:

$$x_a(t) = x(t) + jH\{x(t)\} = x(t) + jx_h(t) = a(t)e^{j\phi(t)} \quad (\text{B.2})$$

where $H\cdot$ denotes the Hilbert transform and $x_h(t)$ is the Hilbert transformed signal. The instantaneous amplitude and phase are given by $a(t)$ and $\phi(t)$. The Hilbert transform is defined as:

$$x_h(t) = H\{x(t)\} = \frac{1}{\pi} p.v. \int_{-\infty}^{\infty} \frac{x(\tau)}{t - \tau} d\tau \quad (\text{B.3})$$

where p.v. denotes the Cauchy principal value of the integral. The Hilbert transform is therefore nonlocal as it requires knowledge over the whole time domain of $x(t)$. The Hilbert transform may also be viewed as a convolution of $x(t)$ with the function $\frac{1}{\pi t}$, so may be expressed as follows:

$$X_h(f) = F\left\{\frac{1}{\pi t}\right\} \cdot X(f) \quad (\text{B.4})$$

and using the Fourier transform pair

$$\frac{1}{t} \xleftrightarrow{F} -j\pi \text{sgn}(f) \quad (\text{B.5})$$

B The concept of instantaneous frequency

$X_h(f)$ may be expressed as

$$X_h(f) = \begin{cases} jX(f) & \text{for } f < 0 \\ 0 & \text{for } f = 0 \\ -jX(f) & \text{for } f > 0 \end{cases} \quad (\text{B.6})$$

The imaginary part of the analytic signal can then be viewed as the original signal with a phase delay of $-\frac{\pi}{2}$. The analytic signal of a harmonic oscillation $x(t) = A_0 \cos(\omega_0 t)$ is therefore $x_a(t) = A_0 \cos \omega_0 t + j A_0 \sin \omega_0 t$.

BIBLIOGRAPHY

- Aetna Inc. (2022). Body surface potential mapping.
- AFFIRM Investigators (2002). A comparison of rate control and rhythm control in patients with atrial fibrillation. *New England Journal of Medicine*, 347(23):1825–1833.
- Akyürek, Ö., Diker, E., Güldal, M., and Oral, D. (2003). Predictive value of heart rate variability for the recurrence of chronic atrial fibrillation after electrical cardioversion. *Clinical cardiology*, 26(4):196–200.
- Alcaraz, R., Abásolo, D., Hornero, R., and Rieta, J. J. (2010). Optimal parameters study for sample entropy-based atrial fibrillation organization analysis. *Computer methods and programs in biomedicine*, 99(1):124–132.
- Allessie, M. A., de Groot, N. M., Houben, R. P., Schotten, U., Boersma, E., Smeets, J. L., and Crijns, H. J. (2010). Electropathological substrate of long-standing persistent atrial fibrillation in patients with structural heart disease: longitudinal dissociation. *Circulation: Arrhythmia and Electrophysiology*, 3(6):606–615.
- Altschuler, J., Bhaskara, A., Fu, G., Mirrokni, V., Rostamizadeh, A., and Zadimoghaddam, M. (2016). Greedy column subset selection: New bounds and distributed algorithms. In *Proceedings of The 33rd International Conference on Machine Learning*, pages 2539–2548. PMLR.
- Andrade, J., Khairy, P., Dobrev, D., and Nattel, S. (2014). The clinical profile and pathophysiology of atrial fibrillation: relationships among clinical features, epidemiology, and mechanisms. *Circulation research*, 114(9):1453–1468.
- Andrade, J. G., Aguilar, M., Atzema, C., Bell, A., Cairns, J. A., Cheung, C. C., Cox, J. L., Dorian, P., Gladstone, D. J., Healey, J. S., et al. (2020). The 2020 canadian cardiovascular society/-canadian heart rhythm society comprehensive guidelines for the management of atrial fibrillation. *Canadian Journal of Cardiology*, 36(12):1847–1948.
- Andrade, J. G., Wells, G. A., Deyell, M. W., Bennett, M., Essebag, V., Champagne, J., Roux, J.-F., Yung, D., Skanes, A., Khaykin, Y., et al. (2021). Cryoablation or drug therapy for initial treatment of atrial fibrillation. *New England Journal of Medicine*, 384(4):305–315.
- Antman, E. M., Leopold, J. A., Sauer, W. H., and Zei, P. C. (2022). Atrial fibrillation and catheter ablation. *New England Journal of Medicine*, 387(14):e31.
- Benjamin, E. J., Muntner, P., Alonso, A., Bittencourt, M. S., Callaway, C. W., Carson, A. P., Chamberlain, A. M., Chang, A. R., Cheng, S., Das, S. R., et al. (2019). Heart disease and

Bibliography

- stroke statistics—2019 update: a report from the American Heart Association. *Circulation*, 139(10):e56–e528.
- Benjamin, E. J., Wolf, P. A., D’Agostino, R. B., Silbershatz, H., Kannel, W. B., and Levy, D. (1998). Impact of atrial fibrillation on the risk of death: the Framingham Heart Study. *Circulation*, 98(10):946–952.
- Blum, S., Aeschbacher, S., Meyre, P., Zwimpfer, L., Reichlin, T., Beer, J. H., Ammann, P., Auricchio, A., Kobza, R., Erne, P., et al. (2019). Incidence and predictors of atrial fibrillation progression. *Journal of the American Heart Association*, 8(20):e012554.
- Blum, S., Muff, C., Aeschbacher, S., Ammann, P., Erne, P., Moschovitis, G., Di Valentino, M., Shah, D., Schläpfer, J., Fischer, A., et al. (2017). Prospective assessment of sex-related differences in symptom status and health perception among patients with atrial fibrillation. *Journal of the American Heart Association*, 6(7):e005401.
- Bonizzi, P., de la Salud Guillem, M., Climent, A. M., Millet, J., Zarzoso, V., Castells, F., and Meste, O. (2010). Noninvasive assessment of the complexity and stationarity of the atrial wavefront patterns during atrial fibrillation. *IEEE Transactions on Biomedical Engineering*, 57(9):2147–2157.
- Brieger, D., Amerena, J., Attia, J. R., Bajorek, B., Chan, K. H., Connell, C., Freedman, B., Ferguson, C., Hall, T., Haqqani, H. M., et al. (2018). National Heart Foundation of Australia and Cardiac Society of Australia and New Zealand: Australian clinical guidelines for the diagnosis and management of atrial fibrillation 2018. *Heart Lung Circ*, 27(10):1209–1266.
- Brundel, B. J., Ai, X., True Hills, M., Kuipers, M. F., Lip, G. Y., and de Groot, N. M. (2022). Atrial fibrillation. *Nature Reviews Disease Primers*, 8(21).
- Burdett, P. and Lip, G. Y. (2022). Atrial fibrillation in the UK: predicting costs of an emerging epidemic recognizing and forecasting the cost drivers of atrial fibrillation-related costs. *European Heart Journal-Quality of Care and Clinical Outcomes*, 8(2):187–194.
- Buttu, A., Pruvot, E., Van Zaen, J., Viso, A., Forclaz, A., Pascale, P., Narayan, S. M., and Vesin, J.-M. (2013). Adaptive frequency tracking of the baseline ECG identifies the site of atrial fibrillation termination by catheter ablation. *Biomedical Signal Processing and Control*, 8(6):969–980.
- Buttu, A., Vesin, J.-M., Van Zaen, J., Ballabeni, P., Pascale, P., Forclaz, A., Bisch, L., Rollin, A., Maury, P., Roten, L., et al. (2016). A high baseline electrographic organization level is predictive of successful termination of persistent atrial fibrillation by catheter ablation. *JACC: Clinical Electrophysiology*, 2(6):746–755.
- Calkins, H., Hindricks, G., Cappato, R., Kim, Y.-H., Saad, E. B., Aguinaga, L., Akar, J. G., Badhwar, V., Brugada, J., Camm, J., et al. (2018). 2017 HRS/EHRA/ECAS/APHRS/SOLAECE expert consensus statement on catheter and surgical ablation of atrial fibrillation. *Heart Rhythm*, 14(10):e275–e444.

- Calò, L., Lamberti, E., Loricchio, M. L., De Ruvo, E., Colivicchi, E., Bianconi, L., Pandozi, C., and Santini, M. (2006). Left atrial ablation versus biatrial ablation for persistent and permanent atrial fibrillation: a prospective and randomized study. *Journal of the American College of Cardiology*, 47(12):2504–2512.
- Capucci, A., Biffi, M., Boriani, G., Ravelli, F., Nollo, G., Sabbatani, P., Orsi, C., and Magnani, B. (1995). Dynamic electrophysiological behavior of human atria during paroxysmal atrial fibrillation. *Circulation*, 92(5):1193–1202.
- Castells, F., Laguna, P., Sörnmo, L., Bollmann, A., and Roig, J. M. (2007). Principal component analysis in ECG signal processing. *EURASIP Journal on Advances in Signal Processing*, 2007(1):98.
- Chao, T.-F., Joung, B., Takahashi, Y., Lim, T. W., Choi, E.-K., Chan, Y.-H., Guo, Y., Sriratanasathavorn, C., Oh, S., Okumura, K., et al. (2022). 2021 Focused update consensus guidelines of the Asia Pacific Heart Rhythm Society on stroke prevention in atrial fibrillation: executive summary. *Thrombosis and haemostasis*, 122(1):20–47.
- Chao, T.-F., Liu, C.-J., Tuan, T.-C., Chen, T.-J., Hsieh, M.-H., Lip, G. Y., and Chen, S.-A. (2018). Lifetime risks, projected numbers, and adverse outcomes in Asian patients with atrial fibrillation: a report from the Taiwan nationwide AF cohort study. *Chest*, 153(2):453–466.
- Chatterjee, N. A., Giulianini, F., Geelhoed, B., Lunetta, K. L., Misialek, J. R., Niemeijer, M. N., Rienstra, M., Rose, L. M., Smith, A. V., Arking, D. E., et al. (2017). Genetic obesity and the risk of atrial fibrillation: causal estimates from Mendelian randomization. *Circulation*, 135(8):741–754.
- Chung, M. K., Eckhardt, L. L., Chen, L. Y., Ahmed, H. M., Gopinathannair, R., Joglar, J. A., Noseworthy, P. A., Pack, Q. R., Sanders, P., Trulock, K. M., et al. (2020). Lifestyle and risk factor modification for reduction of atrial fibrillation: a scientific statement from the American Heart Association. *Circulation*, 141(16):e750–e772.
- Civril, A. (2014). Column subset selection problem is UG-hard. *Journal of Computer and System Sciences*, 80(4):849–859.
- Cohen, L. (1995). *Time-frequency analysis*, volume 778. Prentice Hall New Jersey.
- Cohen, R. J., Berger, R. D., and Dushane, T. E. (1983). A quantitative model for the ventricular response during atrial fibrillation. *IEEE Transactions on Biomedical Engineering*, 30(12):769–781.
- Corino, V. D., Cygankiewicz, I., Mainardi, L. T., Stridh, M., Vasquez, R., Bayes de Luna, A., Holmqvist, F., Zareba, W., and Platonov, P. G. (2013). Association between atrial fibrillatory rate and heart rate variability in patients with atrial fibrillation and congestive heart failure. *Annals of Noninvasive Electrocardiology*, 18(1):41–50.

Bibliography

- Coyne, K. S., Paramore, C., Grandy, S., Mercader, M., Reynolds, M., and Zimetbaum, P. (2006). Assessing the direct costs of treating nonvalvular atrial fibrillation in the United States. *Value in Health*, 9(5):348–356.
- Di Marco, L. Y., Bourke, J. P., and Langley, P. (2012). Spatial complexity and spectral distribution variability of atrial activity in surface ECG recordings of atrial fibrillation. *Medical & biological engineering & computing*, 50(5):439–446.
- Di Marco, L. Y., Raine, D., Bourke, J. P., and Langley, P. (2014). Recurring patterns of atrial fibrillation in surface ECG predict restoration of sinus rhythm by catheter ablation. *Computers in biology and medicine*, 54:172–179.
- Dietzel, J., Haeusler, K. G., and Endres, M. (2018). Does atrial fibrillation cause cognitive decline and dementia? *EP Europace*, 20(3):408–419.
- Duytschaever, M., Demolder, A., Philips, T., Sarkozy, A., El Haddad, M., Taghji, P., Knecht, S., Tavernier, R., Vandekerckhove, Y., and De Potter, T. (2018). Pulmonary vein isolation with vs. without continued antiarrhythmic drug treatment in subjects with recurrent atrial fibrillation (POWDER AF): results from a multicentre randomized trial. *European Heart Journal*, 39(16):1429–1437.
- ECG & Echo Learning (2022). The ECG leads: electrodes, limb leads, chest leads, 12-lead ECG.
- Everett IV, T. H. and Olgin, J. E. (2007). Atrial fibrosis and the mechanisms of atrial fibrillation. *Heart Rhythm*, 4(3):S24–S27.
- Farahat, A. K., Ghodsi, A., and Kamel, M. S. (2011). An efficient greedy method for unsupervised feature selection. In *2011 IEEE 11th International Conference on Data Mining*, pages 161–170. IEEE.
- Feng, X., Bai, B., Wu, Z., Yang, C., and Wu, Z. (2019). Leads selection of body surface potential mapping during atrial fibrillation: A sequential selection based on adapted Botteron’s approach. *IEEE Access*, 7:158064–158074.
- Forclaz, A., Narayan, S. M., Scherr, D., Linton, N., Jadidi, A. S., Nault, I., Rivard, L., Miyazaki, S., Uldry, L., Wright, M., et al. (2011). Early temporal and spatial regularization of persistent atrial fibrillation predicts termination and arrhythmia-free outcome. *Heart Rhythm*, 8(9):1374–1382.
- Gabor, D. (1946). Theory of communication. *Journal of the Institution of Electrical Engineers-part III: radio and communication engineering*, 93(26):429–441.
- Gillis, A. M., Krahn, A. D., Skanes, A. C., and Nattel, S. (2013). Management of atrial fibrillation in the year 2033: new concepts, tools, and applications leading to personalized medicine. *Canadian Journal of Cardiology*, 29(10):1141–1146.

- Goette, A., Kalman, J. M., Aguinaga, L., Akar, J., Cabrera, J. A., Chen, S. A., Chugh, S. S., Corradi, D., D'Avila, A., Dobrev, D., et al. (2016). EHRA/HRS/APHRS/SOLAECE expert consensus on atrial cardiomyopathies: definition, characterization, and clinical implication. *EP Europace*, 18(10):1455–1490.
- Guillem, M. S., Bollmann, A., Climent, A. M., Husser, D., Millet-Roig, J., and Castells, F. (2009). How many leads are necessary for a reliable reconstruction of surface potentials during atrial fibrillation? *IEEE Transactions on Information Technology in Biomedicine*, 13(3):330–340.
- Guillem, M. S., Castells, F., Climent, A. M., Bodí, V., Chorro, F. J., and Millet, J. (2008). Evaluation of lead selection methods for optimal reconstruction of body surface potentials. *Journal of Electrocardiology*, 41(1):26–34.
- Guillem, M. S., Climent, A. M., Millet, J., Arenal, Á., Fernández-Avilés, F., Jalife, J., Atienza, F., and Berenfeld, O. (2013). Noninvasive localization of maximal frequency sites of atrial fibrillation by body surface potential mapping. *Circulation: Arrhythmia and Electrophysiology*, 6(2):294–301.
- Haissaguerre, M., Jaïs, P., Shah, D. C., Takahashi, A., Hocini, M., Quiniou, G., Garrigue, S., Le Mouroux, A., Le Métayer, P., and Clémenty, J. (1998). Spontaneous initiation of atrial fibrillation by ectopic beats originating in the pulmonary veins. *New England Journal of Medicine*, 339(10):659–666.
- Haïssaguerre, M., Sanders, P., Hocini, M., Hsu, L.-F., Shah, D. C., Scavée, C., Takahashi, Y., Rotter, M., Pasquié, J.-L., Garrigue, S., et al. (2004). Changes in atrial fibrillation cycle length and inducibility during catheter ablation and their relation to outcome. *Circulation*, 109(24):3007–3013.
- Haïssaguerre, M., Sanders, P., Hocini, M., Takahashi, Y., Rotter, M., Sacher, F., Rostock, T., HSU, L.-F., Bordachar, P., Reuter, S., et al. (2005). Catheter ablation of long-lasting persistent atrial fibrillation: critical structures for termination. *Journal of cardiovascular electrophysiology*, 16(11):1125–1137.
- Haykin, S. S. (2002). *Adaptive Filter Theory*. Prentice-Hall.
- Heidenreich, P. A., Bozkurt, B., Aguilar, D., Allen, L. A., Byun, J. J., Colvin, M. M., Deswal, A., Drazner, M. H., Dunlay, S. M., Evers, L. R., et al. (2022). 2022 AHA/ACC/HFSA guideline for the management of heart failure: a report of the American College of Cardiology/American Heart Association Joint Committee on Clinical Practice Guidelines. *Journal of the American College of Cardiology*, 79(17):e263–e421.
- Heijman, J., Algalarrondo, V., Voigt, N., Melka, J., Wehrens, X. H., Dobrev, D., and Nattel, S. (2016). The value of basic research insights into atrial fibrillation mechanisms as a guide to therapeutic innovation: a critical analysis. *Cardiovascular research*, 109(4):467–479.

Bibliography

- Heist, E. K., Chalhoub, F., Barrett, C., Danik, S., Ruskin, J. N., and Mansour, M. (2012). Predictors of atrial fibrillation termination and clinical success of catheter ablation of persistent atrial fibrillation. *The American journal of cardiology*, 110(4):545–551.
- Hindricks, G., Potpara, T., Dagres, N., Arbelo, E., Bax, J. J., Blomström-Lundqvist, C., Boriani, G., Castella, M., Dan, G.-A., Dilaveris, P. E., et al. (2021). 2020 ESC Guidelines for the diagnosis and management of atrial fibrillation developed in collaboration with the European Association for Cardio-Thoracic Surgery (EACTS) The Task Force for the diagnosis and management of atrial fibrillation of the European Society of Cardiology (ESC) Developed with the special contribution of the European Heart Rhythm Association (EHRA) of the ESC. *European heart journal*, 42(5):373–498.
- Hocini, M., Ho, S. Y., Kawara, T., Linnenbank, A. C., Potse, M., Shah, D., Jaïs, P., Janse, M. J., Haïssaguerre, M., and De Bakker, J. M. (2002). Electrical conduction in canine pulmonary veins: electrophysiological and anatomic correlation. *Circulation*, 105(20):2442–2448.
- Hocini, M., Nault, I., Wright, M., Veenhuyzen, G., Narayan, S. M., Jaïs, P., Lim, K.-T., Knecht, S., Matsuo, S., Forclaz, A., et al. (2010). Disparate evolution of right and left atrial rate during ablation of long-lasting persistent atrial fibrillation. *Journal of the American College of Cardiology*, 55(10):1007–1016.
- Hohnloser, S. H., Basic, E., and Nabauer, M. (2019). Changes in oral anticoagulation therapy over one year in 51,000 atrial fibrillation patients at risk for stroke: a practice-derived study. *Thrombosis and haemostasis*, 119(06):882–893.
- Holm, M., Pehrson, S., Ingemansson, M., Sörnmo, L., Johansson, R., Sandhall, L., Sunemark, M., Smideberg, B., Olsson, C., and Olsson, S. B. (1998). Non-invasive assessment of the atrial cycle length during atrial fibrillation in man: introducing, validating and illustrating a new ECG method. *Cardiovascular research*, 38(1):69–81.
- Holmqvist, F., Stridh, M., Waktare, J. E., Sörnmo, L., Olsson, S. B., and Meurling, C. J. (2006). Atrial fibrillatory rate and sinus rhythm maintenance in patients undergoing cardioversion of persistent atrial fibrillation. *European heart journal*, 27(18):2201–2207.
- Hong, K., Bjerregaard, P., Gussak, I., and Brugada, R. (2005). Short QT syndrome and atrial fibrillation caused by mutation in KCNH2. *Journal of cardiovascular electrophysiology*, 16(4):394–396.
- Horan, L. G. and Kistler, J. C. (1961). Study of ventricular response in atrial fibrillation. *Circulation research*, 9(2):305–311.
- Ihara, Z., van Oosterom, A., Jacquemet, V., and Hoekema, R. (2007). Adaptation of the standard 12-lead electrocardiogram system dedicated to the analysis of atrial fibrillation. *Journal of electrocardiology*, 40(1):68.e1–68.e8.

- Jaïs, P., Cauchemez, B., Macle, L., Daoud, E., Khairy, P., Subbiah, R., Hocini, M., Extramiana, E., Sacher, F., Bordachar, P., et al. (2008). Catheter ablation versus antiarrhythmic drugs for atrial fibrillation: the A4 study. *Circulation*, 118(24):2498–2505.
- Kalantarian, S., Stern, T. A., Mansour, M., and Ruskin, J. N. (2013). Cognitive impairment associated with atrial fibrillation: a meta-analysis. *Annals of internal medicine*, 158(5_Part_1):338–346.
- Kim, K.-B., Rodefeld, M. D., Schuessler, R. B., Cox, J. L., and Boineau, J. P. (1996). Relationship between local atrial fibrillation interval and refractory period in the isolated canine atrium. *Circulation*, 94(11):2961–2967.
- Kim, M. H., Johnston, S. S., Chu, B.-C., Dalal, M. R., and Schulman, K. L. (2011). Estimation of total incremental health care costs in patients with atrial fibrillation in the United States. *Circulation: Cardiovascular quality and outcomes*, 4(3):313–320.
- Kirchhof, P., Benussi, S., Kotecha, D., Ahlsson, A., Atar, D., Casadei, B., Castella, M., Diener, H.-C., Heidbuchel, H., Hendriks, J., et al. (2016). 2016 ESC Guidelines for the management of atrial fibrillation developed in collaboration with EACTS. *Kardiologia Polska (Polish Heart Journal)*, 74(12):1359–1469.
- Klabunde, R. E. (2019). Cardiovascular physiological concepts: Electrocardiogram.
- Konings, K., Kirchhof, C., Smeets, J., Wellens, H., Penn, O. C., and Allessie, M. A. (1994). High-density mapping of electrically induced atrial fibrillation in humans. *Circulation*, 89(4):1665–1680.
- Kornej, J., Börschel, C. S., Benjamin, E. J., and Schnabel, R. B. (2020). Epidemiology of atrial fibrillation in the 21st century: novel methods and new insights. *Circulation research*, 127(1):4–20.
- Kornej, J., Hindricks, G., Shoemaker, M. B., Husser, D., Arya, A., Sommer, P., Rolf, S., Saavedra, P., Kanagasundram, A., Patrick Whalen, S., et al. (2015). The APPLE score: a novel and simple score for the prediction of rhythm outcomes after catheter ablation of atrial fibrillation. *Clinical Research in Cardiology*, 104:871–876.
- Kotecha, D., Holmes, J., Krum, H., Altman, D. G., Manzano, L., Cleland, J. G., Lip, G. Y., Coats, A. J., Andersson, B., Kirchhof, P., et al. (2014). Efficacy of β blockers in patients with heart failure plus atrial fibrillation: an individual-patient data meta-analysis. *The Lancet*, 384(9961):2235–2243.
- Lang, C., Seyfang, L., Ferrari, J., Gattringer, T., Greisenegger, S., Willeit, K., Toell, T., Krebs, S., Brainin, M., Kiechl, S., et al. (2017). Do women with atrial fibrillation experience more severe strokes? Results from the Austrian stroke unit registry. *Stroke*, 48(3):778–780.
- Langberg, J. J., Burnette, J. C., and McTeague, K. K. (1998). Spectral analysis of the electrocardiogram predicts recurrence of atrial fibrillation after cardioversion. *Journal of electrocardiology*, 31:80.

Bibliography

- Langley, P., Rieta, J. J., Stridh, M., Millet, J., Sornmo, L., and Murray, A. (2006). Comparison of atrial signal extraction algorithms in 12-lead ECGs with atrial fibrillation. *IEEE Transactions on Biomedical Engineering*, 53(2):343–346.
- Lankveld, T., Zeemering, S., Scherr, D., Kuklik, P., Hoffmann, B. A., Willems, S., Pieske, B., Haïssaguerre, M., Jaïs, P., Crijns, H. J., et al. (2016). Atrial fibrillation complexity parameters derived from surface ecgs predict procedural outcome and long-term follow-up of stepwise catheter ablation for atrial fibrillation. *Circulation. Arrhythmia and electrophysiology*, 9(2).
- Lankveld, T. A., Zeemering, S., Crijns, H. J., and Schotten, U. (2014). The ECG as a tool to determine atrial fibrillation complexity. *Heart*, 100(14):1077–1084.
- Lemay, M., Vesin, J.-M., Van Oosterom, A., Jacquemet, V., and Kappenberger, L. (2007). Cancellation of ventricular activity in the ECG: evaluation of novel and existing methods. *IEEE Transactions on Biomedical Engineering*, 54(3):542–546.
- Liao, H.-E. (2005). Two discrete oscillator based adaptive notch filters (OSC ANFs) for noisy sinusoids. *IEEE Transactions on Signal Processing*, 53(2):528–538.
- Lim, K.-T., Davis, M. J., Powell, A., Arnolda, L., Moulden, K., Bulsara, M., and Weerasooriya, R. (2007). Ablate and pace strategy for atrial fibrillation: long-term outcome of AIRCRAFT trial. *Europace*, 9(7):498–505.
- Lip, G. Y. (2017). The ABC pathway: an integrated approach to improve AF management. *Nature Reviews Cardiology*, 14(11):627–628.
- Lip, G. Y., Nieuwlaat, R., Pisters, R., Lane, D. A., and Crijns, H. J. (2010). Refining clinical risk stratification for predicting stroke and thromboembolism in atrial fibrillation using a novel risk factor-based approach: the euro heart survey on atrial fibrillation. *Chest*, 137(2):263–272.
- Lübke-meier, I., Andrié, R., Lickfett, L., Bosen, F., Stöckigt, F., Dobrowolski, R., Draffehn, A. M., Fregeac, J., Schultze, J. L., Bukauskas, F. F., et al. (2013). The Connexin40A96S mutation from a patient with atrial fibrillation causes decreased atrial conduction velocities and sustained episodes of induced atrial fibrillation in mice. *Journal of molecular and cellular cardiology*, 65:19–32.
- Luca, A., Baskaralingam, A., McCann, A., Vesin, J., Pascale, P., Le Bloa, M., Herrera, C., Roten, L., Kuhne, M., Spies, F., et al. (2022). Amplitude of fibrillatory wave correlates with long-term maintenance of sinus rhythm after ablation in persistent atrial fibrillation. *Europace*, 24(Supplement_1):euac053–063.
- Luca, A., Pittet, A., Buttu, A., McCann, A., Vesin, J.-M., Pascale, P., Le Bloa, M., Herrera, C., Park, C.-I., Rollin, A., et al. (2020). Severe and uniform bi-atrial remodeling measured by dominant frequency analysis in persistent atrial fibrillation unresponsive to ablation. *Journal of interventional cardiac electrophysiology*, 59(2):431–440.

- Lux, R. L., Smith, C. R., Wyatt, R. F., and Abildskov, J. (1978). Limited lead selection for estimation of body surface potential maps in electrocardiography. *IEEE Transactions on Biomedical Engineering*, 25(3):270–276.
- Macfarlane, P. W., Van Oosterom, A., Pahlm, O., Kligfield, P., Janse, M., and Camm, J. (2010). *Comprehensive Electrocardiology*. Springer Science & Business Media.
- Marwan, N., Romano, M. C., Thiel, M., and Kurths, J. (2007). Recurrence plots for the analysis of complex systems. *Physics Reports*, 438(5-6):237–329.
- Marwan, N., Wessel, N., Meyerfeldt, U., Schirdewan, A., and Kurths, J. (2002). Recurrence-plot-based measures of complexity and their application to heart-rate-variability data. *Physical review. E*, 66(2):026702.
- Matsuo, S., Lellouche, N., Wright, M., Bevilacqua, M., Knecht, S., Nault, I., Lim, K.-T., Arantes, L., O'Neill, M. D., Platonov, P. G., et al. (2009). Clinical predictors of termination and clinical outcome of catheter ablation for persistent atrial fibrillation. *Journal of the American College of Cardiology*, 54(9):788–795.
- Mayo Clinic (2022). Holter monitor.
- Mayo Clinic (2023). SR vs AF.
- McCann, A., Luca, A., Pascale, P., Pruvot, E., and Vesin, J.-M. (2022). Novel spatiotemporal processing tools for body-surface potential map signals for the prediction of catheter ablation outcome in persistent atrial fibrillation. *Frontiers in physiology*, 13:1001060.
- McCann, A., Luca, A., Pruvot, E., Roten, L., Sticherling, C., and Vesin, J.-M. (2021a). Ventricular response regularity in atrial fibrillation and its relationship to successful catheter ablation. In *2020 28th European Signal Processing Conference (EUSIPCO)*, pages 910–914. IEEE.
- McCann, A., Luca, A., Pruvot, E., Roten, L., Sticherling, C., and Vesin, J.-M. (2023). Heart rate variability analysis in atrial fibrillation for assessing response to catheter ablation. *Physiological measurement*. In submission.
- McCann, A., Vesin, J.-M., Pruvot, E., Roten, L., Sticherling, C., and Luca, A. (2021b). ECG-based indices to characterize persistent atrial fibrillation before and during stepwise catheter ablation. *Frontiers in physiology*, 12:654053.
- Menown, I. and Adgey, A. (2000). Improving the ECG classification of inferior and lateral myocardial infarction by inversion of lead aVR. *Heart*, 83(6):657–660.
- Meo, M., Pambrun, T., Derval, N., Dumas-Pomier, C., Puyo, S., Duchateau, J., Jais, P., Hocini, M., Haissaguerre, M., and Dubois, R. (2018). Noninvasive assessment of atrial fibrillation complexity in relation to ablation characteristics and outcome. *Frontiers in physiology*, 9:929.

Bibliography

- Meo, M., Zarzoso, V., Meste, O., Latcu, D. G., and Saoudi, N. (2012). Spatial variability of the 12-lead surface ECG as a tool for noninvasive prediction of catheter ablation outcome in persistent atrial fibrillation. *IEEE Transactions on Biomedical Engineering*, 60(1):20–27.
- Meo, M., Zarzoso, V., Meste, O., Latcu, D. G., and Saoudi, N. (2013). Catheter ablation outcome prediction in persistent atrial fibrillation using weighted principal component analysis. *Biomedical Signal Processing and Control*, 8(6):958–968.
- Mesquita, J., Ferreira, A. M., Cavaco, D., Moscoso Costa, F., Carmo, P., Marques, H., Morgado, F., Mendes, M., and Adragao, P. (2018). Development and validation of a risk score for predicting atrial fibrillation recurrence after a first catheter ablation procedure—atlas score. *EP Europace*, 20(FI_3):f428–f435.
- Michaud, G. F. and Stevenson, W. G. (2021). Atrial fibrillation. *New England Journal of Medicine*, 384:353–361.
- Middeldorp, M. E., Pathak, R. K., Meredith, M., Mehta, A. B., Elliott, A. D., Mahajan, R., Twomey, D., Gallagher, C., Hendriks, J. M., Linz, D., et al. (2018). PREVENTion and regReSSive Effect of weight-loss and risk factor modification on Atrial Fibrillation: the REVERSE-AF study. *EP Europace*, 20(12):1929–1935.
- Milaire, P., Rothman, Z., and Courneya, C. (2017). Cardiology: Re-entry circuits.
- Miller, J. M., Kowal, R. C., Swarup, V., Daubert, J. P., Daoud, E. G., Day, J. D., Ellenbogen, K. A., Hummel, J. D., Baykaner, T., Krummen, D. E., et al. (2014). Initial independent outcomes from focal impulse and rotor modulation ablation for atrial fibrillation: multicenter FIRM registry. *Journal of cardiovascular electrophysiology*, 25(9):921–929.
- Moe, G. (1959). Atrial fibrillation as a self-sustaining arrhythmia independent of focal discharge. *American heart journal*, 58:59–70.
- Mou, L., Norby, F. L., Chen, L. Y., O’Neal, W. T., Lewis, T. T., Loehr, L. R., Soliman, E. Z., and Alonso, A. (2018). Lifetime risk of atrial fibrillation by race and socioeconomic status: ARIC Study (Atherosclerosis Risk in Communities). *Circulation. Arrhythmia and electrophysiology*, 11(7):e006350.
- Mujović, N., Marinković, M., Marković, N., Shantsila, A., Lip, G. Y., and Potpara, T. S. (2017). Prediction of very late arrhythmia recurrence after radiofrequency catheter ablation of atrial fibrillation: the mb-later clinical score. *Scientific reports*, 7(1):1–11.
- Murase, Y., Inden, Y., Shibata, R., Yanagisawa, S., Fujii, A., Ando, M., Otake, N., Takenaka, M., Funabiki, J., Sakamoto, Y., et al. (2020). The impact of the dominant frequency of body surface electrocardiography in patients with persistent atrial fibrillation. *Heart and Vessels*, 35(7):967–976.
- Nademanee, K., McKenzie, J., Kosar, E., Schwab, M., Sunsaneewitayakul, B., Vasavakul, T., Khunnawat, C., and Ngarmukos, T. (2004). A new approach for catheter ablation of atrial

- fibrillation: mapping of the electrophysiologic substrate. *Journal of the American College of Cardiology*, 43(11):2044–2053.
- Nattel, S., Burstein, B., and Dobrev, D. (2008). Atrial remodeling and atrial fibrillation: mechanisms and implications. *Circulation. Arrhythmia and electrophysiology*, 1(1):62–73.
- Nattel, S. and Dobrev, D. (2016). Electrophysiological and molecular mechanisms of paroxysmal atrial fibrillation. *Nature Reviews Cardiology*, 13(10):575–590.
- Nattel, S., Heijman, J., Zhou, L., and Dobrev, D. (2020). Molecular basis of atrial fibrillation pathophysiology and therapy: a translational perspective. *Circulation research*, 127(1):51–72.
- Nault, I., Lellouche, N., Matsuo, S., Knecht, S., Wright, M., Lim, K.-T., Sacher, F., Platonov, P., Deplagne, A., Bordachar, P., et al. (2009). Clinical value of fibrillatory wave amplitude on surface ECG in patients with persistent atrial fibrillation. *Journal of interventional cardiac electrophysiology*, 26(1):11–19.
- Nielsen, J. B., Thorolfsdottir, R. B., Fritsche, L. G., Zhou, W., Skov, M. W., Graham, S. E., Herron, T. J., McCarthy, S., Schmidt, E. M., Sveinbjornsson, G., et al. (2018a). Biobank-driven genomic discovery yields new insight into atrial fibrillation biology. *Nature Genetics*, 50:1234–1239.
- Nielsen, J. C., Johannessen, A., Raatikainen, P., Hindricks, G., Walfridsson, H., Pehrson, S. M., Englund, A., Hartikainen, J., Mortensen, L. S., and Hansen, P. S. (2017). Long-term efficacy of catheter ablation as first-line therapy for paroxysmal atrial fibrillation: 5-year outcome in a randomised clinical trial. *Heart*, 103(5):368–376.
- Nielsen, P. B., Skjøth, F., Overvad, T. F., Larsen, T. B., and Lip, G. Y. (2018b). Female sex is a risk modifier rather than a risk factor for stroke in atrial fibrillation: should we use a CHA2DS2-VA score rather than CHA2DS2-VASc? *Circulation*, 137(8):832–840.
- Nikolaidou, T. and Channer, K. (2009). Chronic atrial fibrillation: a systematic review of medical heart rate control management. *Postgraduate medical journal*, 85(1004):303–312.
- Nilsson, F., Stridh, M., Bollmann, A., and Sörnmo, L. (2006). Predicting spontaneous termination of atrial fibrillation using the surface ECG. *Medical engineering & physics*, 28(8):802–808.
- Noubiap, J. J., Sanders, P., Nattel, S., and Lau, D. H. (2021). Biomarkers in atrial fibrillation: pathogenesis and clinical implications. *Cardiac Electrophysiology Clinics*, 13(1):221–233.
- Okumura, Y., Watanabe, I., Kofune, M., Nagashima, K., Sonoda, K., Mano, H., Ohkubo, K., Nakai, T., and Hirayama, A. (2012). Characteristics and distribution of complex fractionated atrial electrograms and the dominant frequency during atrial fibrillation: relationship to the response and outcome of circumferential pulmonary vein isolation. *Journal of interventional cardiac electrophysiology*, 34(3):267–275.

Bibliography

- Oral, H., Chugh, A., Good, E., Wimmer, A., Dey, S., Gadeela, N., Sankaran, S., Crawford, T., Sarrazin, J. F., Kuhne, M., et al. (2007). Radiofrequency catheter ablation of chronic atrial fibrillation guided by complex electrograms. *Circulation*, 115(20):2606–2612.
- O'Neill, M. D., Jaïs, P., Takahashi, Y., Jönsson, A., Sacher, F., Hocini, M., Sanders, P., Rostock, T., Rotter, M., Pernet, A., et al. (2006). The stepwise ablation approach for chronic atrial fibrillation—evidence for a cumulative effect. *Journal of interventional cardiac electrophysiology*, 16(3):153–167.
- Packer, D. L., Kowal, R. C., Wheelan, K. R., Irwin, J. M., Champagne, J., Guerra, P. G., Dubuc, M., Reddy, V., Nelson, L., Holcomb, R. G., et al. (2013). Cryoballoon ablation of pulmonary veins for paroxysmal atrial fibrillation: first results of the North American Arctic Front (STOP AF) pivotal trial. *Journal of the American College of Cardiology*, 61(16):1713–1723.
- Pandit, S. V. and Jalife, J. (2013). Rotors and the dynamics of cardiac fibrillation. *Circulation research*, 112(5):849–862.
- Pappone, C., Rosanio, S., Oreto, G., Tocchi, M., Gugliotta, F., Vicedomini, G., Salvati, A., Dicandia, C., Mazzone, P., Santinelli, V., et al. (2000). Circumferential radiofrequency ablation of pulmonary vein ostia: a new anatomic approach for curing atrial fibrillation. *Circulation*, 102(21):2619–2628.
- Pastori, D., Pignatelli, P., Menichelli, D., Violi, F., and Lip, G. Y. (2019). Integrated care management of patients with atrial fibrillation and risk of cardiovascular events: the abc (atrial fibrillation better care) pathway in the athero-af study cohort. *Mayo Clinic proceedings*, 94(7):1261–1267.
- Pathak, R. K., Elliott, A., Middeldorp, M. E., Meredith, M., Mehta, A. B., Mahajan, R., Hendriks, J. M., Twomey, D., Kalman, J. M., Abhayaratna, W. P., et al. (2015a). Impact of CARDIOrespiratory FITness on arrhythmia recurrence in obese individuals with atrial fibrillation: the CARDIO-FIT study. *Journal of the American College of Cardiology*, 66(9):985–996.
- Pathak, R. K., Middeldorp, M. E., Lau, D. H., Mehta, A. B., Mahajan, R., Twomey, D., Alasady, M., Hanley, L., Antic, N. A., McEvoy, R. D., et al. (2014). Aggressive risk factor reduction study for atrial fibrillation and implications for the outcome of ablation: the ARREST-AF cohort study. *Journal of the American College of Cardiology*, 64(21):2222–2231.
- Pathak, R. K., Middeldorp, M. E., Meredith, M., Mehta, A. B., Mahajan, R., Wong, C. X., Twomey, D., Elliott, A. D., Kalman, J. M., Abhayaratna, W. P., et al. (2015b). Long-term effect of goal-directed weight management in an atrial fibrillation cohort: a long-term follow-up study (LEGACY). *Journal of the American College of Cardiology*, 65(20):2159–2169.
- Petrutiu, S., Ng, J., Nijm, G. M., Al-Angari, H., Swiryn, S., and Sahakian, A. V. (2006). Atrial fibrillation and waveform characterization. *IEEE engineering in medicine and biology magazine*, 25(6):24–30.

- Petrutiu, S., Sahakian, A. V., Fisher, W., and Swiryn, S. (2009). Manifestation of left atrial events and interatrial frequency gradients in the surface electrocardiogram during atrial fibrillation: contributions from posterior leads. *Journal of cardiovascular electrophysiology*, 20(11):1231–1236.
- Piccini, J. P. and Fauchier, L. (2016). Rhythm control in atrial fibrillation. *The Lancet*, 388(10046):829–840.
- Pilia, N., Nagel, C., Lenis, G., Becker, S., Dössel, O., and Loewe, A. (2021). ECGdeli-an open source ECG delineation toolbox for MATLAB. *SoftwareX*, 13:100639.
- Pisters, R., Lane, D. A., Marin, F., Camm, A. J., and Lip, G. Y. (2012). Stroke and thromboembolism in atrial fibrillation—systematic review of stroke risk factors and risk stratification schema—. *Circulation journal: official journal of the Japanese Circulation Society*, 76(10):2289–2304.
- Pithon, A., McCann, A., Buttu, A., Vesin, J.-M., Pascale, P., Le Bloa, M., Herrera, C., Park, C.-I., Roten, L., Kühne, M., et al. (2021). Dynamics of intraprocedural dominant frequency identifies ablation outcome in persistent atrial fibrillation. *Frontiers in physiology*, 12:731917.
- Platonov, P. G., Mitrofanova, L. B., Orshanskaya, V., and Ho, S. Y. (2011). Structural abnormalities in atrial walls are associated with presence and persistency of atrial fibrillation but not with age. *Journal of the American College of Cardiology*, 58(21):2225–2232.
- Proietti, M., Romiti, G. F., Olshansky, B., Lane, D. A., and Lip, G. Y. (2018). Improved outcomes by integrated care of anticoagulated patients with atrial fibrillation using the simple ABC (Atrial Fibrillation Better Care) pathway. *The American journal of medicine*, 131(11):1359–1366.
- Prudat, Y. and Vesin, J. (2009). Multi-signal extension of adaptive frequency tracking algorithms. *Signal Processing*, 89(6):963–973.
- Rawles, J. M. and Rowland, E. (1986). Is the pulse in atrial fibrillation irregularly irregular? *Heart*, 56(1):4–11.
- Richman, J. S. and Moorman, J. R. (2000). Physiological time-series analysis using approximate entropy and sample entropy. *American journal of physiology. Heart and circulatory physiology*, 278(6):H2039–H2049.
- Rienstra, M., Hobbelt, A. H., Alings, M., Tijssen, J. G., Smit, M. D., Brügemann, J., Geelhoed, B., Tieleman, R. G., Hillege, H. L., Tukkie, R., et al. (2018). Targeted therapy of underlying conditions improves sinus rhythm maintenance in patients with persistent atrial fibrillation: results of the RACE 3 trial. *European heart journal*, 39(32):2987–2996.
- Rissanen, J. (1978). Modeling by shortest data description. *Automatica*, 14(5):465–471.

Bibliography

- Roselli, C., Chaffin, M. D., Weng, L.-C., Aeschbacher, S., Ahlberg, G., Albert, C. M., Almgren, P., Alonso, A., Anderson, C. D., Aragam, K. G., et al. (2018). Multi-ethnic genome-wide association study for atrial fibrillation. *Nature Genetics*, 50(9):1225–1233.
- Rostock, T., Salukhe, T. V., Steven, D., Drewitz, I., Hoffmann, B. A., Bock, K., Servatius, H., Müllerleile, K., Sultan, A., Gosau, N., et al. (2011). Long-term single-and multiple-procedure outcome and predictors of success after catheter ablation for persistent atrial fibrillation. *Heart Rhythm*, 8(9):1391–1397.
- Salinet, J., Molero, R., Schlindwein, F. S., Karel, J., Rodrigo, M., Rojo-Álvarez, J. L., Berenfeld, O., Climent, A. M., Zenger, B., Vanheusden, F., et al. (2021). Electrocardiographic imaging for atrial fibrillation: a perspective from computer models and animal experiments to clinical value. *Frontiers in physiology*, 12:653013.
- Scherr, D., Khairy, P., Miyazaki, S., Aurillac-Lavignolle, V., Pascale, P., Wilton, S. B., Ramoul, K., Komatsu, Y., Roten, L., Jadidi, A., et al. (2015). Five-year outcome of catheter ablation of persistent atrial fibrillation using termination of atrial fibrillation as a procedural endpoint. *Circulation. Arrhythmia and electrophysiology*, 8(1):18–24.
- Schnabel, R. B., Michal, M., Wilde, S., Wiltink, J., Wild, P. S., Sinning, C. R., Lubos, E., Ojeda, F. M., Zeller, T., Munzel, T., et al. (2013). Depression in atrial fibrillation in the general population. *PLoS one*, 8(12):e79109.
- Schnabel, R. B., Yin, X., Gona, P., Larson, M. G., Beiser, A. S., McManus, D. D., Newton-Cheh, C., Lubitz, S. A., Magnani, J. W., Ellinor, P. T., et al. (2015). 50 year trends in atrial fibrillation prevalence, incidence, risk factors, and mortality in the Framingham Heart Study: a cohort study. *The Lancet*, 386(9989):154–162.
- Schreiber, D., Rostock, T., Fröhlich, M., Sultan, A., Servatius, H., Hoffmann, B. A., Lüker, J., Berner, I., Schäffer, B., Wegscheider, K., et al. (2015). Five-year follow-up after catheter ablation of persistent atrial fibrillation using the stepwise approach and prognostic factors for success. *Circulation. Arrhythmia and electrophysiology*, 8(2):308–317.
- Serpytis, R., Navickaite, A., Serpytiene, E., Barysiene, J., Marinskis, G., Jatuzis, D., Petrulioniene, Z., Laucevicius, A., and Serpytis, P. (2018). Impact of atrial fibrillation on cognitive function, psychological distress, quality of life, and impulsiveness. *The American journal of medicine*, 131(6):703.e1–703.e5.
- Shaffer, F. and Ginsberg, J. P. (2017). An overview of heart rate variability metrics and norms. *Frontiers in public health*, page 258.
- Shaffer, F., McCraty, R., and Zerr, C. L. (2014). A healthy heart is not a metronome: an integrative review of the heart's anatomy and heart rate variability. *Frontiers in psychology*, 5:1040.
- Skolnik, M. I. (1980). *Introduction to Radar Systems*. McGraw-Hill Book Co.

- Slocum, J., Sahakian, A., and Swiryn, S. (1992). Diagnosis of atrial fibrillation from surface electrocardiograms based on computer-detected atrial activity. *Journal of electrocardiology*, 25(1):1–8.
- Sörnmo, L., Petrénas, A., and Marozas, V. (2018). *Atrial fibrillation from an engineering perspective*. Springer.
- Staerk, L., Sherer, J. A., Ko, D., Benjamin, E. J., and Helm, R. H. (2017). Atrial fibrillation: epidemiology, pathophysiology, and clinical outcomes. *Circulation research*, 120(9):1501–1517.
- Staerk, L., Wang, B., Preis, S. R., Larson, M. G., Lubitz, S. A., Ellinor, P. T., McManus, D. D., Ko, D., Weng, L.-C., Lunetta, K. L., et al. (2018). Lifetime risk of atrial fibrillation according to optimal, borderline, or elevated levels of risk factors: cohort study based on longitudinal data from the Framingham Heart Study. *BMJ : British medical journal / British Medical Association*, 361.
- Steinberg, J. S., O’Connell, H., Li, S., and Ziegler, P. D. (2018). Thirty-second gold standard definition of atrial fibrillation and its relationship with subsequent arrhythmia patterns: analysis of a large prospective device database. *Circulation. Arrhythmia and electrophysiology*, 11(7):e006274.
- Stridh, M. and Sörnmo, L. (2001). Spatiotemporal QRST cancellation techniques for analysis of atrial fibrillation. *IEEE Transactions on Biomedical Engineering*, 48(1):105–111.
- Szilágyi, J., Walters, T. E., Marcus, G. M., Vedantham, V., Moss, J. D., Badhwar, N., Lee, B., Lee, R., Tseng, Z. H., and Gerstenfeld, E. P. (2018). Surface ECG and intracardiac spectral measures predict atrial fibrillation recurrence after catheter ablation. *Journal of cardiovascular electrophysiology*, 29(10):1371–1378.
- Takens, F. (1981). Detecting strange attractors in turbulence. In *Dynamical systems and turbulence, Warwick 1980*, pages 366–381. Springer.
- Tamborero, D., Mont, L., Berruezo, A., Matiello, M., Benito, B., Sitges, M., Vidal, B., de Caralt, T. M., Perea, R. J., Vatasescu, R., et al. (2009). Left atrial posterior wall isolation does not improve the outcome of circumferential pulmonary vein ablation for atrial fibrillation: a prospective randomized study. *Circulation. Arrhythmia and electrophysiology*, 2(1):35–40.
- Teh, A. W., Kistler, P. M., Lee, G., Medi, C., Heck, P. M., Spence, S., Morton, J. B., Sanders, P., and Kalman, J. M. (2011). Electroanatomic properties of the pulmonary veins: slowed conduction, low voltage and altered refractoriness in af patients. *Journal of cardiovascular electrophysiology*, 22(10):1083–1091.
- Tilz, R. R., Rillig, A., Thum, A.-M., Arya, A., Wohlmuth, P., Metzner, A., Mathew, S., Yoshiga, Y., Wissner, E., Kuck, K.-H., et al. (2012). Catheter ablation of long-standing persistent atrial fibrillation: 5-year outcomes of the Hamburg Sequential Ablation Strategy. *Journal of the American College of Cardiology*, 60(19):1921–1929.

Bibliography

- Trulla, L., Giuliani, A., Zbilut, J., and Webber Jr, C. (1996). Recurrence quantification analysis of the logistic equation with transients. *Physics Letters A*, 223(4):255–260.
- Tse, H.-F., Wang, Y.-J., Ai-Abdullah, M. A., Pizarro-Borromeo, A. B., Chiang, C.-E., Krittayaphong, R., Singh, B., Vora, A., Wang, C.-X., Zubaid, M., et al. (2013). Stroke prevention in atrial fibrillation—an Asian stroke perspective. *Heart Rhythm*, 10(7):1082–1088.
- Uldry, L., Duchêne, C., Prudat, Y., Murray, M. M., and Vesin, J.-M. (2009). Adaptive tracking of EEG frequency components. In *Advanced biosignal processing*, pages 123–144. Springer.
- up Investigation of Rhythm Management (AFFIRM) Investigators, A. F. F. (2002). A comparison of rate control and rhythm control in patients with atrial fibrillation. *New England Journal of Medicine*, 347(23):1825–1833.
- Van Den Berg, M. P., Van Noord, T., Brouwer, J., Haaksma, J., Van Veldhuisen, D. J., Crijns, H. J., and Van Gelder, I. C. (2004). Clustering of RR intervals predicts effective electrical cardioversion for atrial fibrillation. *Journal of cardiovascular electrophysiology*, 15(9):1027–1033.
- Van Zaen, J. (2012). Efficient schemes for adaptive frequency tracking and their relevance for EEG and ECG. Technical report, EPFL.
- Van Zaen, J., Uldry, L., Duchêne, C., Prudat, Y., Meuli, R. A., Murray, M. M., and Vesin, J.-M. (2010). Adaptive tracking of EEG oscillations. *Journal of neuroscience methods*, 186(1):97–106.
- Velleca, M., Costa, G., Goldstein, L., Bishara, M., and Ming, L. (2019). A review of the burden of atrial fibrillation: understanding the impact of the new millennium epidemic across Europe. *Cardiology*.
- Verma, A., Jiang, C.-y., Betts, T. R., Chen, J., Deisenhofer, I., Mantovan, R., Macle, L., Morillo, C. A., Haverkamp, W., Weerasooriya, R., et al. (2015). Approaches to catheter ablation for persistent atrial fibrillation. *New England Journal of Medicine*, 372(19):1812–1822.
- Wazni, O. M., Dandamudi, G., Sood, N., Hoyt, R., Tyler, J., Durrani, S., Niebauer, M., Makati, K., Halperin, B., Gauri, A., et al. (2021). Cryoballoon ablation as initial therapy for atrial fibrillation. *New England Journal of Medicine*, 384(4):316–324.
- Webber Jr, C. L. and Zbilut, J. P. (1994). Dynamical assessment of physiological systems and states using recurrence plot strategies. *Journal of applied physiology*, 76(2):965–973.
- Werner, J. (2014). 5.01 - electrical activities in the body. In Brahme, A., editor, *Comprehensive Biomedical Physics*, pages 1–24. Elsevier, Oxford.
- Wilber, D. J., Pappone, C., Neuzil, P., De Paola, A., Marchlinski, F., Natale, A., Macle, L., Daoud, E. G., Calkins, H., Hall, B., et al. (2010). Comparison of antiarrhythmic drug therapy and radiofrequency catheter ablation in patients with paroxysmal atrial fibrillation: a randomized controlled trial. *Journal of the American Medical Association*, 303(4):333–340.

- Yang, P.-S., Park, Y.-A., Kim, T.-H., Uhm, J.-S., Joung, B., Lee, M.-H., and Pak, H.-N. (2017). Which patients recur as atrial tachycardia rather than atrial fibrillation after catheter ablation of atrial fibrillation? *PLoS One*, 12(11):e0188326.
- Yazdani, S., Fallet, S., and Vesin, J.-M. (2017). A novel short-term event extraction algorithm for biomedical signals. *IEEE Transactions on Biomedical Engineering*, 65(4):754–762.
- Yiin, G. S., Howard, D. P., Paul, N. L., Li, L., Luengo-Fernandez, R., Bull, L. M., Welch, S. J., Gutnikov, S. A., Mehta, Z., and Rothwell, P. M. (2014). Age-specific incidence, outcome, cost, and projected future burden of atrial fibrillation–related embolic vascular events: a population-based study. *Circulation*, 130(15):1236–1244.
- Yoo, B. (2014). Normal sinus rhythm on an ECG.
- Yoon, M., Yang, P.-S., Jang, E., Yu, H. T., Kim, T.-H., Uhm, J.-S., Kim, J.-Y., Sung, J.-H., Pak, H.-N., Lee, M.-H., et al. (2019). Improved population-based clinical outcomes of patients with atrial fibrillation by compliance with the simple ABC (Atrial Fibrillation Better Care) pathway for integrated care management: a nationwide cohort study. *Thrombosis and haemostasis*, 119(10):1695–1703.
- Zarzoso, V., Latcu, D. G., Hidalgo-Muñoz, A. R., Meo, M., Meste, O., Popescu, I., and Saoudi, N. (2016). Non-invasive prediction of catheter ablation outcome in persistent atrial fibrillation by fibrillatory wave amplitude computation in multiple electrocardiogram leads. *Archives of cardiovascular diseases*, 109(12):679–688.
- Zbilut, J. P., Thomasson, N., and Webber, C. L. (2002). Recurrence quantification analysis as a tool for nonlinear exploration of nonstationary cardiac signals. *Medical engineering & physics*, 24(1):53–60.
- Zbilut, J. P. and Webber Jr, C. L. (1992). Embeddings and delays as derived from quantification of recurrence plots. *Physics letters A*, 171(3-4):199–203.
- Zeemering, S., Lankveld, T. A., Bonizzi, P., Limantoro, I., Bekkers, S. C., Crijns, H. J., and Schotten, U. (2018). The electrocardiogram as a predictor of successful pharmacological cardioversion and progression of atrial fibrillation. *Europace*, 20(7):e96–e104.
- Zhang, J., Johnsen, S. P., Guo, Y., and Lip, G. Y. (2021). Epidemiology of atrial fibrillation: geographic/ecological risk factors, age, sex, genetics. *Cardiac electrophysiology clinics*, 13(1):1–23.
- Zoni-Berisso, M., Lercari, F., Carazza, T., and Domenicucci, S. (2014). Epidemiology of atrial fibrillation: European perspective. *Clinical epidemiology*, 6:213.

Anna McCann

☎ +41 77 902 29 69 • ✉ amccann95@gmail.com • in 🐦 🌐 📺

Nationalities: Irish, American ~ Date of birth: 04 August 1995

Strengths

- Experienced with signal processing and machine learning for biomedical applications.
- Skilled in software development (ML frameworks, scientific Python, open-source software).
- Published in peer-reviewed journals and domain-specific venues.

Education

2019–Present **PhD Biomedical Signal Processing**, *École Polytechnique Fédérale de Lausanne (EPFL)*, Applied Signal Processing Group, Department of Electrical Engineering

I co-lead several interdisciplinary clinical studies, collaborating with research teams of engineers and medical doctors, to develop software, collect patient data, and perform clinical studies resulting in peer-reviewed publications.

- Thesis: Finding information-rich electrocardiographic biomarkers to characterize atrial fibrillation.
- Adviser: Dr. Jean-Marc Vesin.
- Co-adviser: Prof. Etienne Pruvot.

2014–2018 **B.Eng. Electrical and Electronic Engineering**, *University College Dublin (UCD)*, Dublin, IE, *GPA 93%, First Class Honours*

- Thesis: Design and implementation of elderly fall detection using wireless communications.
- Adviser: Prof. Nam Tran.
- Courses and projects in signal processing, embedded systems, computer architecture, electronic design, analog and digital circuits.

Experience

2019–Present **Doctoral Assistant**, *EPFL, UNIL*

Assisted students with course material during exercise sessions, acted as liaison between students and professors, and contributed to creation of exams. I also designed a more equitable and efficient grading system to use for correcting project work and exams.

- Courses: Biomedical Signal Processing, Signaux et Systèmes (*Signals and Systems*), Acquisition et traitement de données (*Data Acquisition and Processing*)

2018–2019 **Hardware Engineer**, *Qualcomm*, Cork, IE

Working within the Security team, implemented hardware verification (SystemVerilog) for new security features of next-generation Snapdragon system on chip mobile platform.

Summer 2017 **Software Engineer Intern**, *Spot Trading*, Chicago, IL, USA

Contributed to the development of algorithmic and architectural changes to speed up a market data decoder (Rust).

Summer 2016 **Summer Research Intern**, *Center for Neurotechnology*, University of Washington, Seattle, WA, USA

Developed stand-alone software for OpenEphys, an open source platform for collecting and analyzing neurological signals, currently in use for computational neuroscience research.

Skills

Statistical signal processing, Machine learning, Deep learning, Matlab, Python (PyTorch, ScikitLearn, NumPy, SciPy, Pandas, Seaborn, Matplotlib), High performance computing, Time Series, Multivariate data, Git, Linux

Awards

2014-2018 UCD Global Excellence Scholarship for outstanding international students

2018 Cylon Award for the best electronic engineering bachelor project

2023 Ma thèse en 180 secondes EPFL finalist

Languages

English Native language

French Advanced (C1)

Publications

- [1] A. Luca, A. Baskaralingam, A. McCann, J.-M. Vesin, P. Pascale, M. Le Bloa, C. Herrera, L. Roten, M. Kuhne, F. Spies. "Amplitude of fibrillatory wave correlates with long-term maintenance of sinus rhythm after ablation in persistent atrial fibrillation". *Europace* 24.Supplement_1 (2022), euac053–063.
- [2] A. McCann, A. Luca, P. Pascale, E. Pruvot, J.-M. Vesin. "Novel spatiotemporal processing tools for body-surface potential map signals for the prediction of catheter ablation outcome in persistent atrial fibrillation". *Front Physiol* (2022), p. 2041.
- [3] A. McCann, A. Luca, E. Pruvot, L. Roten, C. Sticherling, J.-M. Vesin. "Ventricular response regularity in atrial fibrillation and its relationship to successful catheter ablation". *2020 28th European Signal Processing Conference (EUSIPCO)*. IEEE. 2021, pp. 910–914.
- [4] A. McCann, J.-M. Vesin, E. Pruvot, L. Roten, C. Sticherling, A. Luca. "ECG-based indices to characterize persistent atrial fibrillation before and during stepwise catheter ablation". *Front Physiol* 12 (2021), p. 383.
- [5] A. Pithon, A. McCann, A. Buttu, J.-M. Vesin, P. Pascale, M. Le Bloa, C. Herrera, C.-I. Park, L. Roten, M. Kühne. "Dynamics of Intraprocedural Dominant Frequency Identifies Ablation Outcome in Persistent Atrial Fibrillation". *Front Physiol* 12 (2021).
- [6] A. Luca, A. Pittet, A. Buttu, A. McCann, J.-M. Vesin, P. Pascale, M. Le Bloa, C. Herrera, C.-I. Park, A. Rollin. "Severe and uniform bi-atrial remodeling measured by dominant frequency analysis in persistent atrial fibrillation unresponsive to ablation". *J Interv Card Electrophysiol* 59.2 (2020), pp. 431–440.